2015-07-01

Evaluation of Empirical Prediction Methods for Liquefaction-Induced Lateral Spread from the 2010 Maule, Chile, M_W 8.8 Earthquake in Port Coronel

Nicole D. Williams
Brigham Young University

Evaluation of Empirical Prediction Methods for Liquefaction-Induced Lateral Spread from the 2010 Maule, Chile, M_w 8.8 Earthquake in Port Coronel

Nicole D. Williams

A thesis submitted to the faculty of
Brigham Young University
in partial fulfillment of the requirements for the degree of

Master of Science

Kyle M. Rollins, Chair
Kevin W. Franke
Norman L. Jones

Department of Civil and Environmental Engineering

Brigham Young University

July 2015

ABSTRACT

Evaluation of Empirical Prediction Methods for Liquefaction-Induced Lateral Spread from the 2010 Maule, Chile, M_w 8.8 Earthquake in Port Coronel

Nicole D. Williams
Department of Civil and Environmental Engineering, BYU
Master of Science

Over the past several decades, empirical formulas have been developed and improved to predict liquefaction and lateral spread based on a database of case histories from observed earthquakes, such as Youd et al. (2002) and Rauch and Martin (2000). The 2010 Maule Chile earthquake is unique first of all because it is recent and was not used to develop recent liquefaction and lateral spread evaluation methods, and therefore can be reasonably used to evaluate the effectiveness of such equations. Additionally, the 8.8 magnitude megathrust event fills a significant gap in the databases used to develop these empirical formulas, which tends to under represent large magnitude earthquakes and events which occur along subduction zones. Use of case histories from this event will therefore effectively test the robustness and accuracy of these methods.

As a part of this comparison, data will be collected from two piers in Port Coronel, Chile: Lo Rojas or Fisherman's Pier, and el Carbonero. Lo Rojas is a municipally owned pier which failed in the 2010 earthquake. Dr. Kyle Rollins gathered detailed engineering survey data defining lateral spread displacements along this pier in a reconnaissance visit with other GEER investigators after the earthquake. El Carbonero was under construction during the earthquake, but no known lateral displacements were observed. Collaboration with local universities and personnel contributed a great deal of knowledge about the soil profile. In early April 2014, collection of SPT and CPT data began in strategic locations to fill gaps of understanding about the stratigraphy near the two piers. Additional testing will provide necessary information to carry out predictions of displacements using current empirical models, which can then be compared with observed displacements collected after the earthquake. Collected data will also be complied, and this alone will provide useful information as it represents a unique case history for future evaluation.

The goals of this study are therefore: (1) Collect data for two piers (Lo Rojas and el Carbonero) in Port Coronel, Chile to provide a useful case history of lateral displacements observed; (2) Conduct a liquefaction and lateral spread analysis to predict displacement of the two piers in question, considering lateral spread and slope stability; (3) Compare predicted values with observed displacements and draw conclusions on the predictive capabilities of analyzed empirical equations for similar earthquakes (4) Make recommendations to improve when possible.

Keywords: Maule Chile 2010 earthquake, liquefaction, lateral spread.

ACKNOWLEDGEMENTS

Funding for this study was provided by the National Science Foundation, Division of Civil, Mechanical, and Manufacturing Innovation (CMMI) under Grant No. CMMI-1235526. This support is gratefully acknowledged. Nevertheless, the opinions, conclusions, and recommendations expressed in this study are those of the authors and do not necessarily reflect the views of NSF.

Thank you Claudio Vega and those at Port Coronel that made testing at the port possible; Anne Lemnitzer and Ricardo Moffat, owners of Lemnitzer and Moffat Geotechnica Ltd. for providing discounted CPT services and assistance; Dr. Esteban Saez, Dr. Christian Ledezma, and Gabriel de la Maza from the Pontifical Catholic University of Chile for their technical expertise and assistance performing laboratory tests on field samples; Gonzalo Montalva for his help obtaining data and contacts in preparation for field investigations; and Dr. Peter Robertson for providing a free copy of the CPT analysis program CLiq for use in this study.

I am also grateful for the continuous guidance I have received from my advisor Dr. Kyle M. Rollins, who has patiently helped me with every step of this project. Thank you Dr. Kevin W. Franke and Dr. Norman L. Jones for your time and feedback during both the analysis and revisions process. I am also grateful for Dr. T. Leslie Youd, and his insights into existing liquefaction and lateral spread methods, as well as advice and technical expertise.

Finally, thank you Ginger Tryon for blazing the trail by completing the first portion of this project, and for always offering additional support and feedback. The study would not be where it is today without your dedication and technical insight.

TABLE OF CONTENTS

LIST OF TABLES

LIST OF FIGURES

1 INTRODUCTION

Loss of life and property remains an unavoidable consequence of major earthquakes. Throughout history, studies of the effects of major earthquakes have attempted to assess the damage and provide recommendations to mitigate loss in the case of future earthquakes. Of these effects, liquefaction induced lateral spread ground failure is considered one of the most common and detrimental.

Liquefaction occurs when saturated soil loses strength, changing from a solid to a liquid state due to an increase in pore-water pressure, as typically observed in loose saturated sands with silt or even gravels with seams of impermeable layers that prevents proper drainage. Applied cyclic shear stresses causes loose soils to compact, increasing the water pressure in pore spaces. As pore water pressure increases, effective soil stress decreases to near zero reducing the soil strength and allowing the ground to deform. Settlement, lateral spreading, and slope failure are all examples of observed liquefaction induced ground deformation (Kramer, 1996).

When cyclic stresses cause the soil to become unstable, such that the static shear force required to maintain soil in equilibrium exceeds the shear strength of the soil, flow failures occur. Since the amount of deformation is often large, flow failures can be catastrophic. In the 1971 San Fernando earthquake, liquefaction induced ground failures almost resulted in the loss of the Lower San Fernando Dam.

Lateral spreading, defined in this study according to Youd et al. (2002), occurs when mostly intact discrete blocks of soil slide over a liquefied soil layer, moving generally down a gentle slope or toward a free-face. Static shear forces remain lower than the soil shear strength, resulting in smaller deformations that develop incrementally during the earthquake shaking. Movement typically ranges from a few centimeters (cm) to tens of meters (m), affecting areas up to a few square kilometers (km) (Bardet et al., 2002). As saturated soil is a requirement for liquefaction, both flow failures and lateral spreads are frequently observed near bodies of water.

Though lateral spreading will not necessarily cause the catastrophic failures observed in other forms of liquefaction failures such as deep-seated flow failures, it is considered one of the most pervasive forms of liquefaction-induced failure, partially because damage to lifelines is significant. Water, transportation, and communication lines often break under the displacements caused by lateral spread, exacerbating all other impacts and impeding relief efforts. For example, fires generated in the 1906 San Francisco earthquake were devastating due to a lack of water from broken pipelines (Barlett and Youd, 1995).

Though the effects of lateral spreading observed in the 1906 San Francisco earthquake resulted in significant loss of life and property, the phenomena was not well understood and did not begin to catch international attention until the 1960s, following extensive liquefaction observed in the 1964 Alaska and Niigata earthquakes. Significant damage to railroads and port facilities in Alaska and riverfront facilities in Japan lead to the development of several empirical models which attempt to predict ground displacement expected from similar earthquakes.

In 2010, an 8.8 moment magnitude (M_w) earthquake struck of the coast of Concepción in the Maule region, Chile. This earthquake was the fifth largest earthquake in recorded history, lasting 90 to 150 seconds. Extensive liquefaction and lateral spreading were observed among

port facilities around the area, a critical lifeline facilitating relief efforts and rebuilding of the economy. Port Coronel demonstrated signs of significant lateral spread among various piers, resulting in almost 3 m of movement in some locations and the failure of one pier.

Current methods for predicting the amount of displacement frequently rely on empirical methods, as mechanistic models require parameters that are difficult to measure or estimate. However, due to the nature of empirically generated formulas, use on sites with parameters that vary significantly from the cases selected to develop the formulas may result in erroneous predictions. Development of these models is limited to the current data recorded from past earthquakes, with updates allowing the incorporation of more recently collected data and modifications to improve predictive capabilities. Although the M9.2 1964 Alaskan earthquake was in the database this is the only earthquake with a moment magnitude over 8.0 included in current empirical correlations, due to a general lack of availability and documentation of large magnitude earthquakes. As the moment magnitude of the Muale Chile earthquake falls above the generally acceptable range of 8.0 for extrapolation with current empirical prediction techniques, predicted displacements may not correlate well to actual observed displacements.

The purpose of this study is:

(1) to document geotechnical, structural, and performance data collected from two Port Coronel piers that underwent the 2010 Maule, Chile earthquake as case histories

(2) to evaluate the current state of the art for empirical lateral displacement prediction methods for large magnitude earthquakes in subduction zones using two Port Coronel piers case histories, and

(3) to suggest modifications in lateral spreading analysis procedures to improve their predictive capabilities, particularly for large magnitude earthquakes.

Seismic, topographic, and geotechnical data has been collected for each pier, several liquefaction and lateral spread methods are evaluated, and accuracy is evaluated by comparing predicted displacement to observed displacements measured in the Geo-Engineering Extreme Events Reconnaissance (GEER) report (Bray et al. 2010). Conclusions on the applicability of each method to the specific case histories are drawn, and future research is suggested. Methods for evaluating liquefaction triggering include: Youd et al. (2001), Idriss and Boulanger (2004) and Cetin et al. (2004). Methods for evaluating lateral spread displacements will include: Youd, Hansen, and Bartlett (2002), Rauch and Martin (2000), Bardet et al. (2002), Zhang et al. (2012), Faris et al. (2006), and Zhang et al. (2004).

2 CURRENT EMPIRICAL MODEL REVIEW

Several common methods for liquefaction triggering and lateral spreading are reviewed in this section. While numerous versions of each method often exist with previous iterations highlighting advancements, only the most recent versions are examined here. See the references for more detail on the development of each method.

2.1 Liquefaction Triggering Equations

In order for lateral spread to occur, a continuous layer of liquefiable soil must be present. Most empirical techniques require a liquefaction triggering study to identify a layer that is likely to liquefy. Three common liquefaction triggering methods are examined: Youd et al. (2002), Cetin et al. (2004), and Idriss and Boulanger (2004). Since developers of lateral spread and liquefaction techniques often collaborate or are the same authors, an attempt is made to associate the favored liquefaction method with each lateral spread method.

2.1.1 Youd et al. (2001)

Developed during the 1996 NCEER and 1998 NCEER/NSF workshops on evaluation of liquefaction resistance of soils, this method is based on the earlier "simplified procedure" developed by Seed and Idriss in 1971 that was standard practice at the time. No major update had

been made since 1985, and the conference aimed to incorporate additions and modifications to the procedure.

Two terms are required for evaluation: Cyclic Stress Ratio (CSR) and Cyclic Resistance Ratio (CRR). CSR estimates the seismic demand on a soil layer, as shown in equation (2-1) :

$$CSR = 0.65\left(\frac{\sigma_{vo}}{\sigma'_{vo}}\right)\cdot\left(\frac{a_{max}}{g}\right)\cdot r_d \qquad (2\text{-}1)$$

Where a_{max} = peak horizontal acceleration at the ground surface from the earthquake; g= acceleration due to gravity; σ_{v0} and σ'_{v0} are total and effective vertical overburden stresses, respectively; and r_d = stress reduction coefficient defined in equations (2-2) and (2-3).

$$r_d = 1.0 - 0.00765 \text{ for } z \leq 9.15m \qquad (2\text{-}2)$$

$$r_d = 1.174 - 0.0267 \text{ for } 9.15m < z \leq 23m \qquad (2\text{-}3)$$

CRR estimates the capacity of the soil to resist liquefaction, and can be estimated by several types of test data including SPT, CPT, shear wave velocity (V_S), and the Becker penetration test. Field tests are preferred over laboratory testing, due to high sample disturbance during sampling and transportation to the lab.

Advantages of SPT correlations include abundant SPT data from past earthquakes and the ability to retrieve a sample for classification. The equation for estimating CRR for a 7.5 magnitude earthquake from SPT data is shown in equation (2-4):

$$CRR_{7.5} = \frac{1}{34(N1)_{60cs}} + \frac{(N1)_{60cs}}{135} + \frac{1}{(10*(N1)_{60cs}+45)^2} - \frac{1}{200} \quad (2\text{-}4)$$

Where $(N1)_{60}$ is blow count normalized for overburden pressure, and corrected for hammer efficiency, borehole diameter, rod length, sampler, and clean sand equivalent. This equation calculates CRR and is only valid for $(N1)_{60cs}$ less than 30, as larger blow counts are considered non-liquefiable.

Advantages of CPT data include continuous data, good detection of variability within the layer, good quality control, and repeatability. However, CPT data does not always indicate variation in fines content well. CRR is estimated from CPT data using equations (2-5) and (2-6), where $(q_{C1N})_{cs}$ is cone tip resistance normalized for overburden and atmospheric pressure:

$$CRR_{7.5} = 0.833\left[\frac{(q_{c1N})_{cs}}{1000}\right] + 0.05 \; if \; (q_{c1N})_{cs} < 50 \quad (2\text{-}5)$$

$$CRR_{7.5} = 93\left[\frac{(q_{c1N})_{cs}}{1000}\right]^3 + 0.08 \; if \; 50 \leq (q_{c1N})_{cs} < 160 \quad (2\text{-}6)$$

Although not as widely available as SPT and CPT data, V_S data is a basic mechanical property of soil, which is directly related to small-strain shear modulus. However, liquefaction occurs with medium to high-strain. V_S also performs well in gravelly soils, unlike SPT and CPT, but may not detect thin, weakly cemented low V_S strata if the measurement interval is too long.

As there is some debate over the benefits of normalizing V_S data for CRR calculations, CRR can be calculated using both V_S and V_{S1}. Equation (2-7) calculates CRR from V_{S1} :

$$CRR_{7.5} = 0.022\left[\frac{V_{S1}}{100}\right] + 2.8\left(\frac{1}{V^*_{S1}-V_{S1}} - \frac{1}{V_{S1}}\right) \quad (2\text{-}7)$$

For gravels, BPT tests are a good option, as they are able to penetrate these dense materials. However, this test is not discussed in detail here as it is not applicable to the examined case studies.

To correct for magnitude effects, either a Magnitude Scaling Factors (MSF) can be applied to CRR, or CSR is adjusted by dividing by a weighting factor, which is the inverse of a MSF. Both are used to find the corresponding CRR for earthquakes of magnitudes other than 7.5 and achieve the same result. Youd et al. (2001) applies a MSF, where equation (2-25) calculates a factor of safety against liquefaction (FS) using the I. M. Idriss MSF referenced in equation (2-10) where K_σ corrects for overburden pressure:

$$FS = \left(\frac{CRR_{7.5}}{CSR}\right) * MSF * K_\sigma \quad (2\text{-}8)$$

$$MSF = 10^{2.24} / {M_W}^{2.56} \quad (2\text{-}9)$$

Cetin et al. (2004)

Unlike the Youd et al. (2001) paper which considered various forms of in situ field data for determining CRR, Cetin et al. (2004) focuses exclusively on SPT data. Several additional case histories were added, and all case histories were carefully examined for quality and uncertainty and poor quality histories were eliminated. Additionally, this method deals specifically with issues regarding fines content, magnitude correlations, and effective overburden stress corrections. The Cetin et al. (2004) procedure also accounts for improved understanding of SPT data interpretation, assessment of in situ cyclic shear stress ratio, and site-specific earthquake ground motions such as directivity effects and site specific response. Use of high-order Bayesian updating probabilistic tools in addition to case history screening reduced uncertainty. The final method follows the same

pattern as Youd et al. (2001) with a few changes, including a new r_d stress reduction factor and fines correction factor. Equation (2-10) shows r_d for depths less than 20 m, with equation (2-11) for depths greater than 20 m.

$$r_d = \frac{\left[1 + \frac{-23.013 - 2.949a_{max} + 0.999M_w + 0.0525V^*_{s,12m}}{16.258 + 0.201e^{0.341(-20+0.0785V^*_{s,12m}+7.586)}}\right]}{\left[1 + \frac{-23.013 - 2.949a_{max} + 0.999M_w + 0.0525V^*_{s,12m}}{16.258 + 0.201e^{0.341(0.0785V^*_{s,12m}+7.586)}}\right]} \pm \sigma_{\varepsilon_{r_d}} \quad (2\text{-}10)$$

$$r_d = \frac{\left[1 + \frac{-23.013 - 2.949a_{max} + 0.999M_w + 0.0525V^*_{s,12m}}{16.258 + 0.201e^{0.341(-20+0.0785V^*_{s,12m}+7.586)}}\right]}{\left[1 + \frac{-23.013 - 2.949a_{max} + 0.999M_w + 0.0525V^*_{s,12m}}{16.258 + 0.201e^{0.341(0.0785V^*_{s,12m}+7.586)}}\right]} - 0.0046(d - 20) \pm \sigma_{\varepsilon_{r_d}} \quad (2\text{-}11)$$

Where,

$$\sigma_{\varepsilon_{r_d}} = d^{0.8500} * 0.0198. \quad (2\text{-}12)$$

Equation (2-12) defines standard deviation $\sigma_{\varepsilon rd}$ as a function of depth (d), where d is limited to a maximum of 12 m, remaining constant after that depth. The stiffness factor $V^*_{s,\ 12\ m}$ is measured or estimated with a minimum of 120 m/s for very soft soils and a maximum of 250 m/s

for very stiff soils. The necessity of estimating shear wave velocity for site stiffness when evaluating SPT data could be considered a weakness.

SPT blow counts are also corrected for fines, by multiplying $N_{1,60,CS}$ values by C_{Fines}:

$$C_{Fines} = (1 + 0.004 * FC) + 0.05 * \left(\frac{FC}{N_{1,60}}\right) \quad (2\text{-}13)$$

Where FC is percent fines, with a maximum of 35% and a value equal to zero for fines less than 5%. Magnitude is correlated from a duration weighting factor (DWF_M), as shown in Figure 1 and equation (2-14).

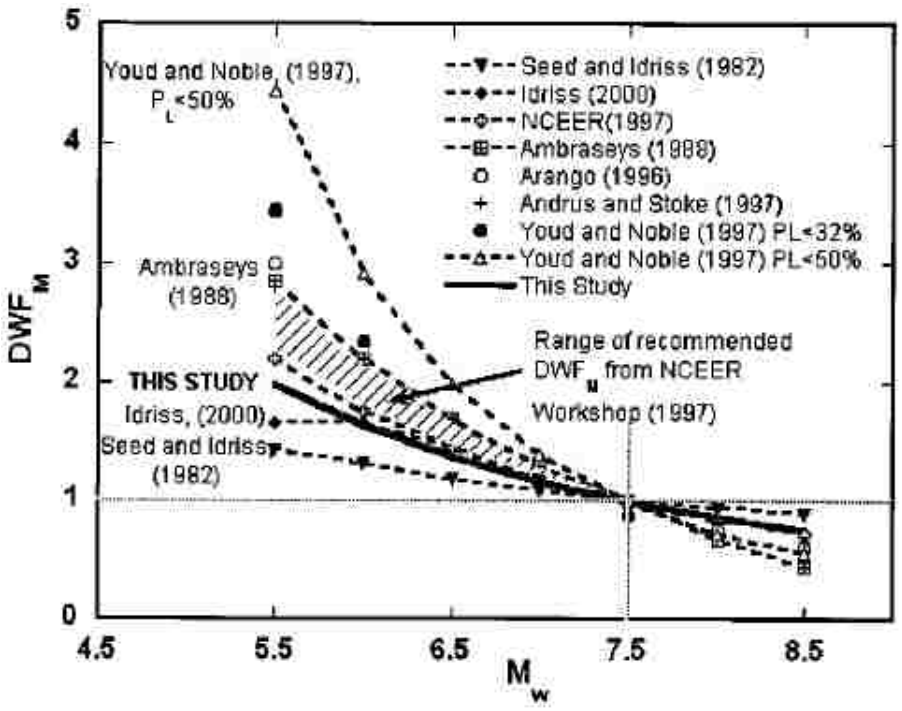

Figure 1. Cetin et al. (2004) recommendations for magnitude scaling (labeled as THIS STUDY) compared with previous methods.

$$CSR^*_{eq} = CSR_{eq}/DWF_M \quad (2\text{-}14)$$

2.1.2 Idriss and Boulanger (2004)

Building on the same framework as Youd et al. (2001) and Cetin et al. (2004), Idriss and Boulanger (2004) redefine parameters r_d, MSF, K_σ and C_N. Idriss performed several hundred parametric site response analyses as a basis to redefine these variables, and derived equations (2-15) – (2-17):

$$ln(r_d) = \alpha(z) + \beta(z) \cdot M \tag{2-15}$$

$$\alpha(z) = -1.012 - 1.126 \sin\left(\frac{Z}{11.73} + 5.13\right) \tag{2-16}$$

$$\beta(z) = 0.106 + 0.118 \sin\left(\frac{Z}{11.28} + 5.142\right) \tag{2-17}$$

Where depth (Z) is less than or equal to 34 m. To correct for magnitude effects, CSR is multiplied by the MSF factor given by (2-18) instead of multiplying CRR by MSF as proposed by Youd et al. (2001). Nevertheless, the effect on the factor of safety against liquefaction is the same in both cases, as described in equation (2-19), with MSF limited to a maximum of 1.8.

$$MSF = 6.9e^{\left(\frac{-M}{4}\right)} - 0.058 \tag{2-18}$$

$$CSR_M = MSF * CSR_{M=7.5} \tag{2-19}$$

Figure 2 shows curves for re-evaluated K_σ by Boulanger and Idriss, with several equations to obtain these curves described in more detail in Idriss and Boulanger (2004).

C_N relations are re-evaluated as well, with final recommendations in equations (2-20):

$$C_N = \left(\frac{P_a}{\sigma'_{vo}}\right)^m \leq 1.7 \qquad (2\text{-}20)$$

Where $m = 0.784 - 0.0768 * ((N_1)_{60})^{0.5}$ for SPT data and $m = 1.338 - 0.249 * (q_{C1N})^{0.264}$ for CPT data. $(N_1)_{60}$ values are limited to a maximum of 46, with q_{C1N} limited to a maximum of 254. Note that solving equation (2-20) requires iteration, as $(N_1)_{60} = C_N(N)_{60}$ and $q_{C1} = C_N q_c$. Idriss and Boulanger (2004) discuss V_S data, but only briefly, as they do not recommend using liquefaction estimations from V_S data outside of creating limiting bounds.

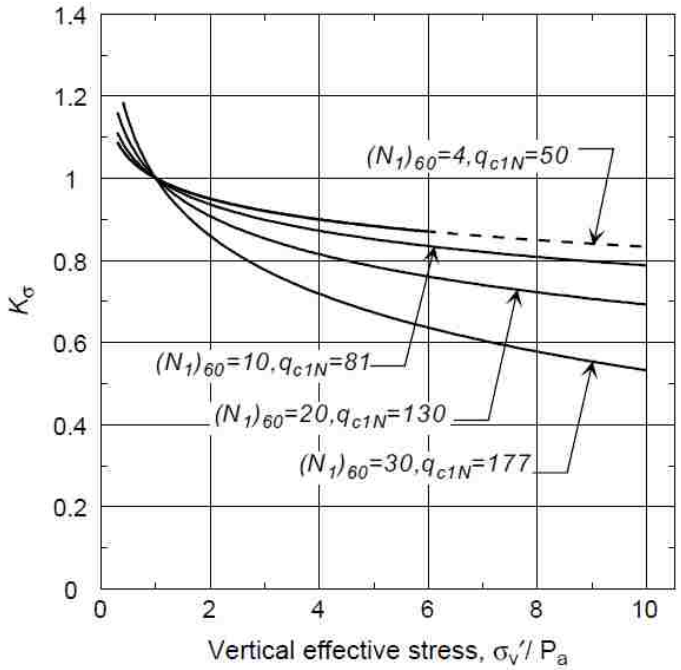

Figure 2. Re-evaluated K_σ curves from Idriss and Boulanger (2004).

2.2 Lateral Spread Prediction Methods

Several deterministic models have been developed to estimate lateral spread, including methods based on SPT and CPT data. Six models are examined here, including: four fully empirical methods for SPT data only, Youd et al. (2002), Rauch and Martin (2000), Bardet et al. (2002), Zhang et al. (2012); one semi-empirical method for SPT data, Faris et al. (2006); and one empirical method for CPT data, Zhang et al. (2004).

Several deterministic methods use Multiple Linear Regression (MLR) analysis to create empirical equations that estimate future behavior based on observations from previous earthquakes. The assumption that a true but unknown relationship exists between measured displacement and site specific or seismic characteristics drives selection of certain parameters which are statistically shown to best approximate the observed movement. Typically, many different parameters are considered, each one evaluated on the availability and quality of data from existing case histories and statistical independence when regressed. One parameter is selected at a time which appears to best reduce error between predicted and observed measurements, and the process is repeated until a consensus is reached on a set that together maximize the coefficient of determination, r^2. More realistic and easily estimated parameters might be selected despite a slightly lower r^2.

2.2.1 Empirical SPT Methods

Several empirical SPT methods are evaluated, including Youd et al. (2002), Rauch and Martin (2000), Bardet et al. (2002), and Zhang et al. (2012).

2.2.1.1 Youd, Hansen, and Bartlett (2002)

Based off an earlier version published by Bartlett and Youd in 1995, this revision offers a simplified technique for estimating ground displacement from liquefaction-induced lateral spreading, which has gained widespread popularity for predictive purposes in current practice. The 82.6% R^2 of the original Bartlett and Youd (1992) method increased to 83.6% for the Youd et al. (2002) model. The revision included additional datasets, corrected some errors, and adjusted the general form slightly. Specifically, the addition of a log function improves predictions for gravels and an added constant to the distance term prevents unrealistically large displacements according to the current case history database.

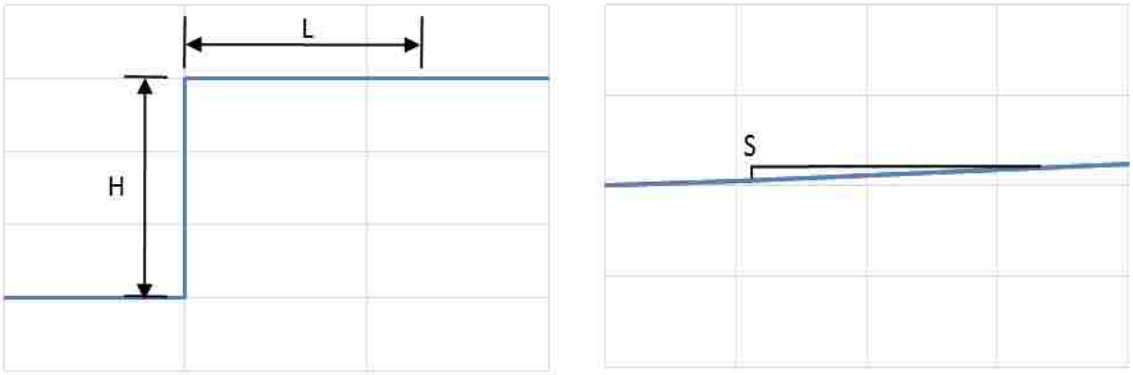

Figure 3. Idealized schematic of Youd et al. (2002) free face and gentle slope scenarios.

The authors found a strong correlation between ground topography and displacement, and developed an equation for two categories of lateral spread displacement: (1) movement towards a free face and (2) movement down a gentle slope where no free face is present. The classic cases of a free face condition and a gentle slope condition are shown in Figure 3. The general form of the revised MLR equation for the free-face condition is:

$$\log(D_H) = -16.713 + 1.532M - 1.406\log(R^*) - 0.012 + 0.592\log(W) + 0.540\log(T_{15}) + 3.413\log(100 - F_{15}) - 0.795\log(D50_{15} + 0.1\,mm) \quad (2\text{-}21)$$

where,

$$R^* = R + R_o, \text{ and} \quad (2\text{-}22)$$

$$R_o = 10^{(0.89M - 5.64)} \quad (2\text{-}23)$$

Using the same definitions of R^* and R_0, the general form of the revised MLR equation for the gentle slope condition is:

$$\log(D_H) = -16.213 + 1.532M - 1.406\log(R^*) - 0.012R + 0.338\log(S) + 0.540\log(T_{15}) + 3.413\log(100 - F_{15}) - 0.795\log(D50_{15} + 0.1\,mm) \quad (2\text{-}24)$$

D_H is the estimated lateral ground displacement, in meters; M is the moment magnitude of the earthquake; R is the nearest horizontal or map distance from the site to the seismic energy source (in kilometers), R_0 is a distance constant that is a function of M; R^* is the modified source distance; T_{15} is the cumulative thickness of saturated layers with corrected blow counts, $(N_1)_{60}$, less than 15 blow/ft, in meters; F_{15} is the average fines content (fraction of sediment sample passing a No. 200 sieve) for materials included within T_{15}, in percent; $D50_{15}$ is the average mean grain size for materials within T_{15}, in millimeters; W is the free-face ratio defined as the height (H) of the free face divided by the distance (L) from the base of the free-face to the site, in percent. Though not included in the equation, Z_T, the depth to the top of the liquefiable layer T_{15}, is included as a limit to prevent application to deeper liquefiable layers than represented in the database. A

liquefaction analysis must be applied previously, as these equations are only considered valid in locations that have already been determined as likely to liquefy.

The liquefiable layer is considered when determining the base of the free face. When calculating the free face ratio W, H is considered the horizontal distance from the site to the toe of the exposed liquefiable layer, and L the vertical distance from the site to the toe of the liquefiable layer. Dr. Leslie Youd described the base of the free face as where the base of the liquefiable layer sees daylight (personal communication, Feb. 26, 2014). Figure 4 shows a schematic for identifying the base of a free face for the Youd et al. (2002) equation.

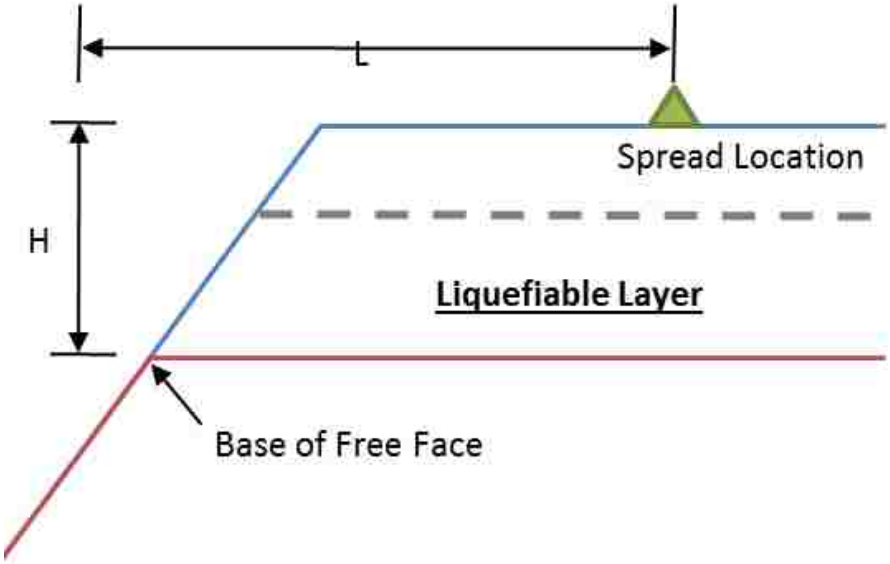

Figure 4. Free face base for the Youd et al. (2002) lateral spread method.

The applicability of these equations is limited by the variability of the data used to develop the equation. Youd et al. (2001) recommend caution when working with W falls outside of the 1% to 20% range, as displacements are generally small when W < 1% and slumping or flow failure may occur near a free face with W > 20%. Extrapolation limits recommended for each parameter due to sufficient representation in the case history database are shown in Table 1. R_f in Ambraseys'

(1988) equation, shown as Equation (2-25) defines the upper limit of R. Acceptable ranges for $D50_{15}$ and F_{15} are shown in Figure 5.

Table 1. Acceptable Range of Parameters for Youd et al. (2002) Lateral Spread Equations

Parameter	Min	Max
M_w	6	8
R or R_{eq} (km)	0.5	Ambraseys (1988)
W (%)	1	20
S (%)	1	5
T_{15} (m)	1	15
Z_T	1	15

Where Ambraseys (1988) equation is:.

$$M_W = 0.18 + 9.2 * 10^{-8} * R_f + 0.9 \log R_f \qquad (2\text{-}25)$$

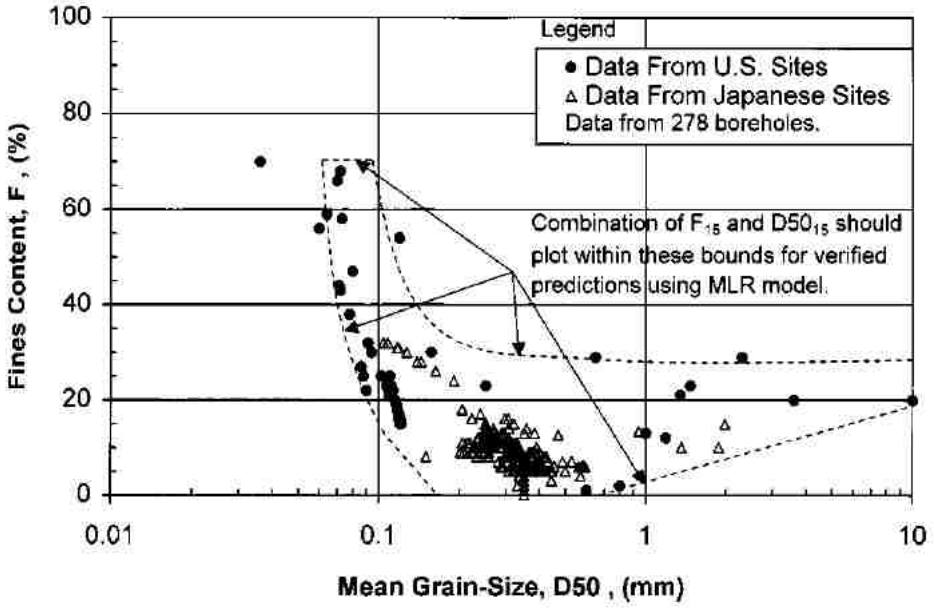

Figure 5. The acceptable range of F_{15} and $D50_{15}$ for Youd et al. (2002) lateral spread equations.

The Bartlett and Youd database from the 1995 version as well as the Youd, Hansen, and Bartlett database from the 2002 revisions consists exclusively of earthquake sites within Japan and the United States. The 2002 revision attempts to account for variations in ground motions among different regions by incorporating a chart that uses three different attenuation relations, correlating average Peak Ground Acceleration (PGA) and earthquake magnitude to an equivalent source distance, R_{eq} which can be used in place of R. This chart, as shown in Figure 6, includes attenuation relations from: Abrahamson and Silva (1997) intended for shallow crustal earthquakes in active tectonic regions; Boore et al. (1997) intended for shallow earthquakes in western North America; and Campbell (1997) intended for worldwide earthquakes with a distance to seismogenic rupture less than 60 km. Locations where boundary effects may have impeded displacement were not included in the 2002 database.

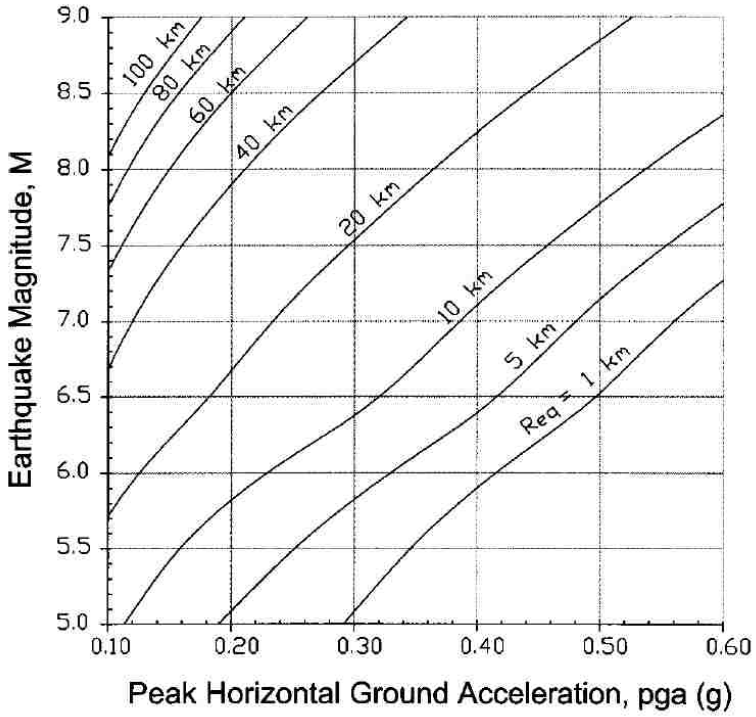

Figure 6. Equivalent distance Req to replace R in Youd et al. (2002) lateral spread equations.

2.2.1.2 Rauch and Martin (2000)

Rauch and Martin generated the Empirical Prediction of Liquefaction-induced Lateral Spreading (EPOLLS) model which is similarly regressed using MLR like the Youd et al. (2002) model but attempts to compensate for varying levels of available information. EPOLLS models consist of three different versions:

- Regional-EPOLLS, requiring only general seismic source and local intensity data
- Site-EPOLLS, requiring all Regional-EPOLLS data plus site specific data like topography and slide area dimensions
- Geotechnical-EPOLLS, requiring all Site-EPOLLS data plus subsurface data from field tests.

By creating models that only include more generalized and easily obtainable information, Rauch and Martin allow the user to enter the model even if there are gaps in collected data. This also allows more sites to be used in developing the Regional and Site EPOLLS models, as less information is required for the site to be included the database for each model. The EPOLLS models are also intended to predict average magnitude of displacement across a general region, unlike Youd et al. (2002) which predicts at a specific site. When compiling the case history database, individual displacement vectors were grouped to create one displacement case study as long as the general direction of the contiguous soil mass remained the same, ignoring slight variations in direction due to local topography and geology. One average horizontal displacement value was then calculated for the whole case study site using individual vectors. Grouping displacements decreases the degree of dependency, where otherwise a few sites with several displacement measurements might become disproportionally represented. This is different from

the Youd et al. (2002) method which can use multiple displacement vectors from the same slide mass.

Lateral spread is limited to mostly horizontal displacement on gentle ground slopes of 5% or less. Sites with embankment slumps, failed retaining walls, and sites with rock-filled dikes or large concrete structures were excluded.

Similar to Youd et al. (2002), all three models require liquefaction assessments to qualify the site prior to entering the EPOLLS models. Equations were similarly regressed until error was minimized, with an emphasis on including parameters which could be easily obtained with reasonable accuracy. Equation (2-26) predicts average horizontal displacement for the Geotechnical-EPOLLS model. Table 2 from Rauch and Martin (2000) defines used parameters.

Rauch and Martin provide the option to use either S_{top} for a gentle slope scenario, H_{face} for a free face scenario, or both for a scenario in which both a free face and gentle slope are present.

Limits are provided in Table 3 for each parameter as well as predicted displacement for the Geotechnical-EPOLLS model. Since the data used to develop their models is primarily from Japan, California, and Alaska, Rauch and Martin acknowledge that reliability of predictions outside of these areas is unknown.

$$Avg_{Horz} = \begin{pmatrix} 0.613M_w - 0.0139R_f - 2.42A_{max} - 0.0114T_d \\ +0.000523L_{slide} + 0.0423S_{top} \\ +0.0313H_{face} + 0.0506Z_{FSmin} - 0.0861Z_{liq} - 2.49 \end{pmatrix}^2 \quad (2\text{-}26)$$
$$+0.124$$

Table 2. Definition of Variables Used in EPOLLS Model from Rauch and Martin (2000).

Parameter	Definition
M_w	Moment magnitude of earthquake
R_f (km)	Shortest horizontal distance from site to surface projection of fault rupture or zone of seismic energy release
A_{max} (g)	Horizontal acceleration at ground surface of site that would occur in absence of excess pore pressures or liquefaction generated by earthquake
T_d (s)	Duration of strong earthquake motions at site, defined as time between first and last occurrences of surface acceleration ≥ 0.05 g
L_{slide} (m)	Maximum horizontal length from head to toe of lateral spread in prevailing direction of movement
S_{top} (%)	Average slope across surface of lateral spread, measured as change in elevation over distance from head to toe • When free face is present, surface slope is measured from head of slide to crest of free face • Negative S_{top} indicates surface that slopes in direction opposite to prevailing direction of movement
H_{face} (m)	Height of free face, measured vertically from toe to crest of free face • H_{face} = 0 when no free face present • When free face is stream bank, measure H_{face} from bottom of stream and do not include height of narrow levees along top
Z_{FSmin} (m)	Average depth to minimum factor of safety in potentially liquefiable soil
Z_{liq} (m)	Average depth to top of liquefied soil
Avg_Horiz (m)	Average horizontal displacement predicted, limited to Geotechnical-EPOLLS here

Table 3. EPOLLS Model Limits

Parameter	Minimum Value	Maximum Value
M_w	6.5	9.2
R_f (km)	0	119
A_{max} (g)	0.16	0.52
T_d (s)	4	88
L_{slide} (m)	20	1360
S_{top} (%)	-0.7	5.2
H_{face} (m)	0	9
Z_{FSmin} (m)	2.4	12.4
Z_{liq} (m)	0.9	7.3
Avg_Horiz	0.23	4.29

2.2.1.3 Bardet, Tobita, Mace, and Hu (2002)

Bardet et al. (2002) provide a more simplified version of the Bartlett and Youd (1992) model intended to provide general estimates of lateral spread displacements over large areas, as would be necessary for a risk assessment across spatially distributed lifeline networks.

Since the geotechnical parameters D_{50} and F_{15} are the most difficult to estimate over large areas, Bardet et al. (2002) dropped these terms, using only a subset of four parameters from the original Bartlett and Youd (1992) equation. The simplified general equation was regressed using the same case history data base and MLR regression techniques as Bartlett and Youd (1992).

Additionally, the four parameter general equations was regressed using a subset of the original case history database which included only cases with measured displacements less than 2 m. As the ability of engineering practice to limit damage to structures that experience displacements greater than 2 m is difficult, this second case history data base was intended to improve estimates for more common applications.

The general equation is shown in (2-27) with coefficients in Table 4. Data Set A consists of all case histories in the original Bartlett and Youd (1992) database, with Data Set B the case histories with less than 2 m of displacement. Note that the Bardet et al. (2002) method limits R to 0.2 – 100 km. For other limits, refer to Bardet et al. (2002).

$$\log(D + 0.01) = \mathrm{b}_0 + \mathrm{b}_{off} + \mathrm{b}_1 \mathrm{M} + \mathrm{b}_2 \log(R) + \mathrm{b}_3 R + \mathrm{b}_4 \log(W) + \mathrm{b}_5 \log(S) + \mathrm{b}_6 (T_{15}) \; . \tag{2-27}$$

Table 4. Regressed Coefficients for Bardet et al. (2002) Model

Coefficients	Data Set A	Data Set B
b_0	-6.815	-6.747
b_{off}	-0.465	-0.162
b_1	1.017	1.001
b_2	-0.278	-0.289
b_3	-0.026	-0.021
b_4	0.497	0.090
b_5	0.454	0.203
b_6	0.558	0.289
R^2 adjusted	64.25%	64.27%
Data points	467	213

Though this model calls for the epicentral distance, Bardet et al. (2002) also define the epicentral distance as "the nearest horizontal distance to seismic energy source or fault rupture" which is almost identical to the Youd et al. (2002) distance R definition, "the horizontal or mapped distance from the site in question to the nearest bound of the seismic energy source". Bardet et al. (2002) reports values from the Youd LD database as "epicentral distances", even though distance values are identical to the database values reported from Dr. Youd's website, which are Joyner-Boore distances. It is therefore determined that the Bardet et al. (2002) model is developed from the same Joyner-Boore distances used by Youd et al. (2002), despite the confusing use of the term epicentral.

In addition to the distance R, Moment magnitude M, liquefiable layer thickness T_{15}, free-face ratio W, and ground surface slope S are all defined the same as Bartlett and Youd (1992). The free face case and slope case are considered separately. R values outside of 0.2 km – 100 km are not recommended, and low values of R with high values of M fall into an area of "No Data" shown in Figure 7.

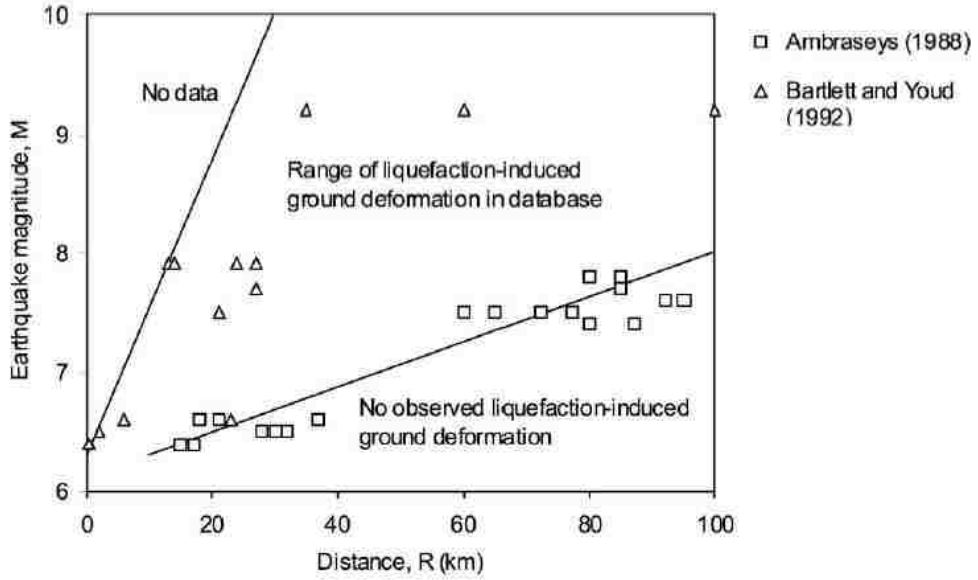

Figure 7. Range of available data from Bartlett and Youd (1992) and Ambraseys (1988) databases.

The accuracy of the Bardet et al. (2002) model is significantly lower with an R^2 at 64%. Bardet et al. (2002) acknowledges the R^2 of the Bartlett and Youd (1992) model is higher when all six parameters are known but claims their model has a higher R^2 if average values of F_{15} = 13% and $D50_{15}$ = 0.292 mm are used.

2.2.1.4 Zhang, Changwei, Zhao, McVerry (2012)

The Zhang et al. (2012) model combines response spectral acceleration from local strong-motion attenuation models with the geotechnical parameters from the lateral displacement dataset on the Youd website, with the intention of increasing the applicability of the model in regions outside of the western United States and Japan. By replacing the source to site distance term with spectral displacement, the model can theoretically predict lateral spreading displacement anywhere local attenuation relations are sufficiently developed to estimate ground shaking.

Equations for the free-face case and gentle slope case are shown in equations (2-28) and (2-29), respectively.

Free-face case:

$$\log(D_H) = 1.8619\log(SD) + 0.608\log(W) + 0.0342T_{15} + 2.4643\log(100 - F_{15}) - 0.8382\log(D50_{15} + 0.1) - 3.4443 \quad (2\text{-}28)$$

Gentle slope case:

$$\log(D_H) = 1.8619\log(SD) + 0.4591\log(S) + 0.0197T_{15} + 2.4643\log(100 - F_{15}) - 0.8382\log(D50_{15} + 0.1) - 2.7096 \quad (2\text{-}29)$$

Parameters are defined as in Youd et al. (2002), with the exception of SD which is pseudo-spectral displacement in meters. SD is found by dividing the spectral acceleration obtained from a local strong-motion attenuation model at a period of 0.5s by $(4\pi)^2$. While the Alaska 1964 earthquake was not included in the database for this model as it did not appear to fit well with the other case histories, successful application to earthquakes in Turkey and New Zealand improves confidence in the Zhang et al. (2012) model.

2.2.2 Strain-Based Semi-Empirical Model: Faris, Seed, Kayen, Wu (2006)

The Faris et al. (2006) model is semi-empirical, combining knowledge from laboratory studies to case history field data. Correlations developed by Wu (2002) between cyclic simple shear obtained in the lab with SPT counts is used to estimate the Strain Potential Index(SPI), the limiting or maximum shear strain experienced due to cyclic loading in Figure 8. SPI is considered indicative of the deformation potential in liquefied soils, and can account for varying probability of displacement within a liquefiable layer as opposed to a uniform parameter such as T_{15} from

Youd et al. (2002) that weights the entire liquefiable layer evenly. Note that curves in Figure 8 are interpolated from extremely limited data with large CSR and small SPT values.

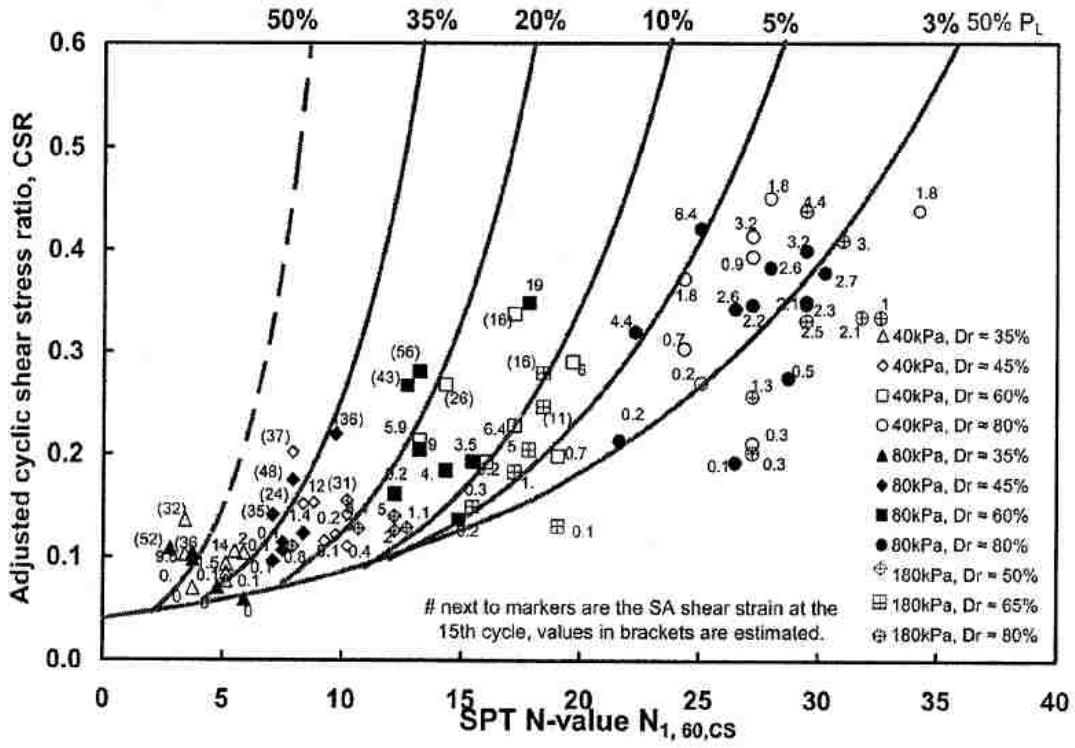

Figure 8. SPI as a function of N1,60,CS and adjusted CSR* for M_w=7.5 (Wu, 2002).

Using the Seed et al. (2003) liquefaction analysis method, SPT blow counts are corrected to $(N_1)_{60}$ and a CSR is obtained. Faris et al. (2006) then corrects SPT counts to a clean sand equivalent ($N_{1,60,CS}$) and CSR to equivalent cycles under a 7.5 magnitude earthquake (CSR*). Using curves based on Wu (2002) but interpolated to include a 75% SPI curve (Figure 9), SPI is obtained from normalized CSR and SPT values. Displacement Potential Index (DPI) is calculated by simply multiplying the SPI for each layer by the layer thickness. Maximum DPI (DPI_{max}) is the summation of the DPI for all liquefiable layers. A final deterministic equation (2-30) is then developed via a Bayesian probabilistic approach to predict H_{max}, the maximum displacement expected due to liquefaction-induced lateral spread. H_{max} and DPI_{max} both are defined in meters.

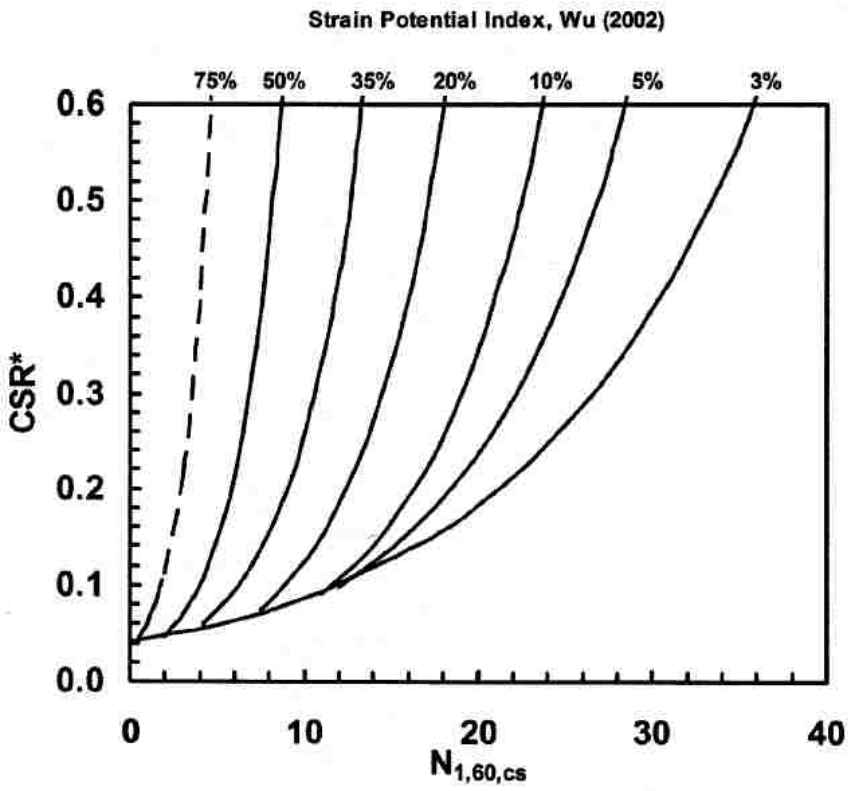

Figure 9. Modified SPI curves given N1,60,CS and adjusted CSR* for M_w=7.5 (Faris et al., 2006).

$$H_{max} = exp(1.0443 \ln(DPI_{max}) + 0.0046 \ln(\alpha) + 0.0029 M_W) \quad (2\text{-}30)$$

Where,

$$\alpha = \begin{cases} \dfrac{H}{0.25L} & for\ free-face\ cases \\ S & for\ sloping\ ground\ cases \\ \dfrac{H}{0.25L} + 0.01S & for\ combination\ cases \end{cases} \quad (2\text{-}31)$$

While DPI_{max} accounts for cyclic shear stress from the earthquake, α represents horizontal driving shear stress from the vertical effective stress of the soil. By defining α separately for a free face and sloping ground scenario, combination scenarios where both a free face and slope exist can be accounted for by applying both terms, as seen in the final definition of α in equation **(2-31)**. M_w is moment magnitude; S the average slope in percent of the ground surface across the entire length of the lateral spread; H the height of the free face in meters and L the distance from the toe of the free face to the site of the lateral spread, in meters.

Lateral spread here is defined similarly to the definition of Rauch and Martin (2000), where displacement of a mass of soil is considered one case history, instead of considering each displacement vector recorded separately, such as in Youd et al. (2002).

2.2.3 Empirical CPT Method: Zhang, Robertson, Brachman (2004)

Similar to Faris et al. (2006), this model presents a semi-empirical approach based on potential maximum cyclic shear strains. However, Zhang et al. (2004) is compatible for both SPT and CPT data. Relative density (D_r) from field data and the Youd et al. (2001) factor of safety against liquefaction (FS) is correlated with laboratory studies on clean sand from Ishihara and Yoshimine (1992) to estimate γ_{max}, the maximum amplitude of cyclic shear strains due to cyclic loading, as shown in Figure 10. A modified version of Meyerhof's (1957) correlation is suggested to obtain D_r from SPT data (2-32), and a modified version of Tatsuoka et al. (1990) with effective overburden stress correction from Robertson and Wride (1998) for CPT data (2-33).

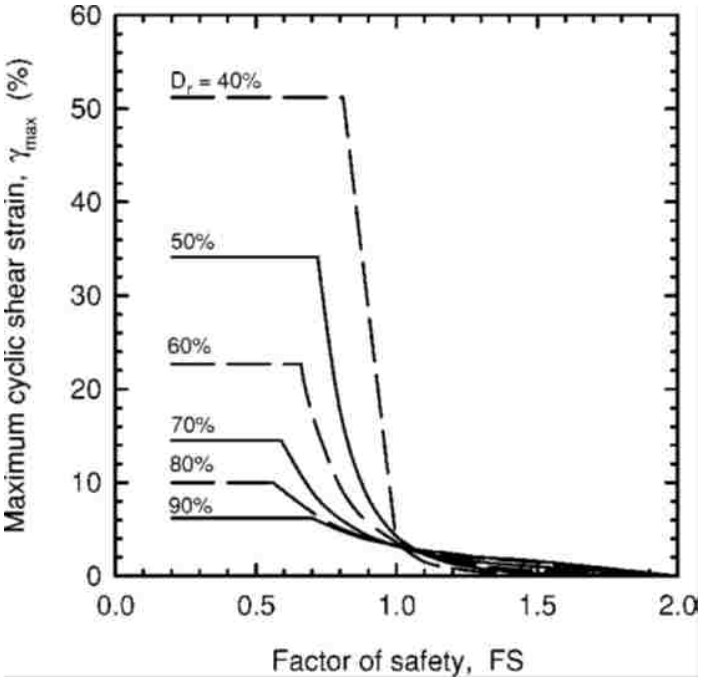

Figure 10. Max cyclic shear strain from D_r and FS against liquefaction (Zhang et al., 2004).

$$Dr = 14 * \sqrt{(N1)_{60}}, \text{ for } (N1)_{60} < 42 \quad (2\text{-}32)$$

$$Dr = -85 + 76\log(q_{C1N}), \text{ for } q_{C1N} \leq 200. \quad (2\text{-}33)$$

A Lateral displacement Index (LDI) is then determined from equation (2-34), which is then combined with geometric parameters to determine total displacement. Z_{max} is the maximum depth below all potential liquefiable layers with a FS below 2.0, with 23 m presented as a maximum within the verified range. Equation (2-35) is used to compute Lateral Displacement (LD) for a free face case, while equation (2-36) is used to calculate LD for a gentle slope case. The case of a free face with gentle slope is examined, but ultimately no equation is presented due to insufficient data. Relationships represented by these equations were fit by-eye rather than statistically with a

regression analysis. Only three earthquakes with CPT data qualified for the Zhang et al. (2004) study, and a need for additional CPT-based case histories is emphasized.

$$LDI = \int_0^{z_{max}} \gamma_{max} d_z \tag{2-34}$$

Free Face:

$$LD = 6\left(L/H\right)^{-0.8} LDI, \text{ for } 4 < L/H < 40 \tag{2-35}$$

Gentle Slope:

$$LD = (S + 0.2) * LDI, \text{ for } 0.2\% < S < 3.5\% \tag{2-36}$$

LD is in meters, L is the horizontal distance from the free face toe to the site in meters, H is the vertical distance from the free face toe to level ground in meters, and S is ground slope in percent.

3 LO ROJAS CASE STUDY

The Lo Rojas Pier and the Granelero Pier are examined as a part of this study, as shown in Figure 11. The North Pier and South Pier were studied in a similar study by Tryon (2014). The Lo Rojas pier experienced the most displacement, totaling approximately 2.85 m; the North Pier experienced about 1.5 m of displacement; the South Pier experienced 0.5 m of displacement; and finally, no displacement was observed at the Grandelero pier.

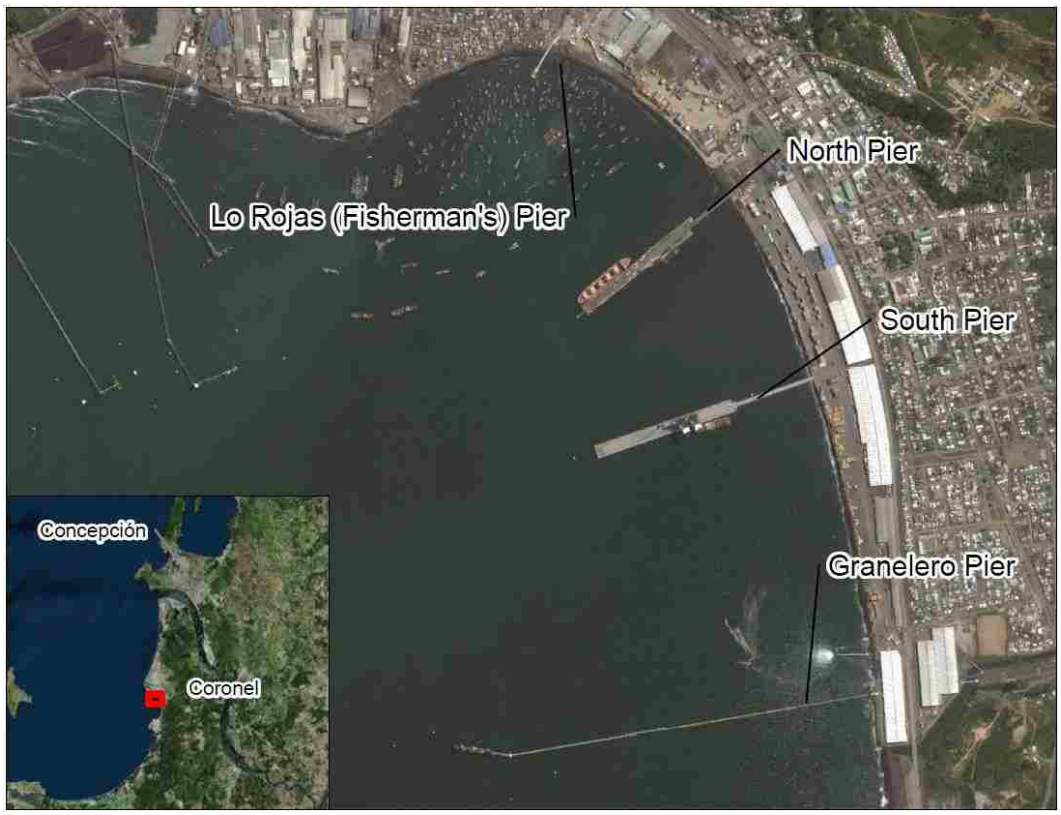

Figure 11. Port Coronel pier locations.

This behavior can be partially explained by the increasing density of the soil moving south from the northernmost Lo Rojas pier to the southernmost Granelero pier, as shown by comparing of SPT blow counts in Figure 11. Corrected cone tip resistance is also compared in Figure 13.

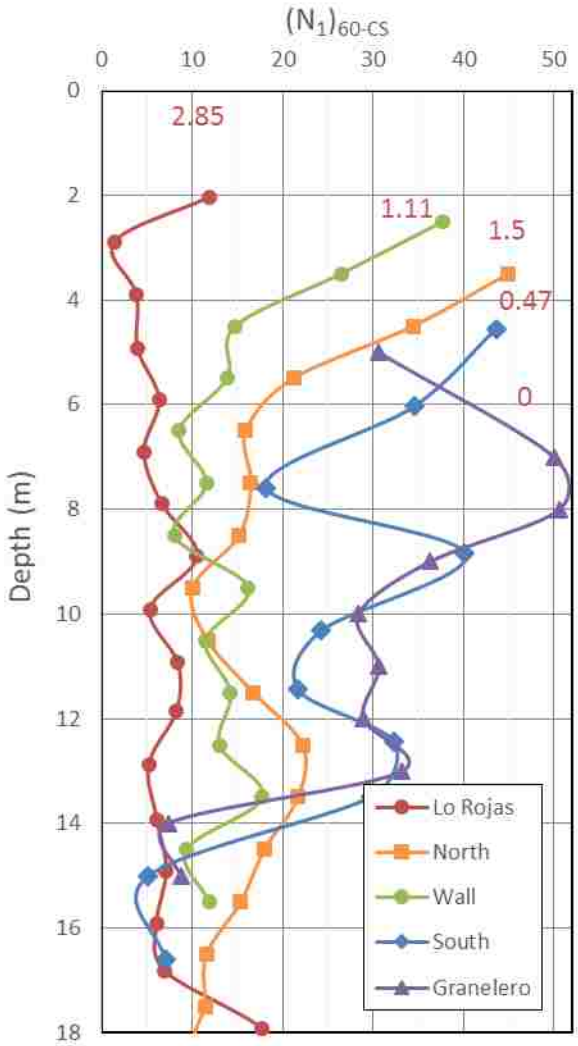

Figure 12. SPT blow counts versus depth for five locations in Port Coronel.

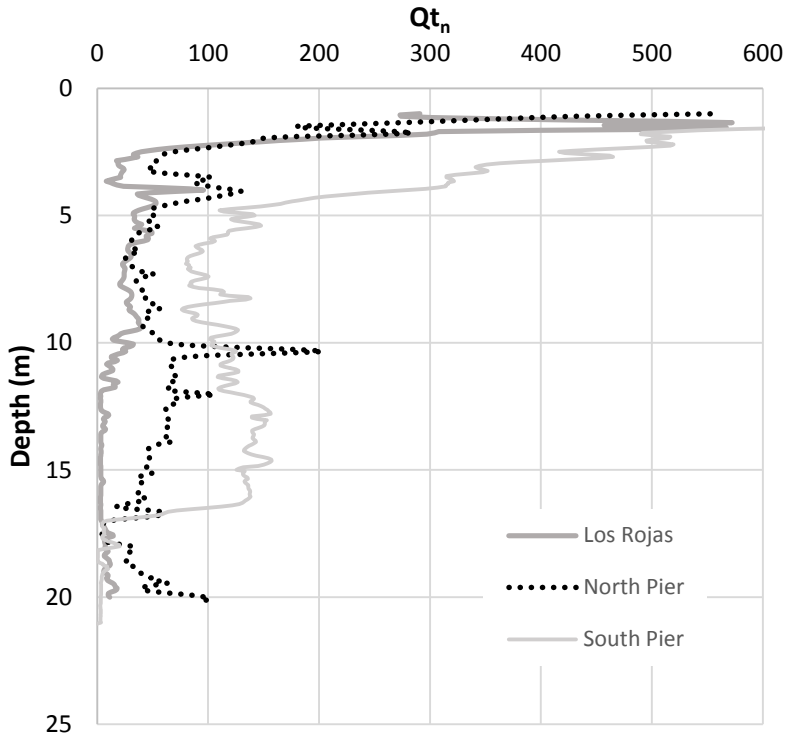

Figure 13. Comparison of corrected cone tip resistance versus depth (Tryon, 2014).

Significant damage occurred to the Lo Rojas or Fisherman's pier during the 2010 Maule, Chile earthquake as described in the Bray et al. (2010) Chile GEER report. As part of the GEER reconnaissance investigation in March of 2010, Rollins, Mylonakis, and Assimaki documented damage and evidence of lateral spreads via pavement cracks.

3.1 Site Layout and Lateral Spread Characteristics

Figure 14 shows damage to the pile supports of the pier, which was compressed at the seaward end and pulled apart at the landside end. A gap of 0.5 to 1.1m was created towards the landside end, and an upwards movement and lack of gaps at the seaward end indicates compression. Additionally, a battered pile pulled out of one of the pile caps towards the landside

end, while the remaining battered pile appears to have moved 0.8 m down and 0.3 m horizontally towards land, missing collision with the pulled out pile by less than 10 cm, as shown in Figure 15 (Bray et al., 2010).

Lateral spreading was evident in pavement cracks behind a retaining wall just east of the pier, as shown in Figure 16. Recorded displacements were summed along a line running perpendicular to the cracks, extending 300 ft or 94.1 m behind the wall. Cracks were measured in several increments along this line, allowing for multiple measurements as show in Figure 17. Note that most of the lateral displacement is observed between 0 and 20 m behind the retaining wall although cracks indicated displacement to a distance of over 80 m behind the wall. The locations of the lateral spread line, SPT and CPT tests are shown in Figure 18.

Figure 14. Damages to Lo Rojas pier in Port Coronel due to lateral spreading.

Figure 15. Lo Rojas pier pile cap with battered piles showing pull out of trailing row piles.

Figure 16. Pavement cracks near Fisherman's (Lo Rojas) pier.

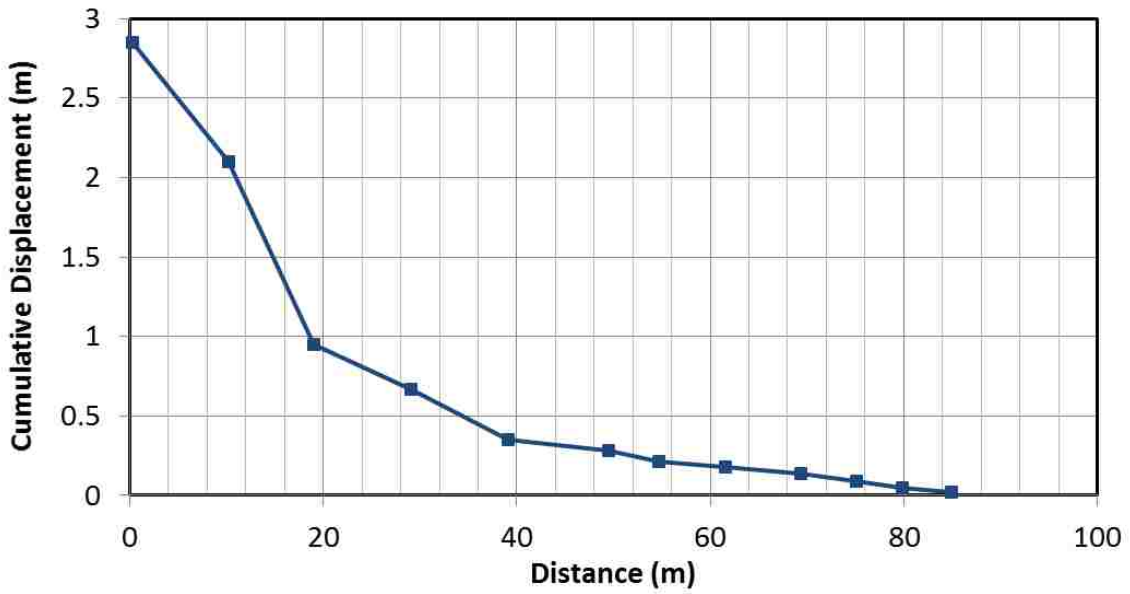

Figure 17. Cumulative horizontal displacement V_S. distance from wall face due to lateral spreading on Lo Rojas pier in Port Coronel, Chile (this study).

Figure 18. Lateral spread line, SPT and CPT locations near Lo Rojas pier and lateral spread line.

The original pier was retrofitted and a new larger pier constructed next to the original as shown in Figure 18. Several forms of data were collected prior to construction of the second pier, including topographic bathymetry data as well as two off shore geotechnical borings. Unfortunately, both borings and the bathymetry data collected fall around the new pier site about 100 m from the measured lateral spread line. As part of this study, additional data was collected in 2014, which included SPT, CPT and topographic data. All the available data is presented in this chapter.

3.2 Seismic Parameters

As indicated previously, the 2010 Maule Chile earthquake was assigned a moment magnitude (M_w) of 8.8 by the USGS (2015). A peak ground acceleration (PGA) of 0.4 g was recorded in Concepción at the nearest seismograph station to the site (Sáez et al., 2013). The Chilean strong ground motion attenuation relations by Contreras & Boroschek predict an acceleration of 0.44 g, which is similar enough that only the actual measured value of 0.40 g is applied for all liquefaction and lateral spread methods. The Contreras & Boroschek attenuation relation is described in more detail in section 3.6.4. The majority of energy was released during the first 90 seconds of shaking, but smaller accelerations continued over the next minute, resulting in reported durations from 90 to 150 seconds among various fault rupture models. Table 5 summarizes the fault rupture durations obtained by a number of researchers.

Defining the source of energy release can be challenging for subduction zone earthquakes. Energy is generally released somewhere along the plane where two tectonic plates slide past each other. The horizontal distance to the source of seismic energy release is relatively simple to define for slip-strike faults, since the slip plane is mostly vertical. However, this becomes more complicated for subduction zones because the fault plane is often moving at an acute angle

underneath the overlying plate as shown in Figure 19. Therefore, the horizontal distance to the zone of energy release might be much less than the horizontal distance to the surface manifestation of the fault (trench) as illustrated in Figure 19.

Table 5. Summary of Fault Rupture Durations

Investigator	Fault Rupture Duration (seconds)
Ruiz et al. 2002	90
Delouis, Nocquet and Vallée 2010	110
Lay, et al. 2010	130 - 150
Sladen n.d.	150
Average Used in this Study	120

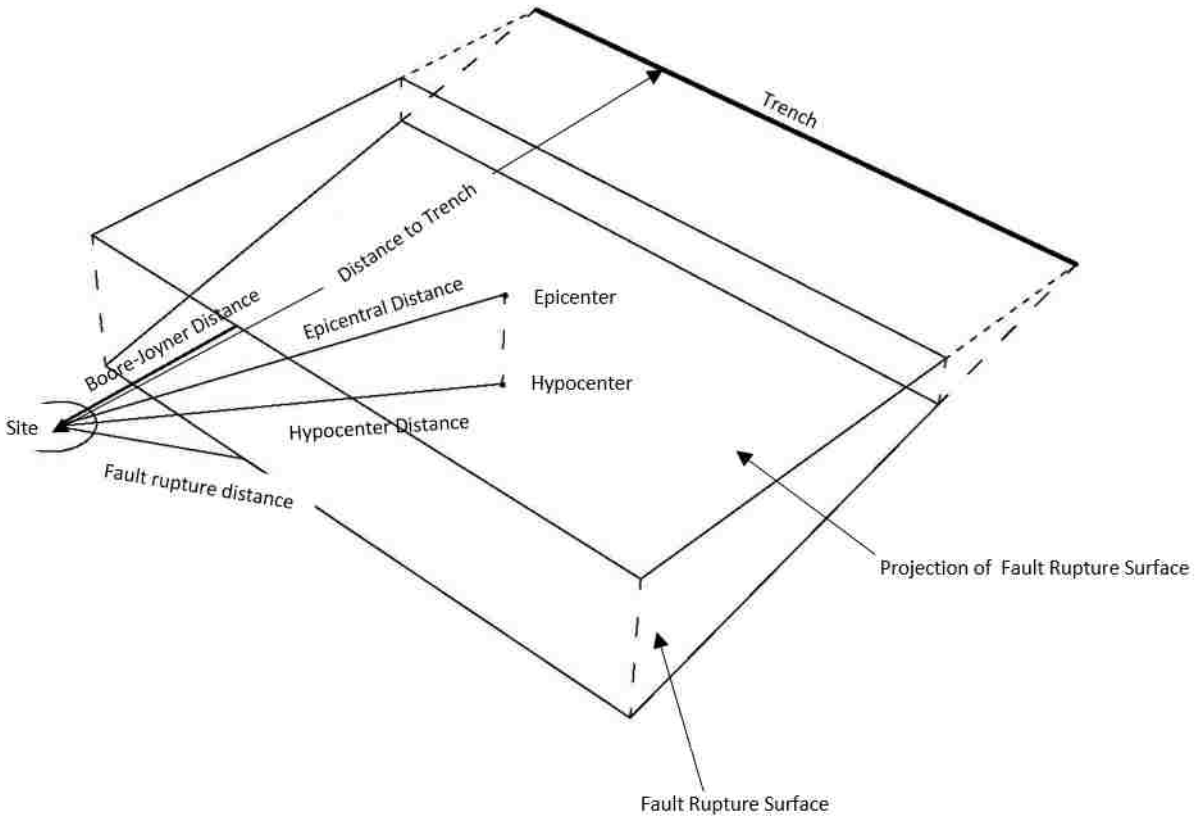

Figure 19. Several methods of defining seismic source to site distances (Tryon, 2014).

Distance to the zone of energy release is an important parameter that is discussed along with individual author interpretations for each method in the lateral spread results section (Section 3.6). Figure 19 displays several common methods of measurement. For most liquefaction and lateral spread applications, authors call for the Joyner-Boore Distance, which for the Coronel, Chile sites is zero since the fault rupture actually extends below the lateral spread site.

The fault rupture distance is another important parameter. In this case, since the fault extends below the site, the fault rupture distance is the depth to the fault below the site. Rupture depth is reported for a number of epicentral locations for the Maule 2010 earthquake, each epicenter representing asperities that released significant amounts of energy at different locations. The USGS relies on far-field stations, the SSN on short-period seismological stations, and Vigny et al. (2001) relied on continuous GPS data that identified two distinct ground pulses. Delouis et al. (2010) identified two areas of large slip indicating the asperities, as shown in red in Figure 20. The hatched areas show the rupture surface for the 1960 south Chile – Valdivia earthquake and the 1985 Central Chile – Valparaiso earthquake, highlighting the large amounts of slip that occurred in the gap between the previous ruptures. There are multiple published epicenters from each source due to updates as new near source data became available. Several focal depths as reported by Tryon (2014) from commonly published epicenters are shown in Table 6, and are used to approximate the fault rupture distance.

Table 6. Epicenter Locations and Depths for the 2010 Maule, Chile Earthquake (Tryon, 2014)

Source	References	Latitude	Longitude	Depth
USGS-Original Epicenter	(U.S. Geological Survey, 2013) (Lay, et al., 2010)	35.909 S	72.733 W	35.0 km
	(Sladen, n.d.)	35.846 S	72.719 W	35.0 km
	(Ruiz, et al., 2012)	35.83 S	72.66 W	35.0 km
USGS-Updated Epicenter	(U.S. Geological Survey, 2014), (Ruiz, et al., 2012)	36.122 S	72.898 W	22.9 km
SSN-Original Epicenter	(Ruiz, et al., 2012)	36.25 S	72.96 W	47.4 km
	(Delouis, Nocquet, & Vallée, 2010)	36.208 S	72.96 W	32 km
SSN-Updated Epicenter	(Conteras & Boroschek, 2012), (Ruiz, et al., 2012)	36.29 S	73.24 W	30.1 km
Vigny et al. (2011) Epicenter	(Ruiz, et al., 2012)	36.41 S	73.18 W	26.0 km
Ruiz et al. (2012) Asperity 1	(Ruiz, et al., 2012)	35.80 S	72.90 W	25.0 km
Ruiz et al. (2012) Asperity 2	(Ruiz, et al., 2012)	34.90 S	72.50 W	25.0 km
Delouis (2010) Asperities	(Delouis, Nocquet, & Vallée, 2010)	See Figure 20		

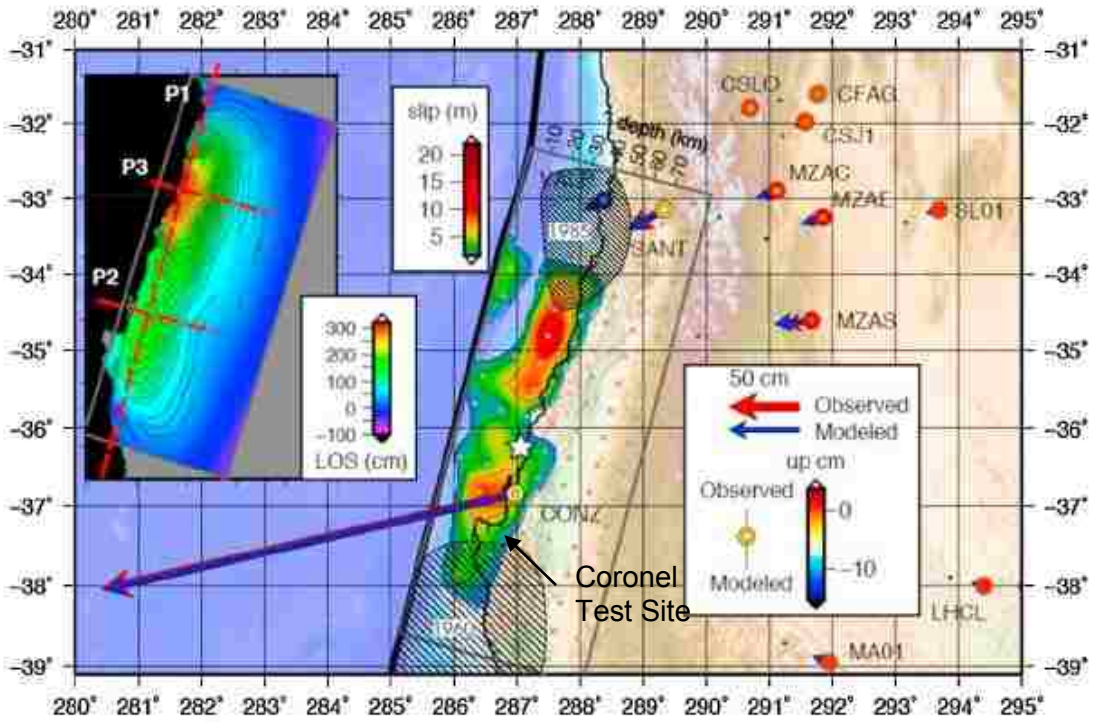

Figure 20. Location of rupture model and slip projected onto the earth surface (Delouis et al., 2010).

3.3 Cross-section Profile Development

One key component in evaluating the potential for a lateral spread is an accurate understanding of the geometry of the cross-section through the slope. Two main high resolution topographic data sets are available around the lateral spread line: (1) survey points collected in July of 2010 for the Ministry of Public Works of the Government of Chile prior to construction of the new Fisherman's pier; and (2) survey points collected during the field investigations as a part of this study in April 2014. During the April 2014 investigation a conventional survey level was used to define the ground surface elevations along the lateral spread measurement line relative to the top of the seawall. In addition, the elevation of the seafloor was measured at selected intervals along the old and new piers to provide additional elevation data. The location of elevation data is shown in Figure 22 and Figure B - 1 of the appendix. Furthermore, relatively sparse topographic data points from Google Earth were used in assessing the slope geometry prior to the earthquake.

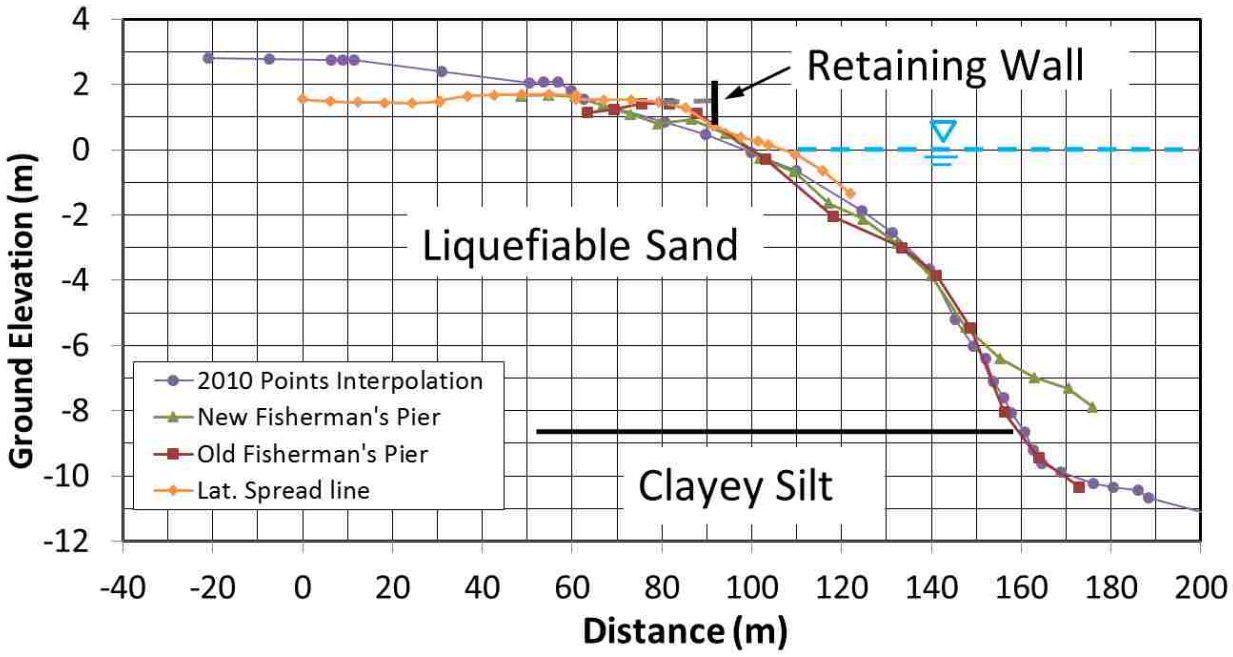

Figure 21. Three elevation profiles lines near the Lo Rojas pier.

Survey points collected by the Chilean government were used to synch the 2014 survey points to real elevations. The synched 2014 points did not match perfectly with 2010 elevation points, so the two sets are plotted separately. The profile created through an interpolation of 2010 data is drawn at a small angle from the top of the spread through the heavily surveyed area to minimize error from a lack of points at the base of the retention wall. The 2010 profile line and elevation profiles from 2014 points along each of the three piers are shown in Figure 10. Each line is shifted vertically up or down until a good fit is obtained among the separate profile lines, with the purpose of characterizing general slope trends of the area. A review of the profiles plotted in Figure 21 indicates that there is generally good agreement between the profiles obtained from the various sources. Typically, the slope is relatively mild (about 1.3 %) beyond a distance of 40 m back from sea level. At closer distances to the water level the slope steepens and has a parabolic shape with slopes ranging from 3.5% to 34%. The slope appears to flatten out at an elevation of about -9 m at a distance of about 40 m into the ocean.

The 2014 data along the lateral slope line indicates a negative slope between about 80 and 92 m from the retaining wall. However, this profile represents the post-failure geometry and the negative slope may be a result of slumping at the head of the slide or post-slide construction activities. To obtain an indication of the average slope in the vicinity of the slide, slopes from the general area perpendicular to the coast on either side of the lateral spread line were obtained from Google Earth for comparison (see Figure 23). Though Google earth uses coarser elevation data than the collected survey data, general trends can be observed as seen in Figure 24.

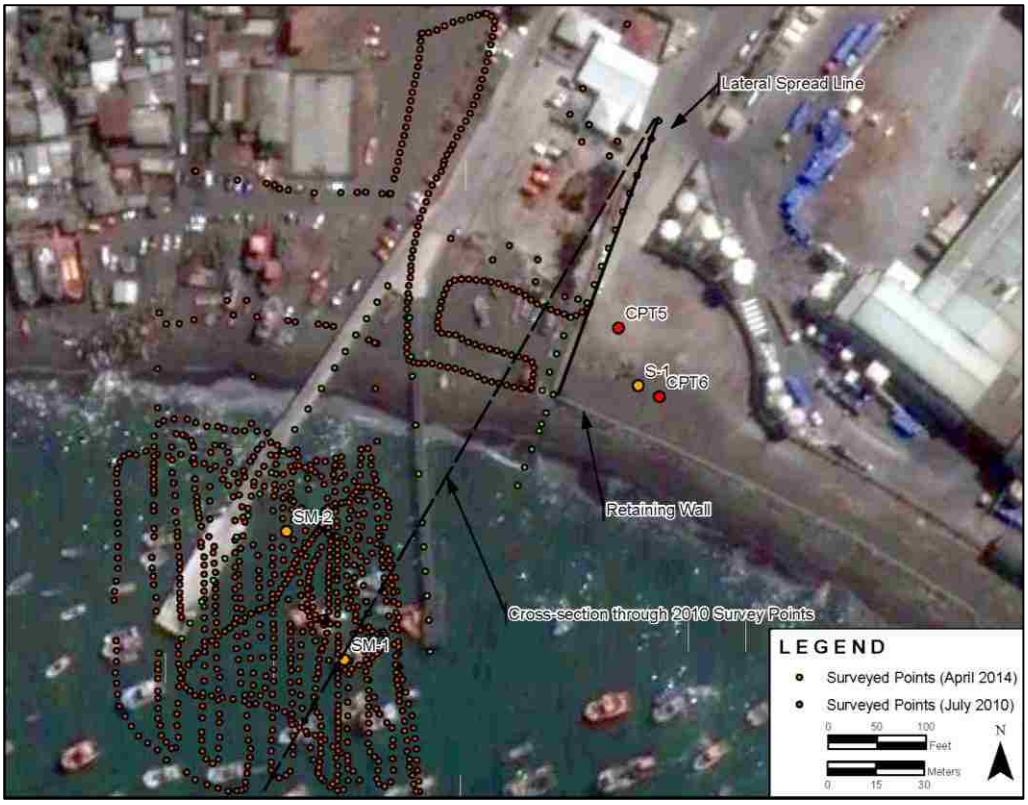

Figure 22. Surveyed data points near the Lo Rojas pier.

Figure 23. Elevation profile line locations in Google Earth; Lines are numbered from left to right.

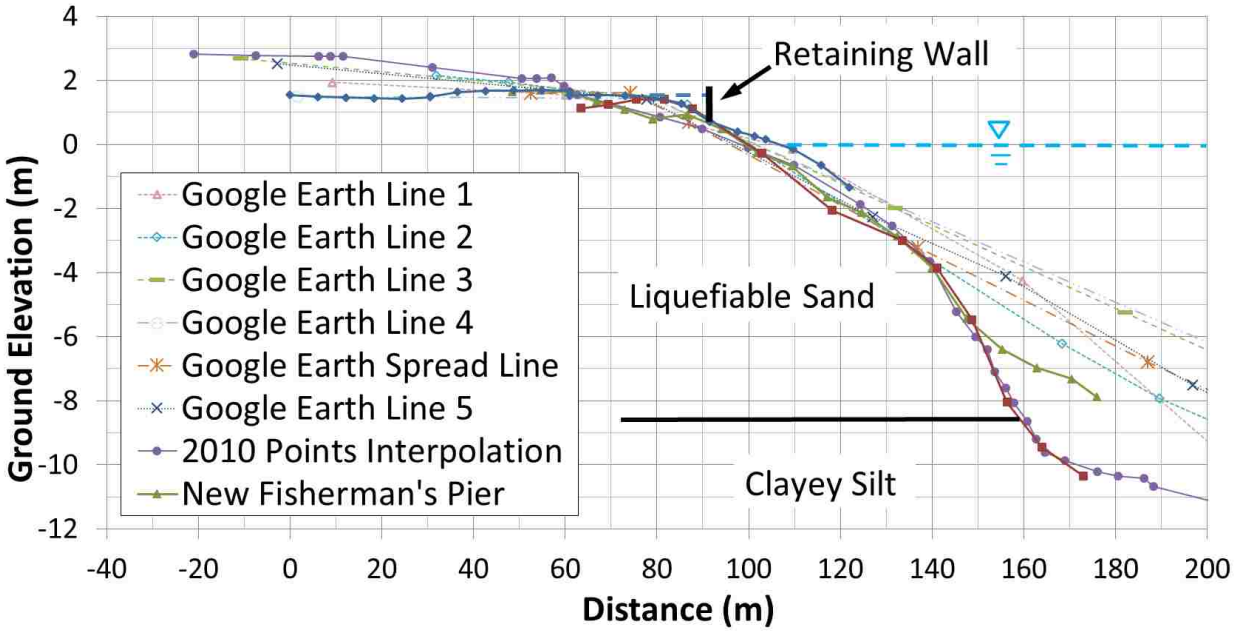

Figure 24. Google Earth elevation profiles compared with elevation profiles from survey data.

Along the lateral spread line, Google Earth also registers a slight decrease in elevation, but only positive slopes are measured on similar lines nearby. This finding suggests that the negative slope observed in the 2014 data is affected by the slope failure, and is not necessarily representative of the area that drove lateral spread.

Based on the available data, a composite topography line (Figure 25) created using 2010, 2014, and Google Earth data, which is considered best representation from existing data of the elevation governing ground displacement near the lateral spread line. The composite line follows data collected along the old Lo Rojas pier. For a to-scale version of the composite elevation profile, see Figure 27 and Figure 28.

Many of the lateral spread methods require classification of each site as either a free face or gentle slope case scenario, including Youd et al. (2002), Bardet et al. (2002), including Zhang et al. (2012). As can be seen from Figure 25, the elevation profile near the Lo Rojas pier is more

of an S-shaped curve instead an idealized free face or gentle slope, as shown in Figure 26. Since the actual geometry is somewhere in between these two cases, both scenarios are explored during lateral spread calculations.

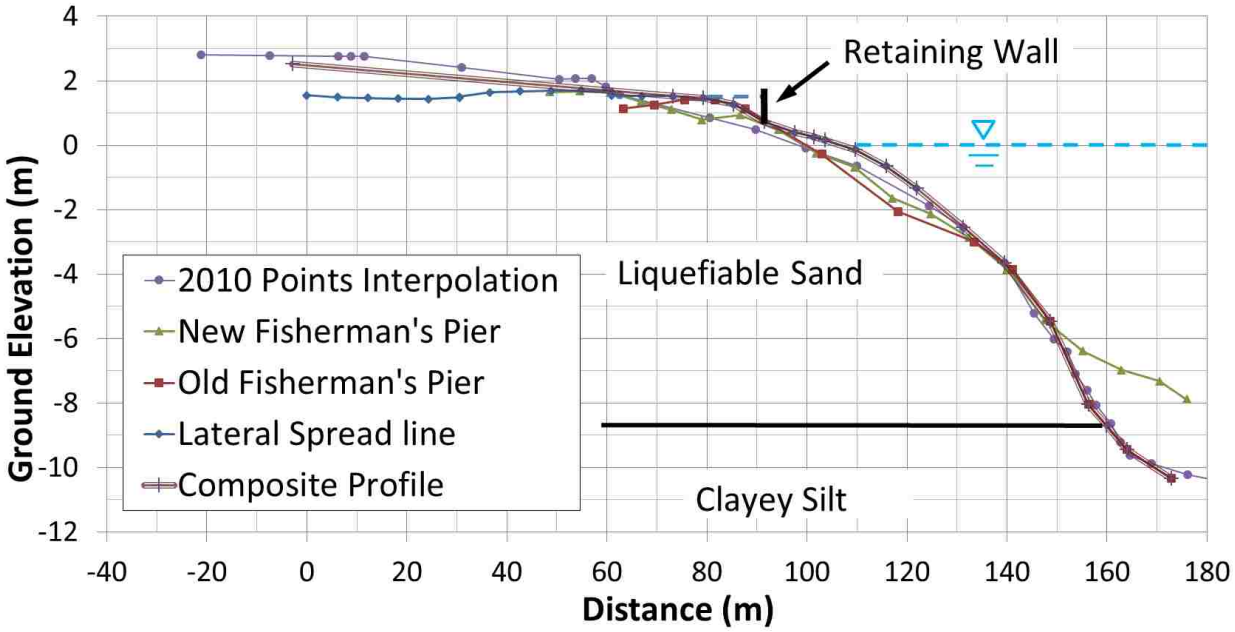

Figure 25. Composite elevation profile near Lo Rojas pier from existing data.

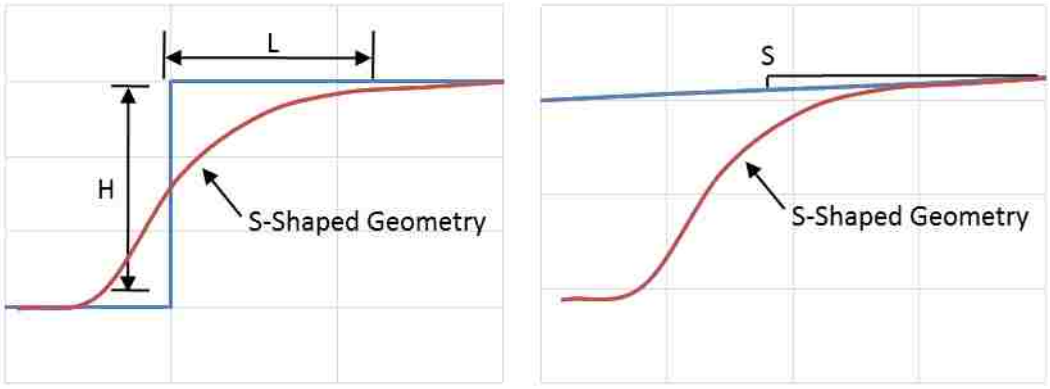

Figure 26. S-shaped curve compared to idealized schematics of Youd et al. (2002) free face and gentle slope scenarios.

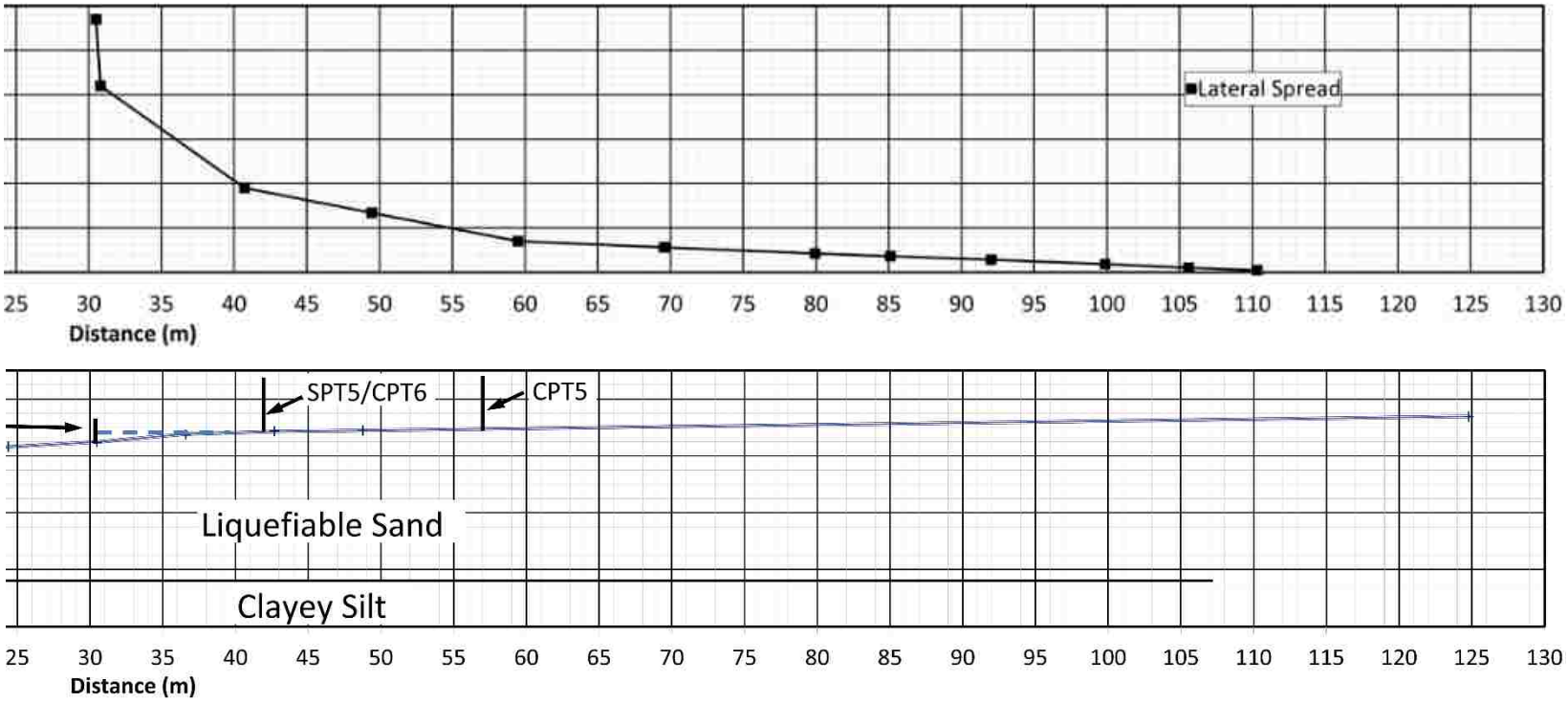

Figure 27. To-scale cross section of composite geometry compared with measured displacement.

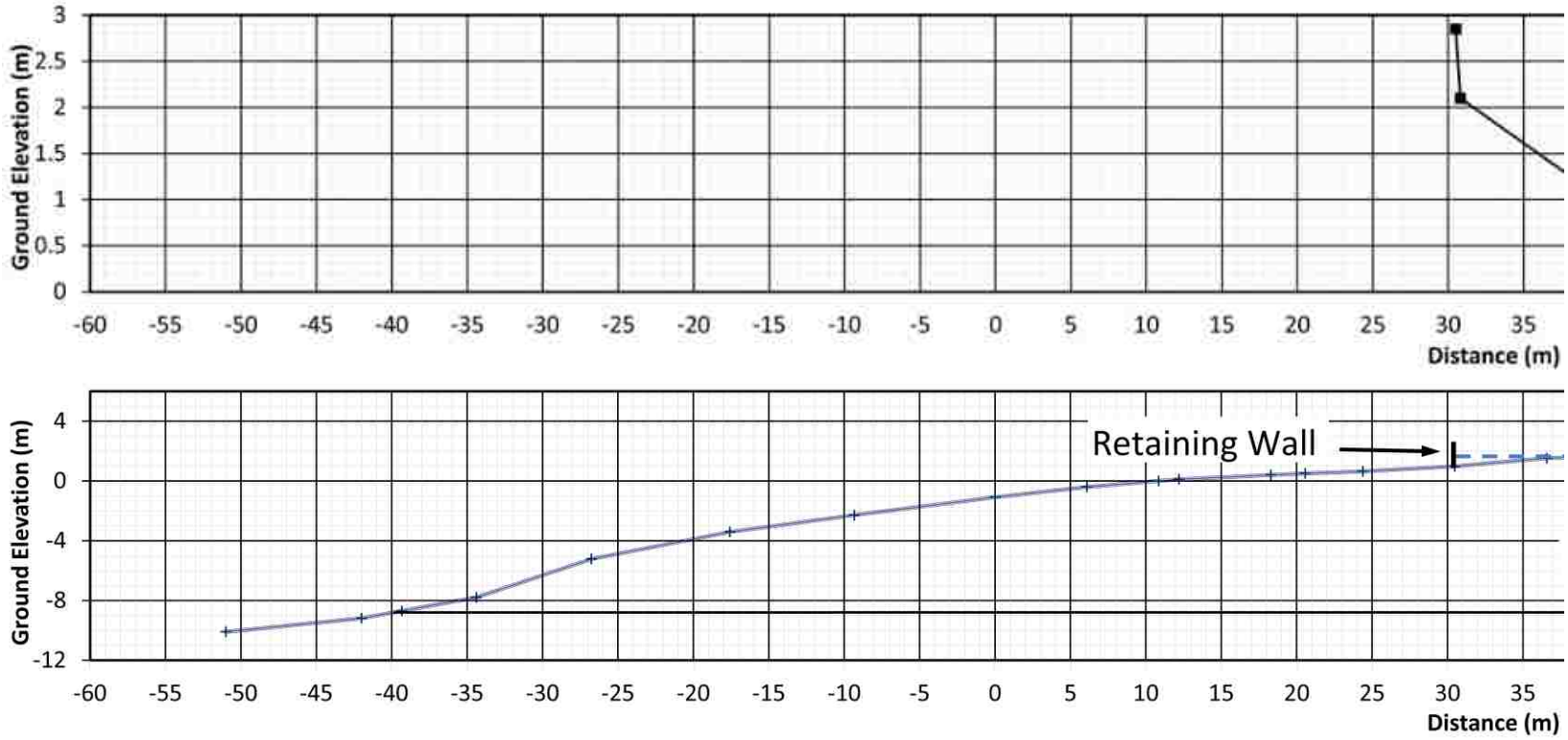

Figure 28. To-scale cross section of composite geometry compared with measured displacement (continued).

3.4 Geotechnical Site Characterization

Geotechnical data collected for the Lo Rojas pier includes, SPT borings, CPT soundings, ground water elevation data, and V_S measurements.

3.4.1 SPT Borings

Records from a total of three SPT borings in the vicinity of the Lo Rojas pier are available. Boring locations and data are shown in Figure 29 along with approximations of the ground surface and estimated liquefiable layer boundary. Test holes SM-1 and SM-2 were drilled off shore by JQ Ingeniería (Engineering) in May of 2010 in preparation for construction of the new Lo Rojas pier. Test hole S-1 was drilled in March of 2014 by EMPRO Ltda. as a part of related research by Gabriel de la Maza, Dr. Esteban Saez, and Dr. Christian Ledezma from the Catholic University of Chile (Maza et al., 2014). The depth of the ground water table (GWT) recorded for test hole S-1 is 1.72 m. Boring locations are shown in Figure 18 and detailed logs for all borings are provided in the appendix. Gradation tests were performed on all samples from test hole S-1 with results shown in Table 7. Atterberg Limit tests were performed on 6 samples, as shown in Table 8. For samples above a depth of 10 m below the surface, enough fines could not be collected to perform Atterberg Limit tests. Interpolated soil profiles from SPT and gradation data suggest a loose poorly graded sand layer extends from the ground surface to a depth of about 10.5 m for S-1 and a depth of about 4 m for SM-1. Below this depths, clayey sand and clay layers with SPT blow counts less than 15 extend about 20 m below the ground surface in S-1, and to a depth of about 11 m for SM-1. Alternating layers of silt and silty sand were interpreted from SM-2, with blow counts below 15 to a depth of about 11 m below the ground surface.

Table 7. Laboratory Index Tests on Samples from Boring S-1

Sample Depth (m)	USCS Classification	Fines (%)	Moisture Content (%)
0.90	SP	2.98	3.87
3.89	SP	0.98	20.43
4.93	SP	0.55	21.71
5.90	SP-SM	6.89	16.84
6.90	SP	0.89	12.05
7.89	SP	4.75	22.71
8.90	SP-SM	8.56	18.04
9.91	SP-SM	13.43	32.12
10.93	SC	32.18	29.06
11.84	SC	17.71	29.61
12.87	SC	49.22	52.48
14.90	CH	67.30	67.91
15.92	CH	71.29	64.87
16.82	CH	57.03	63.15
17.92	SC	45.82	35.44
18.90	CL	75.03	31.70
19.93	CL	74.18	24.17
20.71	CL	66.19	16.94
21.67	CL	58.71	18.03

Table 8. Atterberg Limit Results for Samples from Boring S-1

Sample Depth (m)	USCS Classification	Liquid Limit (LL)	Plastic Limit (PL)	Plasticity Index (PI)
10	CL	31.8	20.4	11.4
12	CL	38.1	21.7	16.4
13	CL	56.6	30.7	25.9
16	CH	59.9	28.3	31.6
18	CL	42.6	23.1	19.5
22	CL	38	19.5	18.5

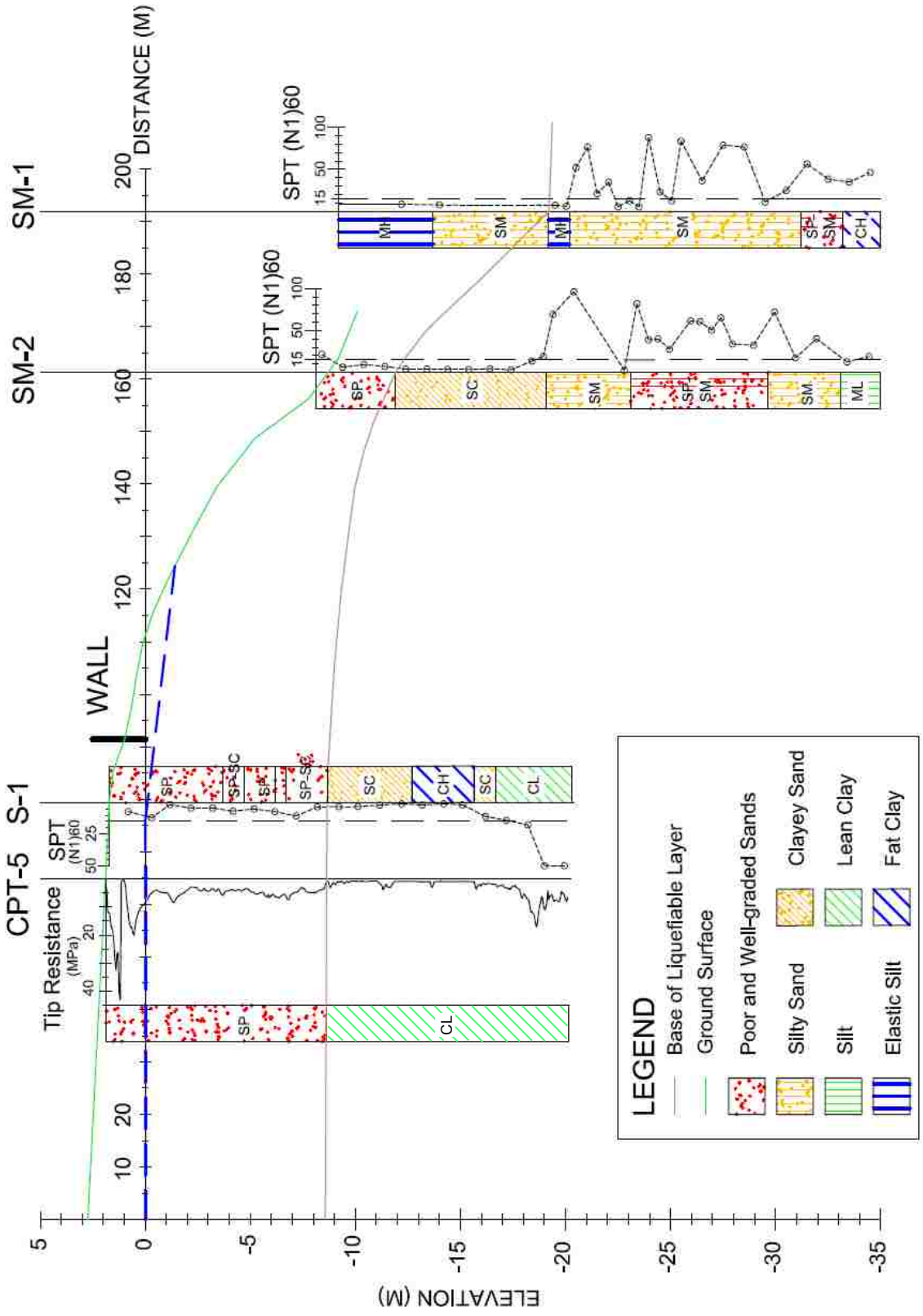

Figure 29. SPT boring data near lateral spread line at Lo Rojas.

A Plasticity Index (PI) ranging from 11.4 to 31.6 in layers 10.5 m below the ground surface indicates clay like behavior, as PI is primarily greater than 7 which is considered a threshold for liquefiable layers according to Idriss and Boulanger (2006). Additionally, high water content values mostly greater than 80% of the LL values further indicate the clay layer is non-liquefiable. CPT data also indicates a transition to clayey soil occurring at a depth of 10.5 m. The estimated liquefiable layer is shown in in Figure 29, having a thickness of 8.7 m according to boring S-1 near the lateral spread line.

3.4.2 CPT Soundings

As part of this study, two CPT soundings, CPT5 and CPT6, were performed in April 2014 at the locations shown in Figure 18 by LMMG Geotechnical Engineers, a company based in Santiago, Chile. CPT6 was originally intended to be performed closer to the ocean, but the soil was too loose to allow the truck access. The recorded GWT is 6 m for CPT5 and 3 m below the ground surface for CPT6. Profiles of cone tip resistance, friction ratio, pore pressure, and soil behavior type are provided for CPT5 and CPT6 in Figure 30 and Figure 31, respectively.

The interpreted soil profiles for CPT5 and CPT6 are very similar and show a relatively loose sand to silty sand layer extending from the ground surface to a depth of about 10.5 m underlain by clay and silty clay to the base of the soundings at a depth of 22 m. The cone tip resistance in the sand layer below about 3 m is typically between 40 and 50 tons/ft^2 (5 MPa) which corresponds to a relative density of about 35 to 40% according to correlations provided by Kulhawy and Mayne (1990). This sand layer would be expected to liquefy when subjected to strong ground shaking. In contrast, the clay layer typically has an I_c value above 2.6 and would not be susceptible to liquefaction.

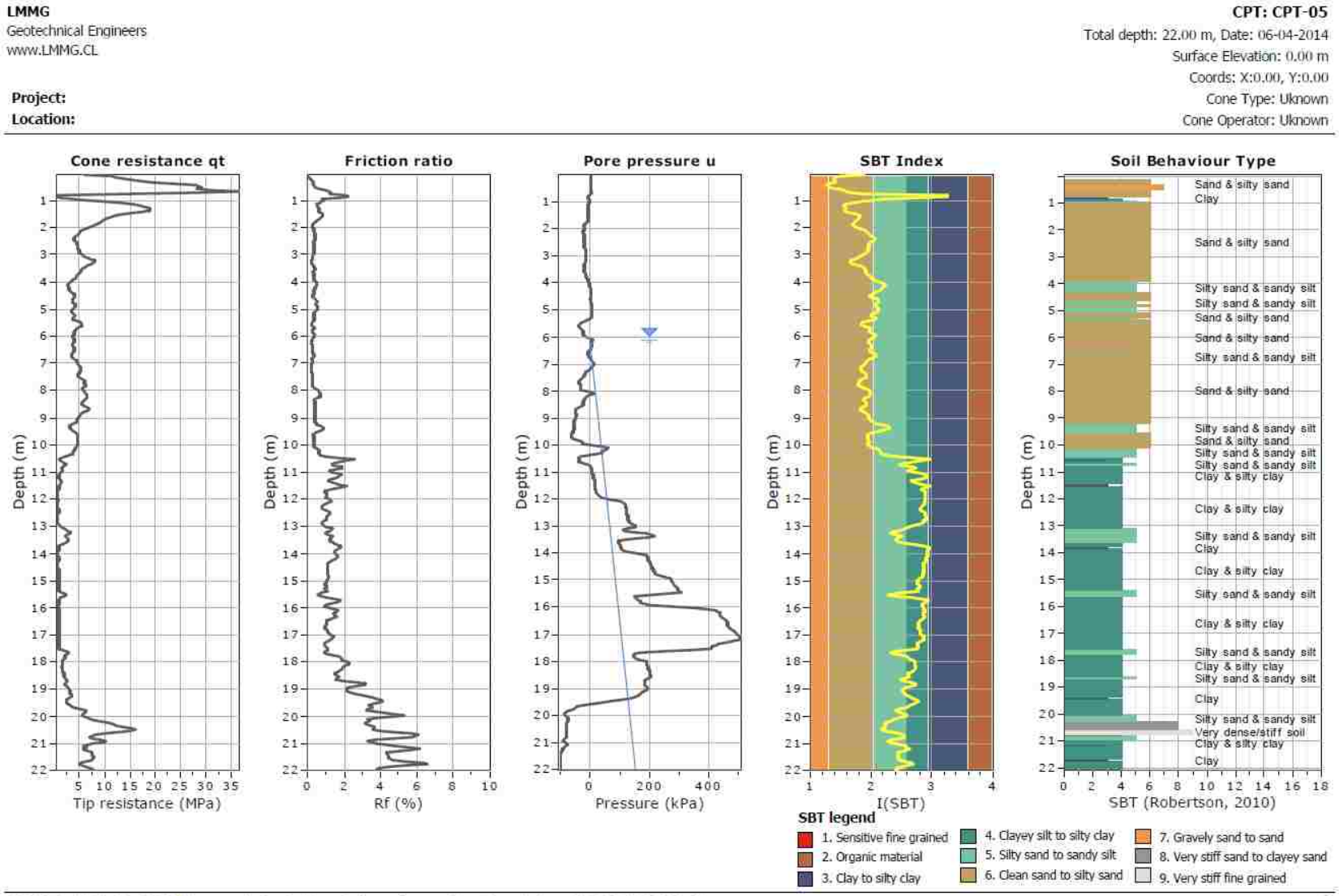

Figure 30. Log from CPT5 near lateral spread line at Lo Rojas

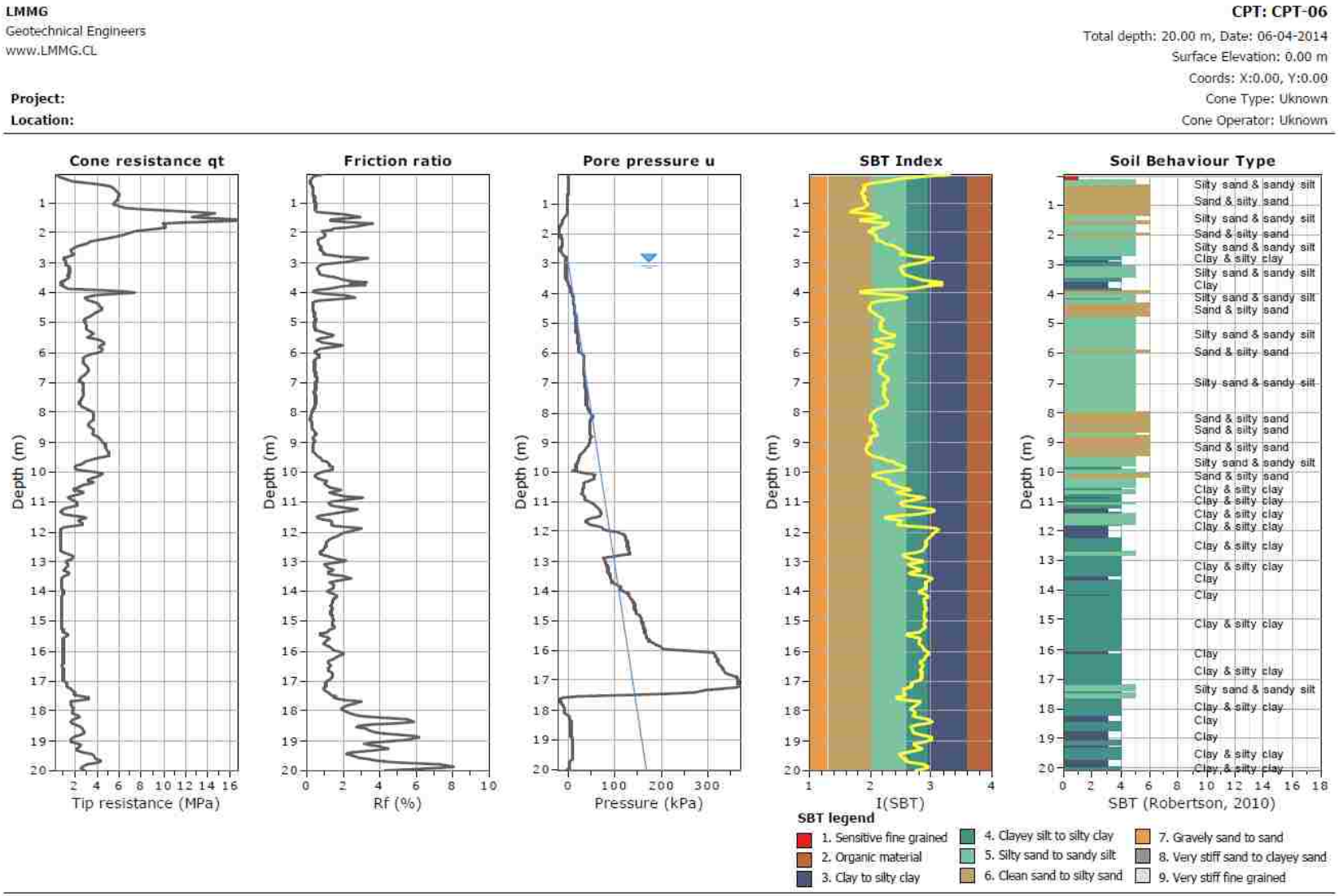

Figure 31. Log from CPT6 near lateral spread line at Lo Rojas

Based on correlations with the cone tip resistance, the undrained shear strength in the clay is approximately 1200 to 1300 psf from 10.5 to 18 m depth and increases to about 3000 to 7000 psf at around 18 m depth. As the soil profile changes from the softer clay to the stiffer clay, the clay transitions from contractive to dilative as shown by the pore pressure response.

CPT data shows liquefiable soil to a depth of about 10.5 m, which is supported by SPT data from boring S-1.

3.4.3 Ground Water Elevation

Because the upper boundary of the liquefied layer appears to be controlled by the groundwater elevation, it becomes important to understand the likely level of the groundwater at the time of the earthquake. Because of the proximity of the site to the ocean, tidal fluctuations are considered. The closest station on the National Oceanic and Atmospheric Administration (NOAA) website to Coronel is Valparaiso, which is about 500 km north, so the Mobile Graphics Tides app which reports tidal predictions for the Talcahuano station about 40 km north of Coronel is preferred. Predictions at the Valparaiso station between the Tides app and NOAA website are compared, and found to differ by only about 2 minutes and 0.1 m. Since the two sources matches reasonably well, the Tides app is used, and the 0.2 m low tide at 04:57 AM CLST recorded in the Tides app for the Talcahuano station is assumed to be the actual low tide on the date of the earthquake. Since the earthquake occurred at 03:34:14 CLST, it is assumed the earthquake hit about an hour and a half before low tide, as shown in Figure 32.

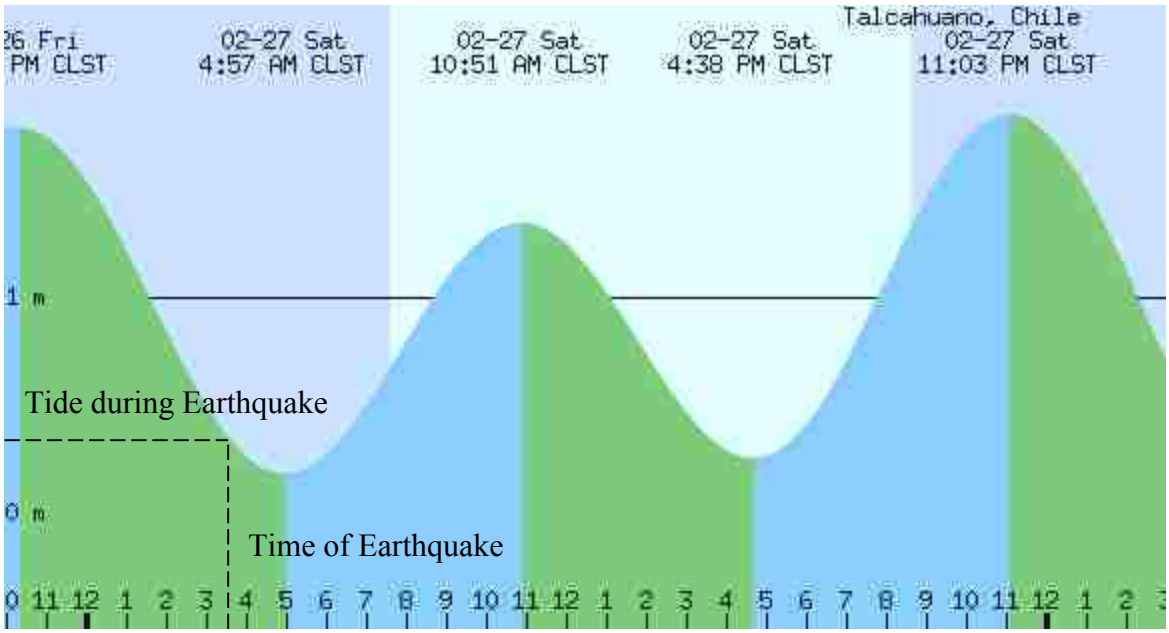

Figure 32. Tidal predictions near Coronel on Feb. 27, 2010 (Adapted from Mobile Graphics).

Similarly, recorded tides for the dates of SPT testing (March 18, 2014) and CPT testing (April 6, 2014) are shown in Figure 33 and Figure 34, respectively. On March 18th there was a fairly consistent predicted high tide of 1.5 m and a low tide of 0.3m. The maximum tide on the afternoon of April 6, 2014 was predicted at 1.4 m with a low of 0.7 m. Although the exact times of the CPT tests are unknown, the best evidence is that CPT5 occurred between 9 and 11 while CPT6 occurred between 12 noon and 2 pm. Since the highest low tide among all three dates occurred approximately during CPT-5 testing when the lowest groundwater table was reported, groundwater table level and tidal levels may not necessarily correlate directly. However, tidal fluctuations are shown to range between 0.7 and 1.6 m, potentially explaining the difference between the water table of 1.72 m and 3 m. It should also be remembered that the GWT will vary and each measurement is only an approximate prediction. Silt layers could also have slowed drainage, decreasing the impact of tidal fluctuations on the GWT.

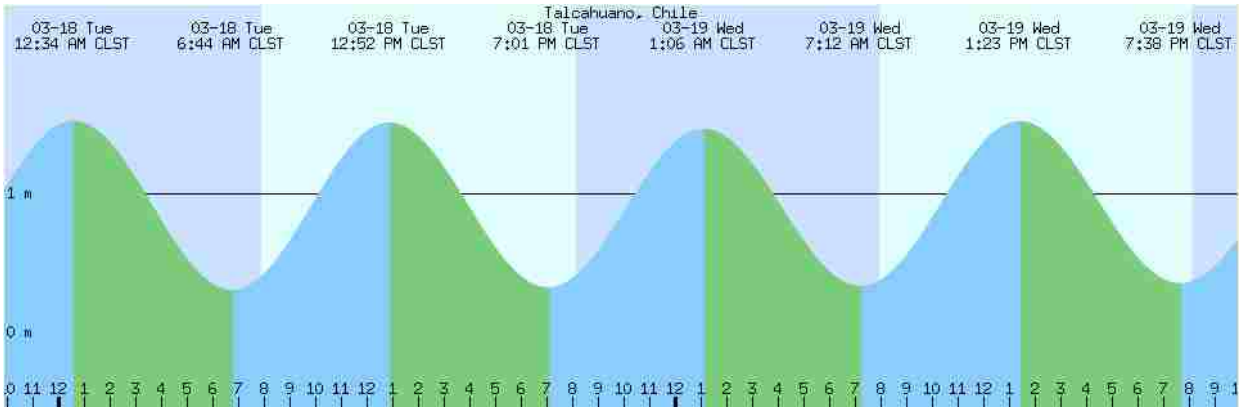

Figure 33. Tidal predictions near Coronel during SPT testing on March 18, 2010 (Adapted from Mobile Graphics).

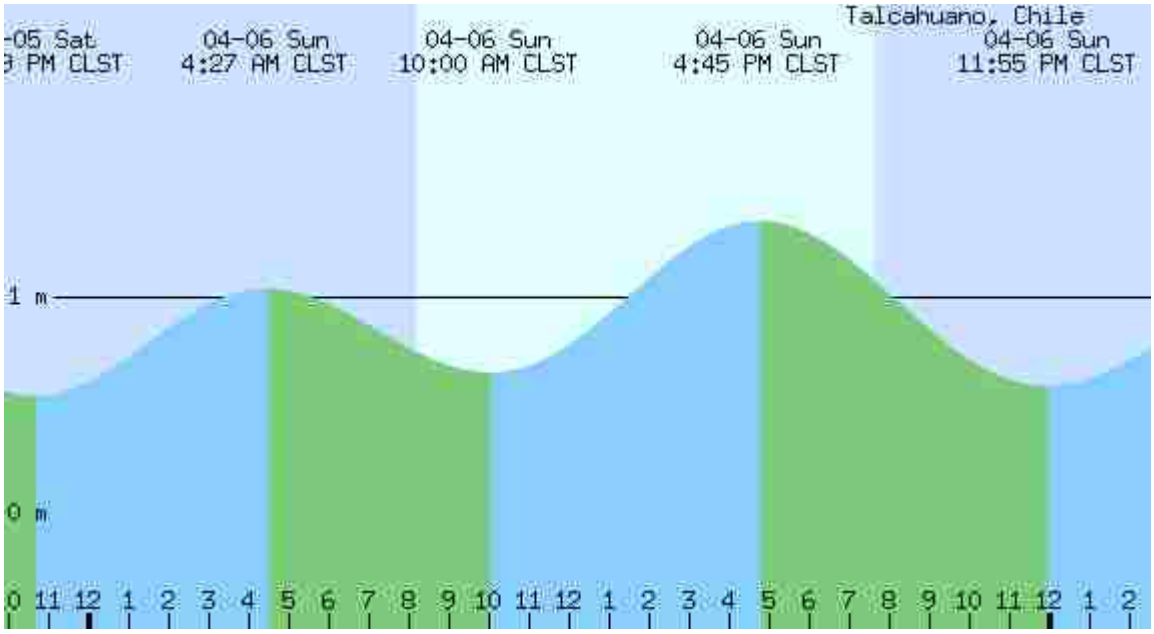

Figure 34. Tidal predictions near Coronel during CPT testing on April 6, 2010 (Adapted from Mobile Graphics).

The reported GWT from CPT-5 of 6 m is assumed to be in error, as it falls significantly outside expected values. During lateral spread and liquefaction calculations, the GWT recorded from SPT testing is used, as it is considered to be more reliable than the highly variant GWTs recorded by CPT soundings.

3.4.4 V_S Measurements

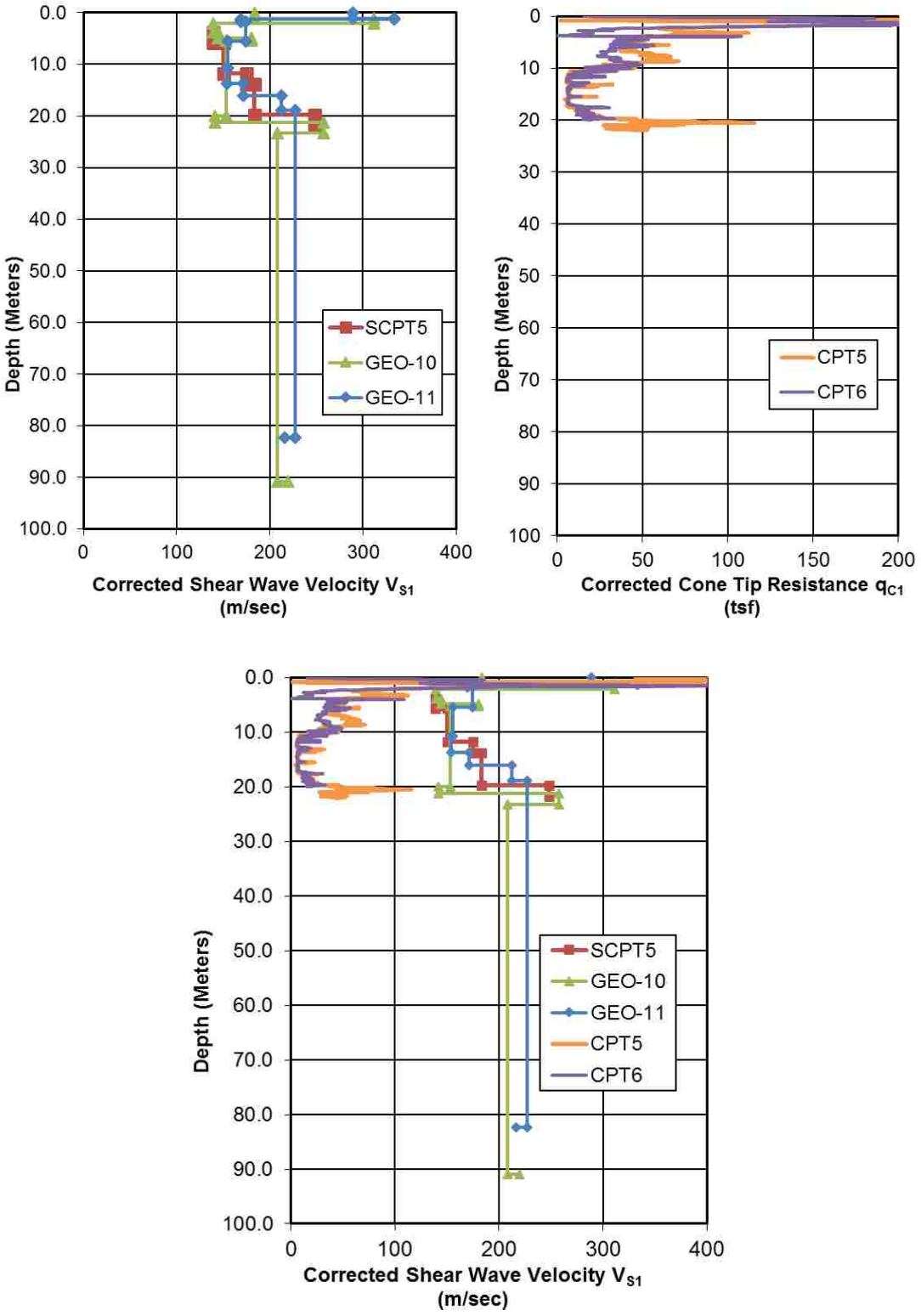

Figure 35. Corrected V_{S1} vs. corrected q_{C1} near Lo Rojas lateral spread line.

Shear wave velocity profiles (V_S) were also measured at the site using both downhole and surface wave methods. During this study, downhole measurements were made using a geophone in the cone penetrometer at CPT5 after inducing shear waves at the ground surface. The measured V_S profile, labeled SCPT5, is shown with CPT5 and CPT6 corrected cone tip resistance in Figure 35. Insufficient V_S data is available from CPT6 to produce another shear wave velocity profile, but likely similar to the V_S profile from CPT5. Dr. Esteban Saez, Dr. Cristian Ledezma, and Gabriel de la Masa also obtained V_S profiles near the site using the Spectral Analysis of Surface Waves (SASW) approach and the profiles from these two measurements are labeled GEO-10 and GEO-11. All recorded V_S data has been converted to V_{S1} by correcting for overburden-stress according to the procedure recommended by Youd et al. (2001).

SCPT5 and GEO-11 are located close together and show similar V_S readings. GEO-10 is closer to the coast and indicates slightly lower V_{S1} values between 15 and 20 m compared to SCPT5 and GEO-10. The V_S value for the sand layers in the upper 10 meters of the profile is considerably less than 210 m/s indicating the sand is susceptible to liquefaction given a large enough earthquake.

3.5 **Liquefaction Triggering**

The liquefaction analysis has been conducted using three methods: Youd et al. (2001); Cetin et al. (2004); and Idriss and Boulanger (2004). In all cases the peak ground acceleration was set at 0.40g ad the appropriate magnitude scaling factors for the various methods were applied to account for the M_w 8.8 earthquake Results from each method are compared in Figure 36 for the SPT test hole and from Figure 37and Figure 38 for the CPT soundings. FS against liquefaction was calculated using the program CLiq and the Robertson 2010 method. More about this program is explained in section 3.6.6.

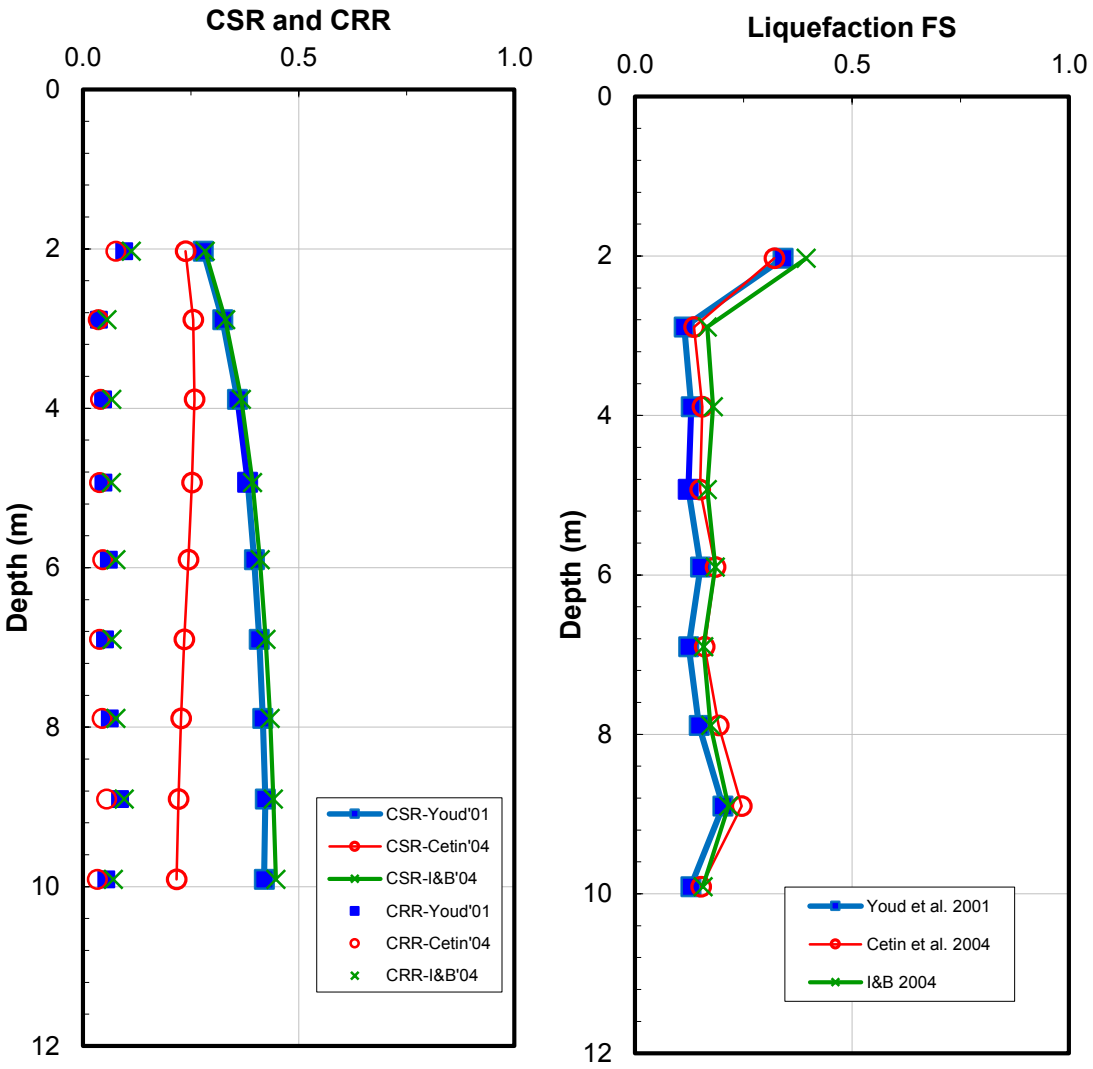

Figure 36. Liquefaction results comparison for Youd et al. (2001), Cetin et al. (2004), and Idriss and Boulanger (2004) methods.

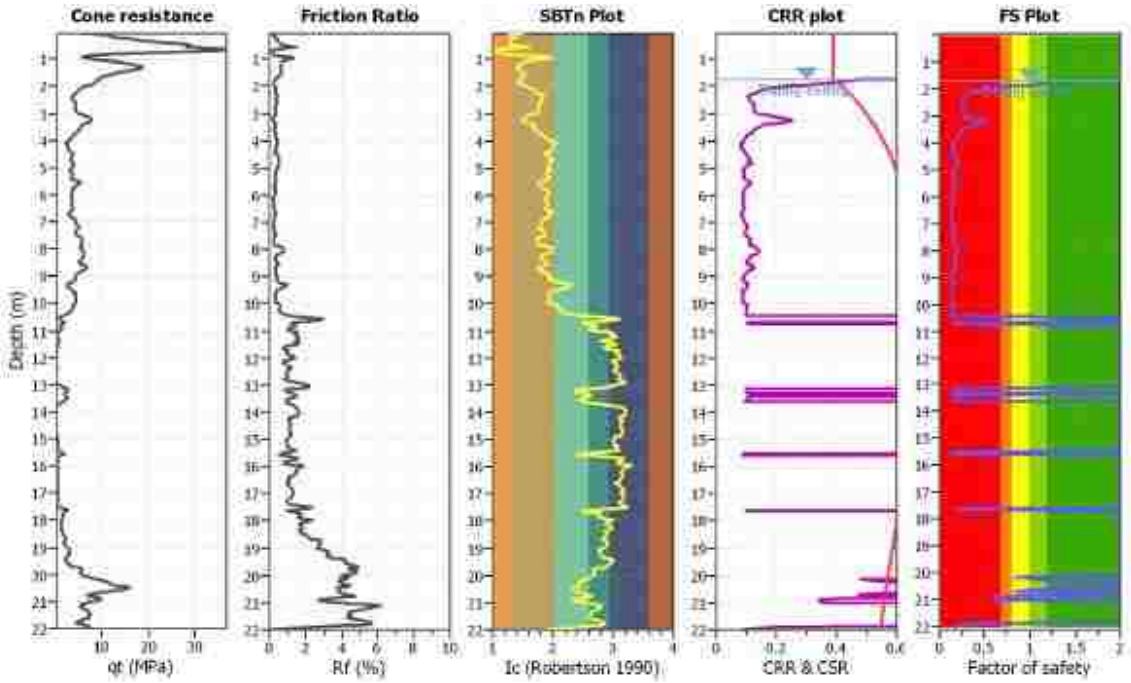

Figure 37. CLiq computed FS against liquefaction for CPT5.

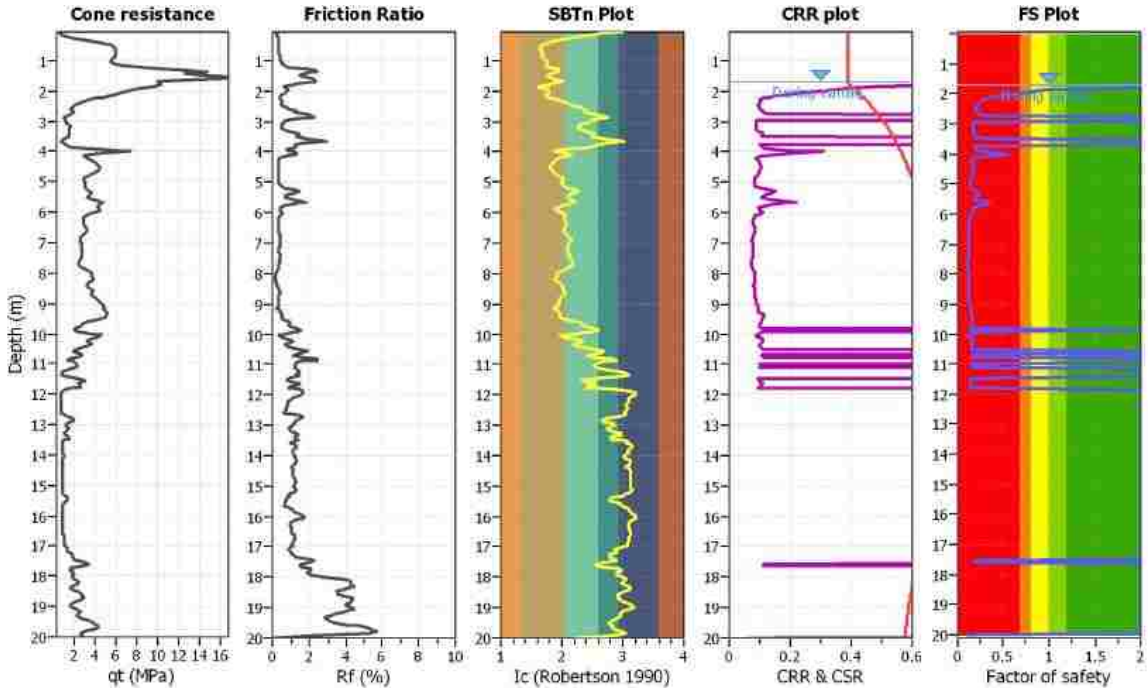

Figure 38. CLiq computed FS against liquefaction for CPT6.

Liquefaction is predicted to a depth of about 10.5 m according to CPT data (Figure 30 and Figure 31), as I_C values consistently exceeded 2.6 below this depth. Generally, soils with Ic values higher than 2.6 are considered too cohesive or plastic to liquefy. SPT blow counts are consistently low from the surface to -18 m below the site, but high PI and fines contents found in samples below a depth of 10.5 m limit the liquefiable layer to sand above this depth.

V_S data indicates potentially liquefiable layers when values are lower than 215 m/s for soil with low fines content (Youd et al., 2001), as can be seen in Figure 33. SCPT5 and GEO-10 indicate the liquefiable layer is above 20 m, while GEO-11 indicates this layer is above about 16 m (see Figure 35). Though V_S data predicts liquefaction over a much higher range than both SPT and CPT data, V_S data is considered less sensitive to distinguishing different types of soil behavior (Idriss and Boulanger, 2004). Because the SPT sample indicates a high PI below 10.5 m, it is assumed that the V_S profiles were unable to identify the clayey sand and clay layers and the soil below 8.4 m is too cohesive to liquefy.

The final liquefiable layer determined from SPT, CPT and V_S data is shown in brown in Figure 29. The depth of the liquefiable layer is then about 8.7 m, which is calculated by interpolating SPT data, with layers assumed halfway between SPT samples that indicate a soil type transition. The liquefiable layer extends from the top of the groundwater table to a depth of 10.5 m near the retaining wall.

3.6 **Lateral Spread Displacement Evaluation**

The following sections present the results from each lateral spread method evaluated. Methods include: Youd et al. (2002); Rauch and Martin (2000); Bardet et al. (2002); Zhang et al. (2012); Faris et al. (2006); and Zhang et al. (2004).

3.6.1 Lateral Spread Evaluation using Youd et al. (2002)

Because the Lo Rojas topography does not clearly meet definitions of a gentle slope nor a free face scenario, both equations are evaluated and compared. Though present, the retaining wall directly at the seaward end of the lateral spread line is not considered a critical geometry as it is only about a meter high. Instead, the gentle slope behind the retaining wall or the steeper drop off of elevation of the seafloor near the lateral spread line are assumed to govern soil behavior. Table 9 lists all parameters used for the Youd et al. (2002) method. Three parameters vary, namely R, W, and S, which are discussed in more detail here. Complications of the R term is also discussed subsequently. Complications in the selection of an appropriate R term are also discussed throughout this section.

Table 9. Parameters for Youd et al. (2002) Lateral Spread Method

Variable	Value	Units
M_w	8.8	
R	Varies	km
T_{15}	8.7	m
F_{15}	4.2	%
$D50_{15}$	0.46	mm
W	Varies	%
S	Varies	%
Z_T	1.72	m

As described in Section 3.5, liquefaction analysis shows low factors of safety against liquefaction from the ground water table to about 10.5 m below the ground surface, indicating lateral spread may occur. Low blow counts and fines content indicate a T_{15} layer approximately 8.7m thick below the water table which is likely to liquefy, as explained in section 3.5 and shown in Figure 29.

Values for the average fines content F_{15} and the average mean grain size $D50_{15}$ are calculated from the SPT data which fell within the assumed liquefiable layer. F_{15} is calculated with an arithmetic average and mean grain size $D50_{15}$ using a geometric average. T_{15}, F_{15}, $D50_{15}$, and Z_T all fit well inside bounds recommended by Youd et al. (2002) as shown in Table 1. Although the M_w 9.2 1964 Alaska Earthquake was included in the Youd et al. (2002) database, there are only seven points for this earthquake in comparison to the other 477 points in the database with M_w < 8.0. Evaluating the ability of the Youd et al. (2002) method to predict displacement for the M_w 8.8 2010 Maule, Chile earthquake is thus an important objective of this study.

Youd et al. (2002) define seismic source to site distance as "the horizontal or mapped distance from the site in question to the nearest bound of seismic energy source". This is similar to the Joyner-Boore distance, which is defined as the closest distance to the surface projection of the fault surface (Kaklamanos, 2011). In this instance, since the subduction zone extends below the coastal crust, the source of seismic energy is directly below the site, such that R=0. The method dictates R values outside minimum limits be increased to R=0.5 km, but this distance still predicts unrealistically large displacements that are over an order of magnitude larger than observed displacement. As Youd et al. (2002) question the accuracy of displacements greater than 6 m, different methods of measuring R were explored to improve method predictions for similar sites with subduction zone fault geometries. Four distances were explored, as shown in Table 10, namely: (1) the Joyner-Boore distance mentioned; (2) the nearest distance to the zone of maximum coastal uplift as described by Vargas et al. (2011); (3) the closest distance to the surface fault rupture or the trench as shown in Figure 39, and (4) an optimal distance for predicting displacement, R=104 km, the lower end of the range recommended for nearby sites by Tryon

(2014). R=0.5 km is used for the Joyner-Boore distance, since this is the minimum value of R allowable for the Youd et al. (2002) equations.

Table 10. Distances Used to Evaluate Lateral Spread

Distance Type	Distance (km)
Joyner-Boore	0
Max Coastal Uplift	47
Optimized (Tryon, 2014)	104
Fault Rupture	160

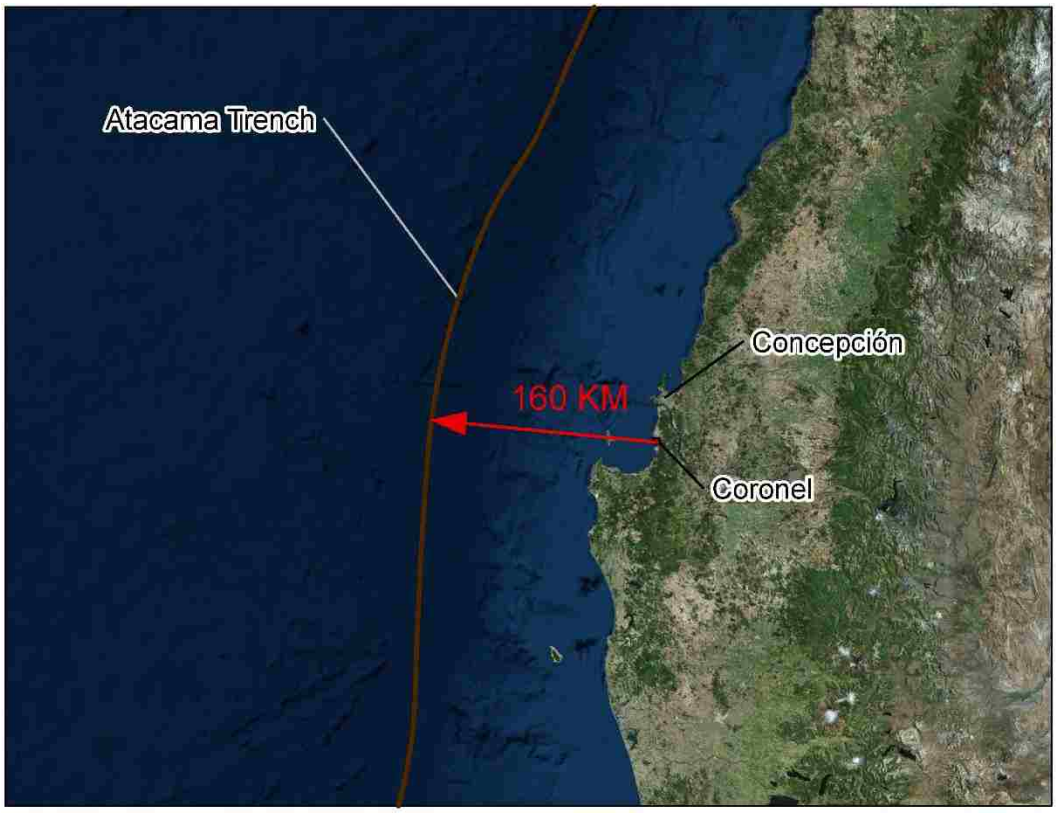

Figure 39. Closest distance from site to visible fault rupture or Atacama Trench.

3.6.1.1 Free Face Type Lateral Spread Geometry

Since multiple displacement measurements can be created by summing different lengths of measured cracks along the lateral spread line, the free face ratio can vary with the location of the end of each lateral spread line. Cracks are summed from the beginning of the lateral spread line, starting 91.4 m behind the retaining wall then moving towards the ocean. As the length of the lateral spread line increases, the distance from the end of the lateral spread line to the base of the free face, L, decreases, in turn decreasing the free face ratio W. Since the height remains relatively constant, W is higher closer to the free face. The reduction in W helps account for the typical reduction in lateral spread displacement at distances further away from the free face. Only displacement measurements within 20 m behind the retaining wall are included in lateral spread predictions because displacement vectors beyond this distance are far enough from collected SPT and CPT data that soil conditions may have changed, potentially causing inaccurate predictions.

Table 11. Calculated W Values for Lo Rojas Elevation Profile

Distance Behind Wall (m)	Elevation Profile		
	L (m)	H (m)	W (%)
0.3	69	9.5	13.8
10.2	79	10.1	12.8
19.0	87	10.2	11.7
29.0	97	10.4	10.6

Calculated W values for the elevation profile developed in section 3.4.3 are shown in Table 11. Figure 40 displays lateral spread predictions from the Youd et al. (2002) method versus measured displacements along the lateral spread line at Lo Rojas. Predicted displacements corresponding to the Joyner-Boore distance are omitted, in this figure, to maintain a reasonable graph scale, since predicted measurements of over 50 m are far outside the range deemed

reasonably accurate by this method. Computed displacement values predicted using the Joyner-Boore R value of 0.5 km are presented in Figure 41 for completeness.

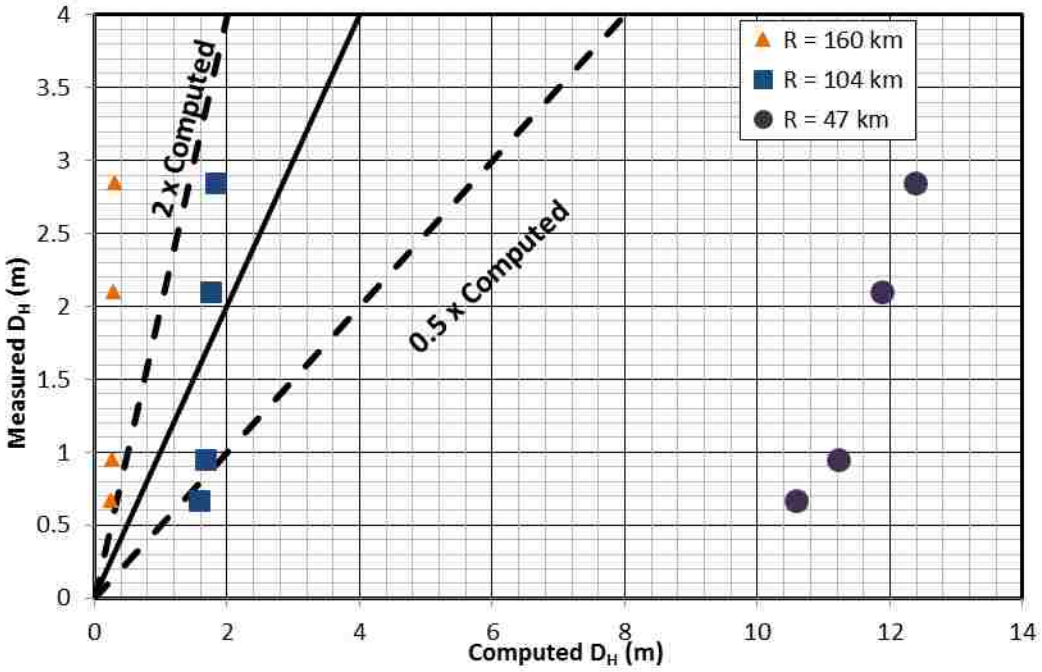

Figure 40. Lo Rojas Youd et al. (2002) prediction vs. measured displacement assuming free face conditions.

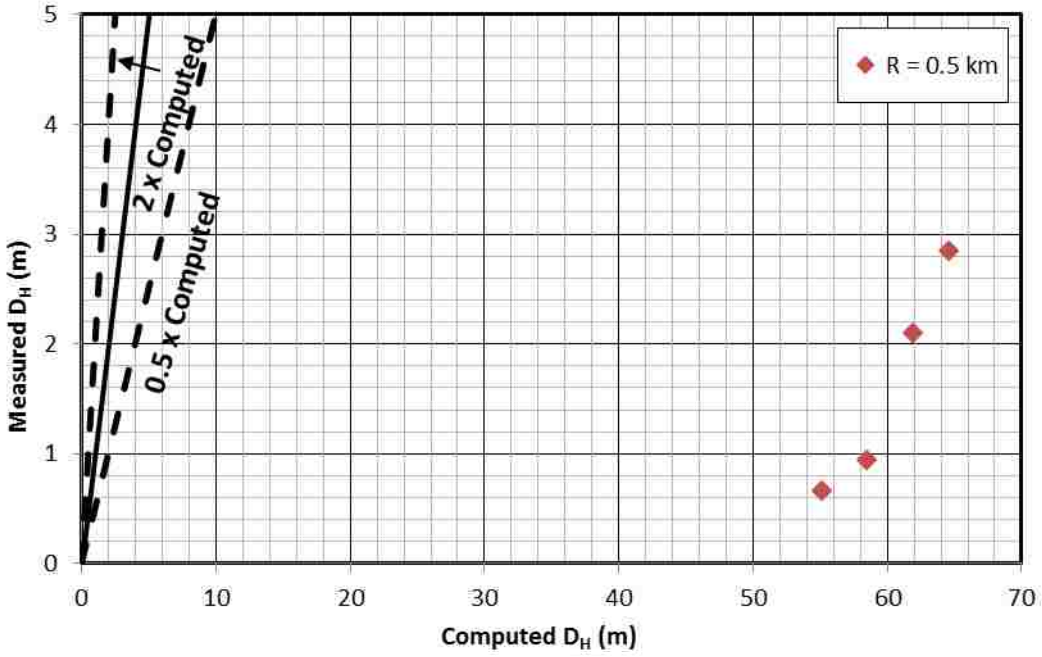

Figure 41. Free face predictions of Youd et al. (2002) vs. measured displacements using Joyner-Boore distance R=0.5 km at Lo Rojas.

3.6.1.2 Gentle Slope Type Lateral Spread Geometry

When using the gentle slope condition, an average slope of 2.73% over a 40 m distance landward from the wall was first employed and compared with the maximum lateral spread displacement measured at the retaining wall. Using this slope, a displacement of 1.7 m is predicted for an R of 104 km, which is in good agreement with the measured displacement as shown in Figure 42. However, using the surface distance to the fault (160 km) yields an unreasonably low value (0.3 m) while the distance to the point of maximum seismic uplift (47 km) yields an unreasonably high value (12 m) as shown in Figure 42. Using the Joyner-Boore distance predicts an unreasonable displacement of 63 m.

An attempt to taper displacement predictions is also made by using the slope at each displacement measurement. As Zhang et al. (2004) restricts slope measurements to average gradients over at least 20 m, this distance was used to define average slope at each point. Figure 43 shows predicted values versus measured values for various assumed R values. Again, Joyner-Boore distance predictions are omitted to maintain a reasonable graph scale and are shown separately in Figure 44. S values calculated by averaging the slope from 10 m behind and 10 m in front of each point along the lateral spread line are shown in Table 12. Beyond 29 m behind the wall, Google Earth governs the composite line and the slope becomes a constant 1.3 %.

Table 12. Slope over 20 m at Each Point Along the Lateral Spread Line

Distance Behind Wall (m)	S (%)
0.3	5.5
10.2	4.1
19.0	1.5
29.0	1.3

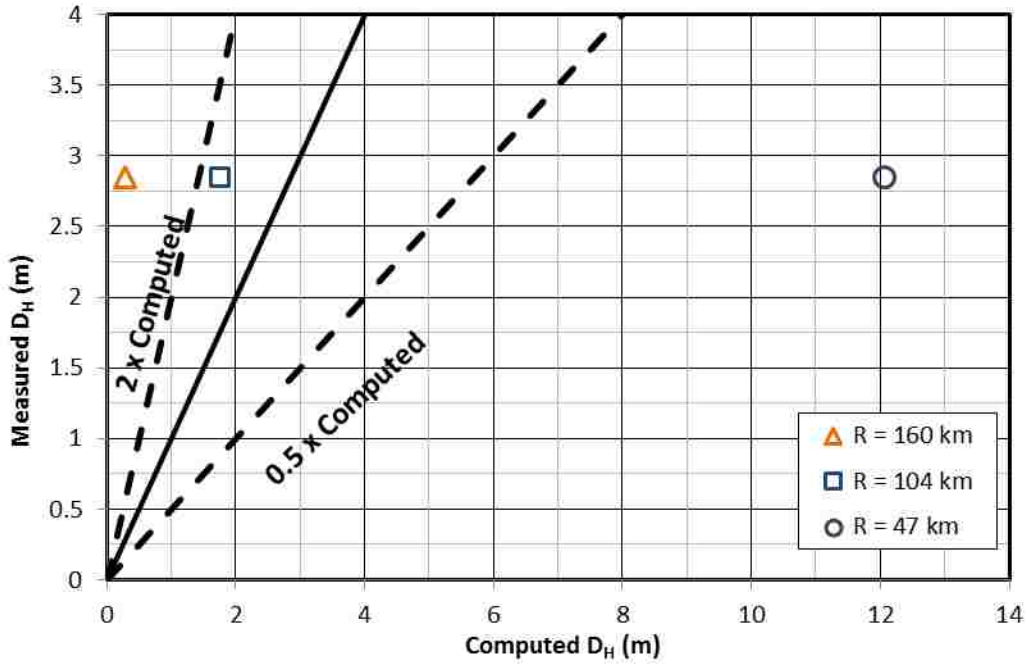

Figure 42. Lo Rojas Youd et al. (2002) prediction vs. measured displacement using one average gentle slope = 2.73%.

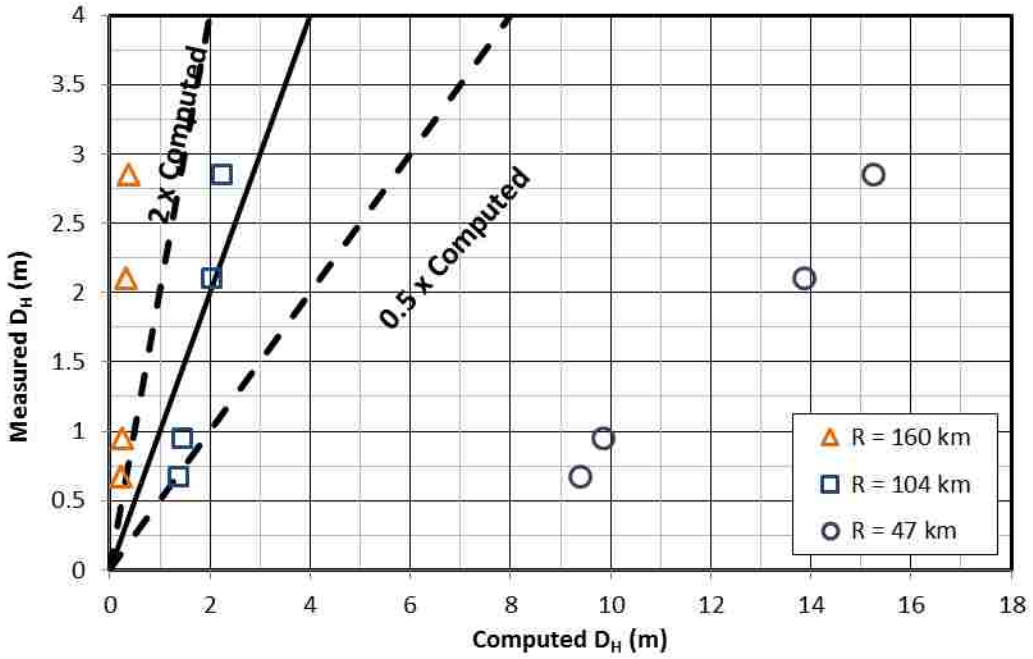

Figure 43. Lo Rojas Youd et al. (2002) prediction vs. measured displacement assuming gentle slope conditions.

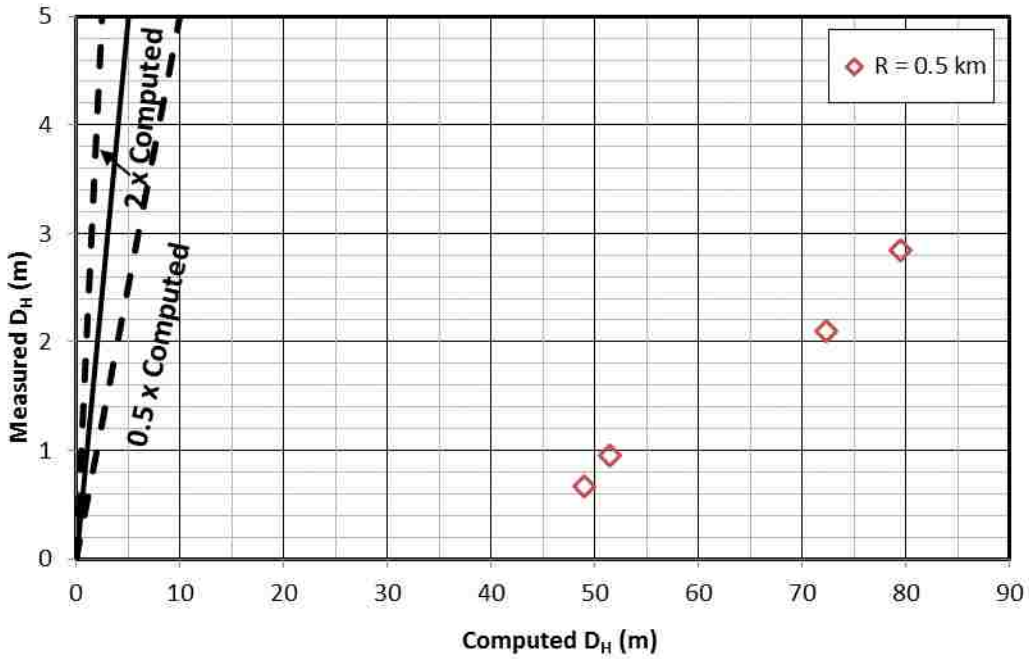

Figure 44. Gentle slope predictions of Youd et al. (2002) vs. measured displacements using Joyner-Boore distance R=0.5 km at Lo Rojas.

3.6.1.3 Comparison

A distance of R=104 km appears to be a good fit between measured and computed displacements for the Lo Rojas site as well as the sites studied in Tryon (2014). In contrast, significant under or overpredictions of displacements were obtained using the surface distance to the fault rupture or the Joyner-Boore distance, respectively. Figure 45 shows the comparison of gentle slope vs. free face scenarios for R=104 km. The gentle slope condition appears to be a good prediction of measured displacement, providing predictions within a factor of two of measured displacement for all four displacement vectors. Using an R value of 104 km also provides good predictions for the free face method, but one prediction falls outside a factor of two of measured displacement.

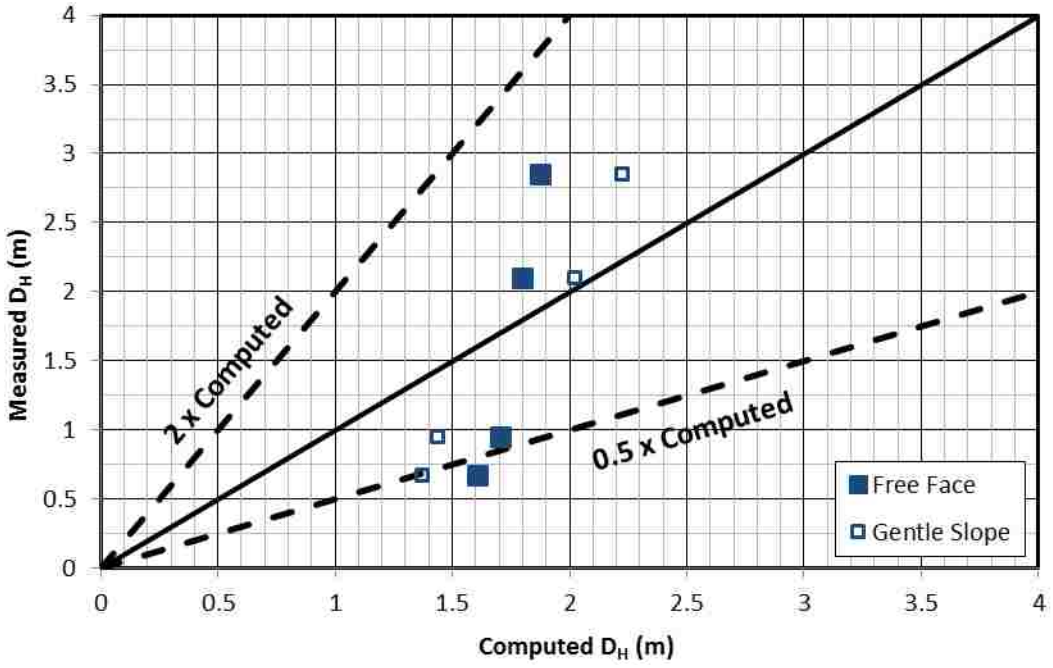

Figure 45. Comparison of free face and gentle slope condition Youd et al. (2002) predictions at Lo Rojas for R = 104 km.

When looking strictly at the graph of measured displacement in Figure 17, it is expected that the free face scenario would be a better predictor of displacement, since the amount of displacement changes with distance instead of remaining fairly constant as is generally anticipated for a gentle slope scenario. However, gentle slope conditions appear to be a better predictor overall for displacement when contrasted with free face conditions. It is possible the gentle slope based geometry is a better predictor than free face based geometry because it more closely represents the steeper gradient in the area behind the retaining wall where the most of measured lateral spread occurred. The lower measured displacements relative to the predicted displacements further inland from the ocean could also be a result of increasing soil density or more cohesive soil types although there is no geotechnical data at present to confirm this speculation. Additional CPT holes further inland would be desirable to examine this possibility. For example, at CPT holes further inland at

the Port of Coronel just south of this site, the sand was significantly denser and was not liquefiable (Tryon, 2014). Predictions are the best over the area where SPT data was collected, which was performed in the zone where the most lateral spread was observed.

Predicted displacement versus measured displacement from the Lo Rojas pier as well as other locations in Port Coronel from Tryon (2014) are shown in Figure 46. Predictions of measured displacement were almost all within a factor of two of measured displacement, with a fairly good distribution between overpredictions and underpredictions of measured displacement. Only one prediction fell outside a factor of two of measured displacement.

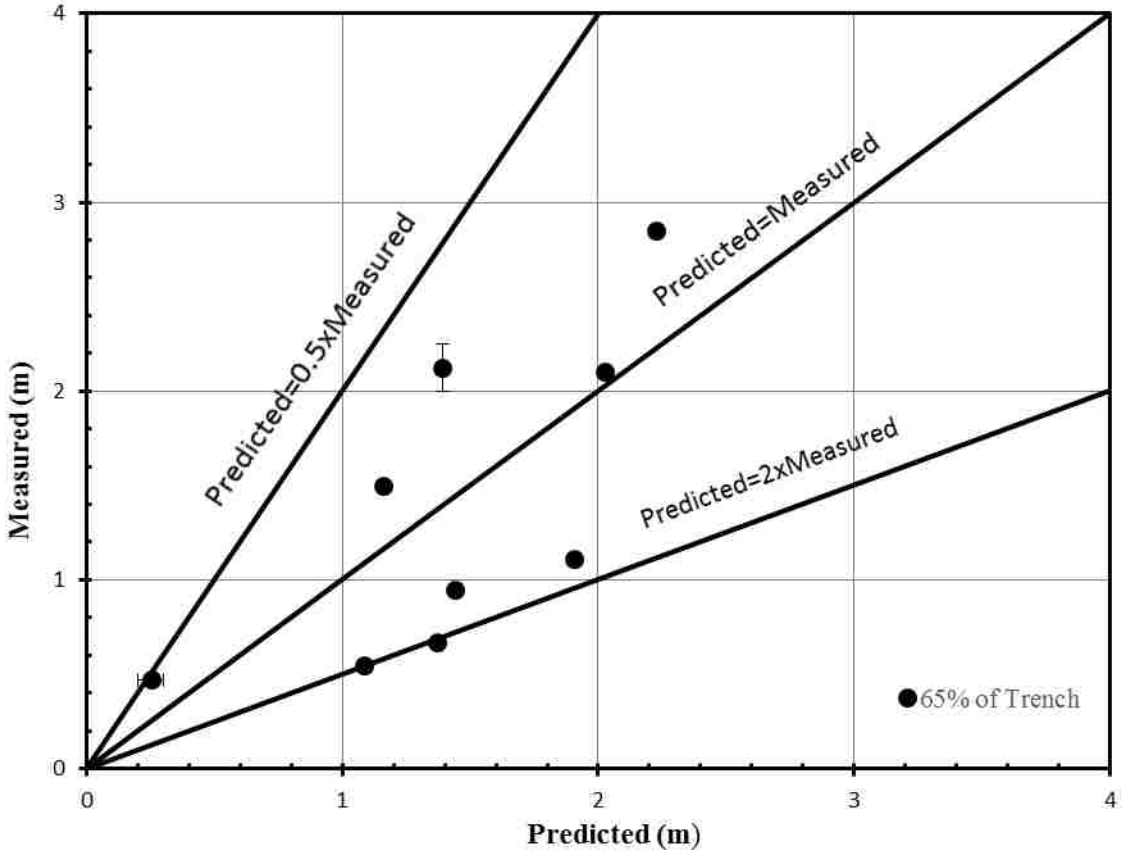

Figure 46. R = 104 km Youd et al. (2002) predictions for the Lo Rojas and Tryon (2014) sites in Port Coronel.

An R value of 65% of the distance to the trench was also applied to sites from the 1964 Alaska earthquake for verification of this method, as shown in Figure 47. This method which worked well for the 2010 Maule, Chile earthquake was not a good predictor of measured displacement for the 1964 Alaska earthquake, providing predictions that were significantly under a factor of two of measured displacement. About 25 to 30 % of the distance to the trench provided reasonable predictions for Youd et al. 2002 method, and these values were used to regress the equation.

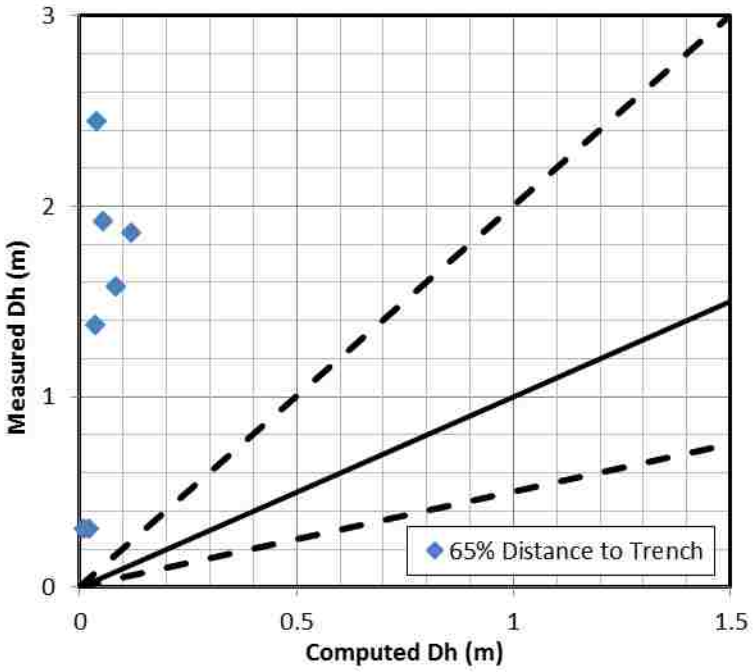

Figure 47. Predicted displacement with R = 65% of the distance to the trench using the Youd et al. (2002) method.

3.6.2 Lateral Spread Evaluation using Rauch and Martin (2000)

Since all of the required parameters for the Geotechnical-EPOLLS model were available, only this model is considered for this study. However, Table 13 lists parameters required for each EPOLLS model. Note that Site-EPOLLS requires all parameters from Regional-EPOLLS and Geotechnical-EPOLLS requires all parameters form both Site-EPOLLS and Regional-EPOLLS.

Table 13. EPOLLS Model Parameters for the Lo Rojas Site

EPOLLS Model	Parameters	
Regional	M_w	8.8
	R_f (km)	0
	A_{max} (g)	0.4
	T_d (s)	120
Site	L_{slide} (m)	91.4
	S_{top} (%)	Varies
	H_{face} (m)	9.5
Geotechnical	Z_{FSmin} (m)	2.89
	Z_{liq} (m)	1.72

Sources for M_w, A_{max} and T_d are discussed in section 3.2. Though several durations were reported, 120 sec represented an average value (see Table 5). L_{slide} is defined as the distance from the head to the toe of the lateral spread, and is assumed as the length of the lateral spread line or 91.4 m. H_{face} is measured from the toe of the free face to the height at the end of the lateral spread line near the retaining wall. Note that since the topography of the site was not a clear free face or gentle slope condition, both S_{top} and H_{face} are employed. Liquefaction analysis conducted according to Youd et al. (2001) on SPT data from boring S-1 indicates the minimum factor of safety occurs at a depth of 2.9 m. This liquefaction analysis also indicates all qualifying soils will liquefy due to extremely low blow counts, and thus the depth to the top of the liquefiable layer Z_{liq}

is assumed as the depth to the ground water table where saturated conditions allow liquefaction to occur.

Multiple ground slopes are compared, similar to the lateral spread analysis performed with the Youd et al. (2002) model. As mentioned in the literature review, Rauch and Martin (2000) specify that a case study is considered "a contiguous mass of soil that moved in one general direction". Only the greatest measured displacement is predicted for this method, compared to Youd et al. (2002) which could consider several separate displacement vectors along the same lateral spread line. When using an overall average slope of 2.73%, the geotechnical model predicts 1.2 m of displacement, which is an under prediction exceeding a factor of two. Using the 5.45% slope which was a good predictor for Youd et al. (2002), predicted displacement was just barely inside of the factor of two from measured displacements.

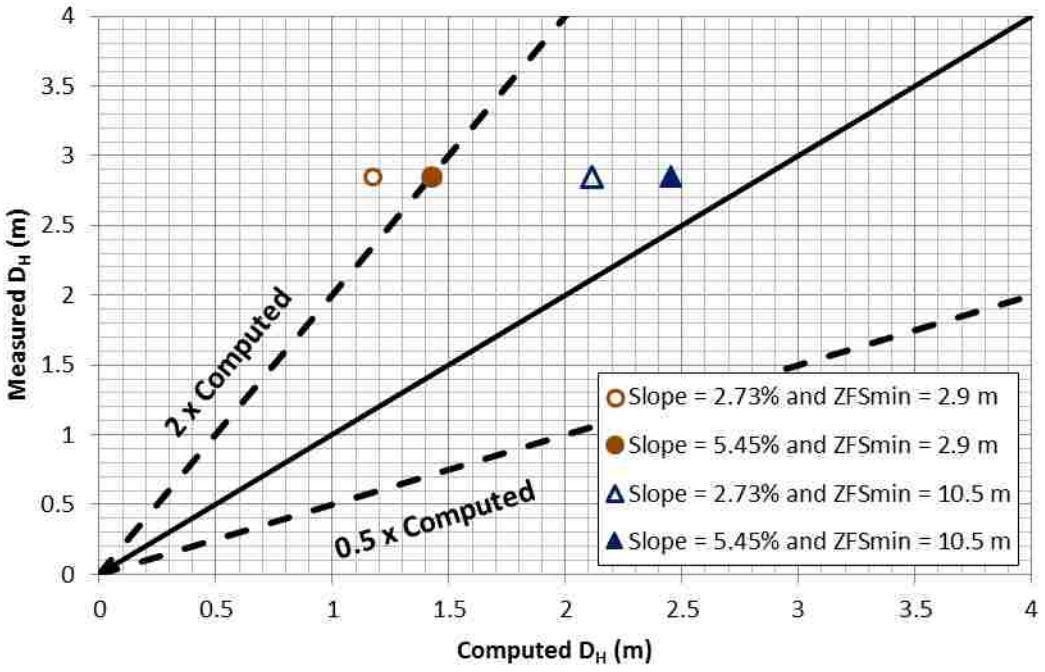

Figure 48. Comparison of Rauch and Martin (2002) predicted and measured displacement with variations in slope and ZFSmin.

Instead of using a term that measures the depth to the base of the liquefiable layer, the Rauch and Martin (2002) method measures the depth to the minimum factor of safety, $Z_{FSmin,}$ to determine the amount of soil that will displace. However, liquefaction analysis with the Youd et al. (2002) and Cetin et al. (2004) models indicated a realatively shallow Z_{FSmin} = 2.9 m, despite extremely low factors of safety against liquefaction down to a depth of 10.5 m, with the final FS against liquefaction at 10.5 m only .02 higher than at 2.9 m. Since it is likely that this entire mass of soil moved during the event, the depth to the base of the liquefiable layer as indicated via liquefaction analysis is substituted for Z_{FSmin} and compared in Figure 48. Using the greater Z_{FSmin} depth and the steeper slope representative of actual gradient where most of the lateral spread occurred more closely approximates measured displacement.

Coefficients on variables A_{max} and T_d are negative, which is counterintuitive. Increasing the peak horizontal acceleration the ground surface experienced at the site and increasing the duration of the earthquake are both generally expected to increase lateral displacement. However, since the coefficients are negative, predicted displacement decreases when PGA or earthquake duration is increased.

All displacement points from Port Cornel examined in this study and Tryon (2014) are shown in Figure 49. Two predictions of measured displacement were within a factor of two of measured displacement, with one prediction under a factor of two of measured displacement, and another over a factor of two of measured displacement.

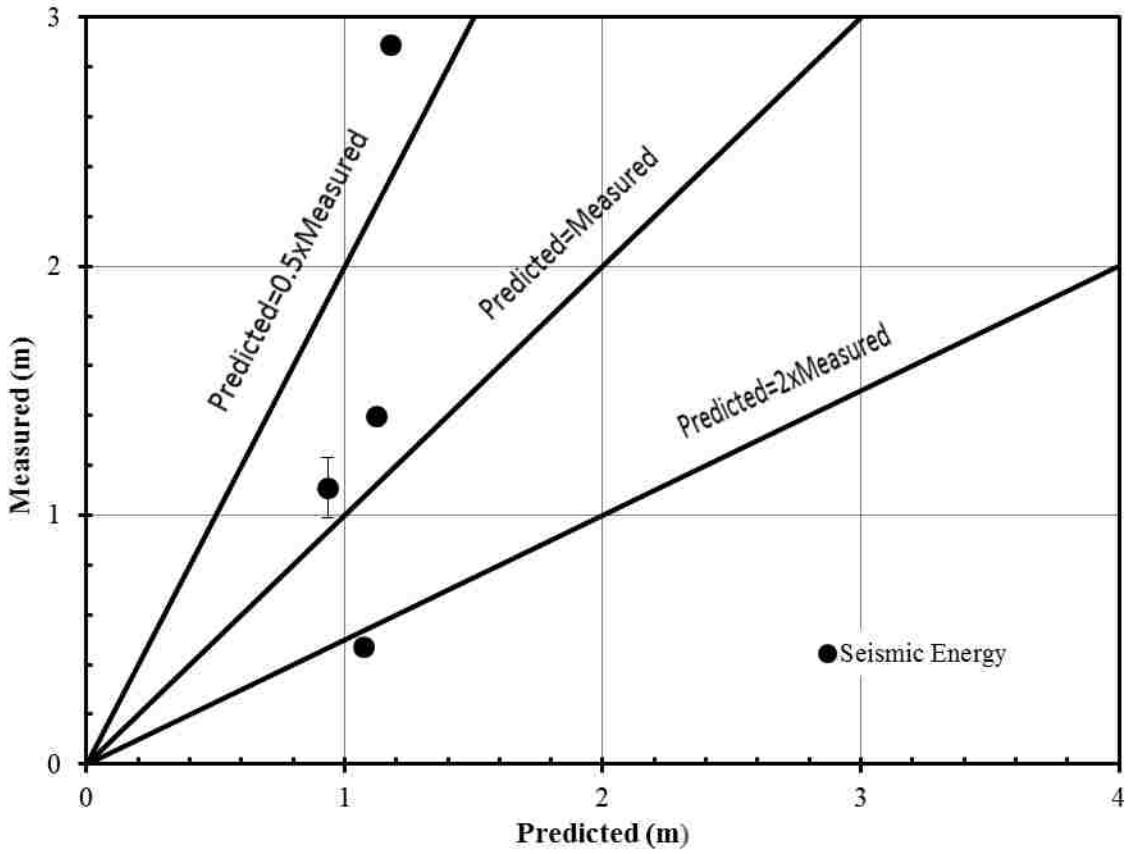

Figure 49. R = Ruach and Martin (2000) predictions for the Lo Rojas and Tryon (2014) sites in Port Coronel.

3.6.3 Lateral Spread Evaluation using Bardet et al. (2002)

The Bardet et al. (2002) model experiences the same difficulties defining R as Youd et al. (2002). Though Bardet et al. (2002) does not specify the replacement of values outside of the recommended range with a minimum R value, a minimum value of 0.2 km is used to allow for calculation using the Joyne-Boore distance, which would produce an error if the true value of zero were used. Various distances of R are examined, similar to the analysis performed for Youd et al. (2002). See section 3.6.1 for a description of why each distance is selected for further analysis.

Values used for each parameter in the Bardet et al. (2002) equation are shown in Table 14. Both the free face and gentle slope cases are considered, where S is the average gradient over 20

m at each displacement point measurement, and W is the slope from the free face to the displacement point in question, similar to the analysis conducted for Youd et al. (2002). Predicted displacements using the free face equation relative to the measured value are shown in Figure 50, with predictions using the gentle slope equation in Figure 51. All predictions using R=0.2 km are over 750 m, and all predictions using R = 47 km are over 10 m. Both are therefore rejected as unrealistic and are not included in graphical form.

The only displacements predicted within a factor of two of measured displacements correspond to measured displacements of 0.95 and 0.67 m, the two lowest considered, using R = 104 km. Because none of the R values used for Youd et al. (2002) provide good predictions for all considered measured displacements, optimum values of R are also calculated for Bardet et al. (2002). An R value of 79 km, or about 50% of the measured distance to the surface trench, provides reasonable predictions for all four measured displacement vectors for the free face based method. Similarly, for the gentle slope based method an R value of 80 km or 50% of the measured distance to the surface trench provides reasonable predictions within a factor of two of measured displacement. However, the slope based geometry provides an overall better fit, with predictions closer to measured displacements than the free face based geometry.

Table 14. Bardet et al. (2002) Model Parameters for Lo Rojas Site

BARDET 2002 (Data set A)	
M_w	8.8
R (km)	Varies, see section 3.6.1
T_{15} (m)	8.7
W (%)	Varies, see section 3.6.1.1
S (%)	Varies, see section 3.6.1.2

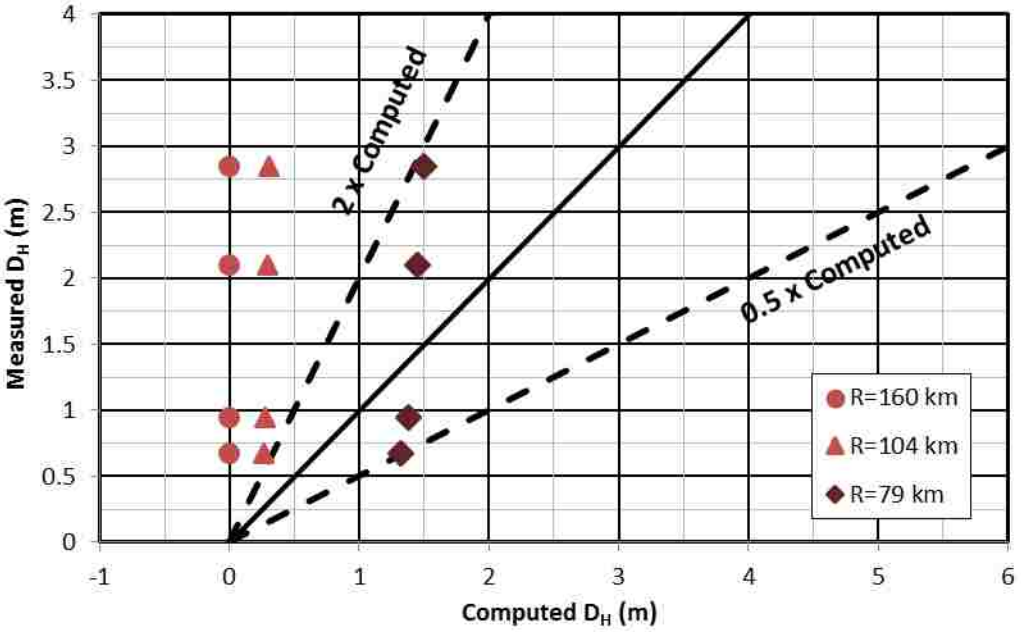

Figure 50. Comparison of Bardet et al. (2002) free face method predicted vs. measured displacement for various R values.

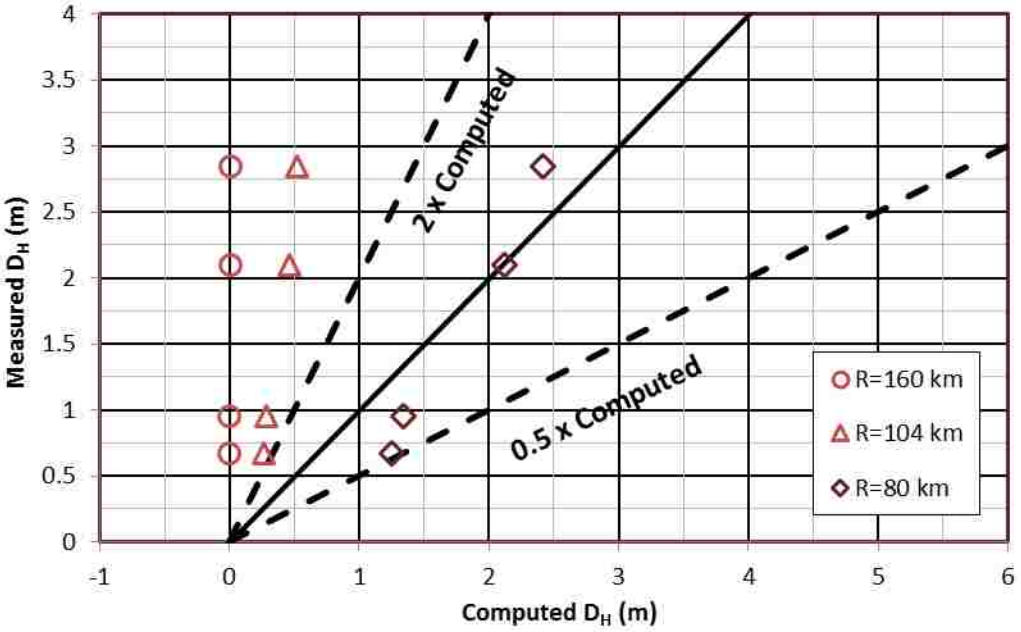

Figure 51. Comparison of Bardet et al. (2002) gentle slope method predicted vs. measured displacement for various R values.

All displacement points from Port Cornel analyzed with the Bardet et al. (2002) method from this study and Tryon (2014) are shown in Figure 58. All predictions are within a factor of two of measured displacement, with a reasonable skew around the line of equal predicted and measured displacement.

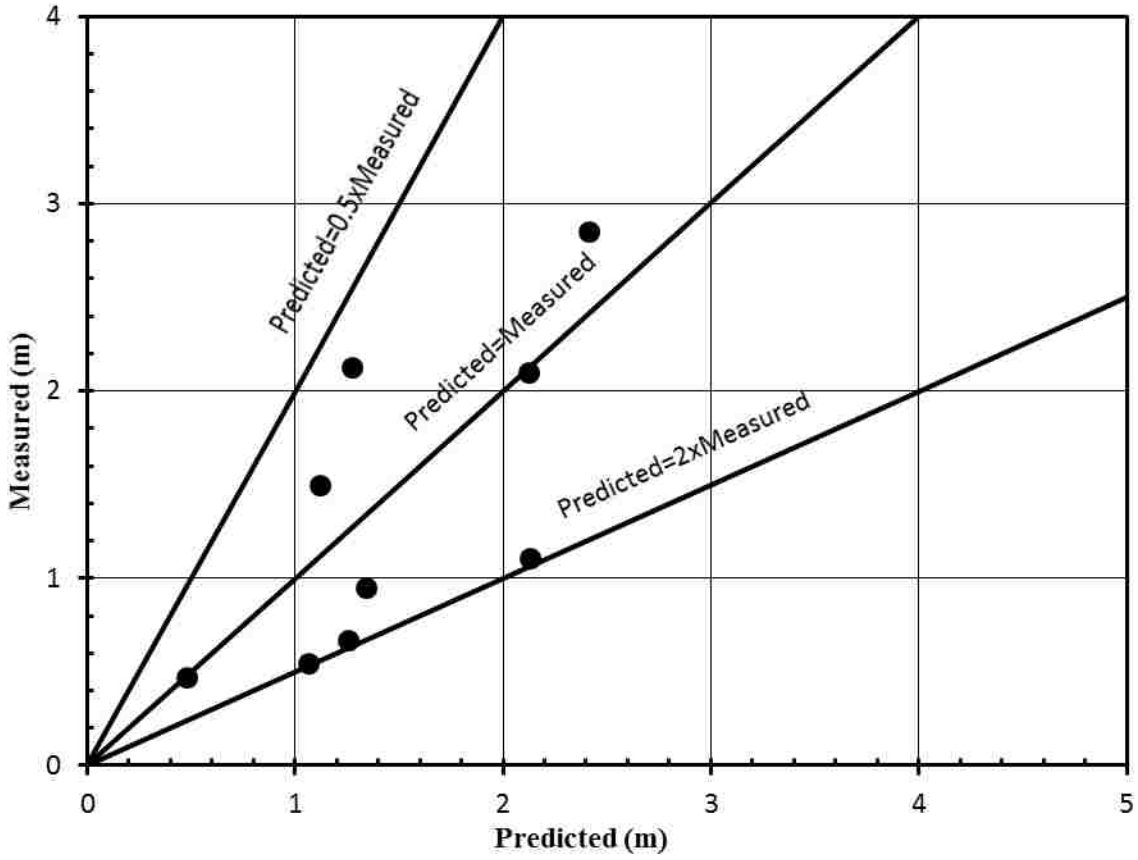

Figure 52. R = 80 km Bardet et al. (2002) predictions for the Lo Rojas and Tryon (2014) sites in Port Coronel.

3.6.4 Lateral Spread Evaluation using Zhang et al. (2012)

To complete the Zhang et al. (2012) model, Chilean strong ground motion attenuation relations proposed by Contreras & Boroschek (2012) are considered. Equation (3-1) estimates spectral acceleration at a period of 0.5 ($SA_{0.5\ s}$) with 5% damping, where M_w is the moment magnitude, H is the focal depth in kilometers, and Z = 0 for rock or Z = 1 for soil. R in kilometers is calculated with equation (3-2).

$$\log(SA_{0.5\ s}) = -2.1228 + 0.3208M_w + 0.0094H - 0.0008R - glog(R) + 0.2834Z \quad (3\text{-}1)$$

$$R = \sqrt{R_{rup}^2 + \Delta^2} \quad (3\text{-}2)$$

R_{rup} is the closest distance to the rupture surface in kilometers, Δ is the near source saturation term described in equation (3-3) and g is the geometrical spreading coefficient in equation (3-4):

$$\Delta = 0.0734 * 10^{0.3552M_w}, \quad (3\text{-}3)$$

$$g = 1.5149 - 0.103M_w, \quad (3\text{-}4)$$

Spectral Displacement (SD) in m is estimated from spectral acceleration by dividing $SA_{0.5s}$ by $(4\pi)^2$. A focal depth of 30 m for the Maule Chile earthquake reported in Contreras & Boroschek (2012) is confirmed from recorded depths listed in Table 6 in section 3.1. A distance of 50 km from Delouis et al. (2010) is used for R_{rup} and Z is assumed to be 1 as site conditions resemble soil over rock. $SA_{0.5s}$ is then estimated to be 0.91 g or 8.92 m/s^2 with SD at 0.054 m. Parameters used for Zhang et al. (2012) are in Table 15 while Figure 53 compares measured and predicted displacements. Both the slope based and free face based methods provide reasonable predictions

of displacement, yielding predictions within a factor of two for three of the four measured displacements considered; however, the slope based method provides a closer prediction of maximum measured displacement.

Table 15. Zhang et al. (2012) Model Parameters for Lo Rojas Site

	Parameters
SD (m)	0.057
T_{15} (m)	8.7
F_{15} (%)	4.2
$D50_{15}$ (mm)	0.46
S_{gs} (%)	Varies, see section 3.6.1.2
W_{ff} (%)	Varies, see section 3.6.1.1

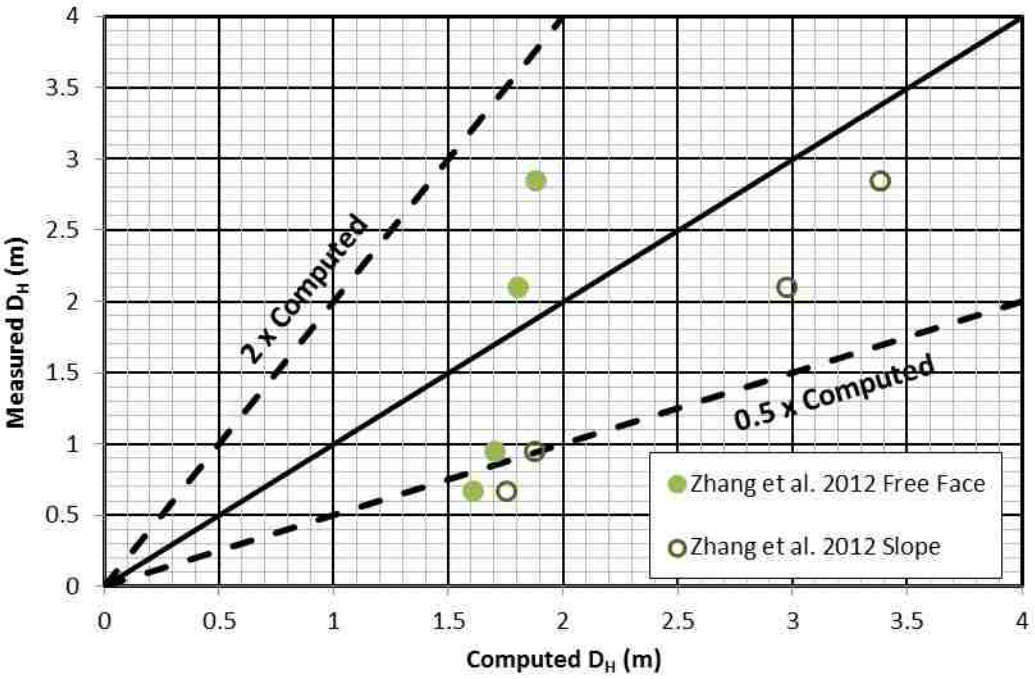

Figure 53. Comparison of Zhang et al. (2012) predicted vs. measured displacement.

All displacement vectors from Port Cornel analyzed with the Zhang et al. (2012) method from this study and Tryon (2014) are shown in Figure 54. The Zhang et al. (2012) method

underpredict measured displacement for most measured displacement vectors, with only two overpredictions of measured displacement out of ten measured displacement vectors. Seven predictions are within a factor of two of measured displacement, with three predictions conservatively underpredicting measured displacement outside a factor of two of measured displacement.

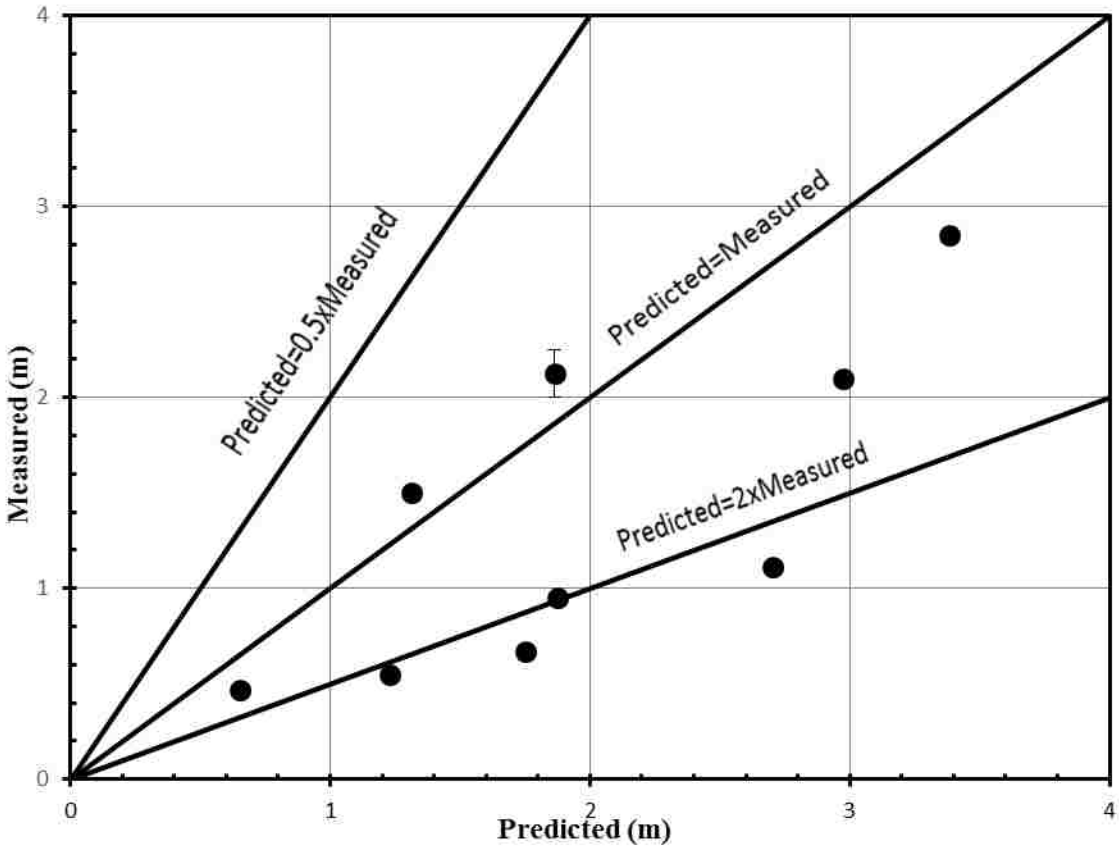

Figure 54. Zhang et al. (2012) predictions for the Lo Rojas and Tryon (2014) sites in Port Coronel.

3.6.5 Lateral Spread Evaluation using Faris et al. (2006)

Values used in the Faris et al. (2006) model are shown in Table 16. The value α is calculated using the combination case, since both a free face and sloping gradient of the ground surface appear

present. The length of the free face is calculated from the place the liquefiable layer becomes visible on the free face to the beginning of the lateral spread line, which for this case is the same as the Youd et al. (2002) free face length. Faris et al. (2006) considers the liquefiable layer thickness based on the CSR instead of SPT $(N_1)_{60}$<15, but the two thicknesses are identical in this instance. The average slope of the entire length of the lateral spread, or 2.73%, is used for the gentle slope gradient. As slope is found to provide an indiscernible contribution to DPImax at three significant figures when free face parameters are considered, other slopes are not attempted. The effect of α is also found to contribute insignificantly when compared to DPI and M_w, resulting in a predicted displacement value 0.2 m smaller when the α term is neglected.

Table 16. Faris et al. (2006) Model Parameters for Lo Rojas Site

Parameters	
H (m)	9.4
L (m)	68
S (%)	2.7
α (%)	57.8
M_W	8.8
DPI_{max} (m)	6.13

The computed maximum lateral spread displacement is compared to the measured value in Figure 55. Because Faris et al. (2006) defines a lateral spread to be one case when a semi-coherent mass of soil moves largely in one direction, similar to Rauch and Martin (2000), only maximum displacements are considered. The computed value of 6.13 is about 2.2 times greater than measured value. This overprediction of the lateral spread displacement by the Faris et al. (2006) approach in this case is similar that determined by Tryon (2014) for two lateral spread cases at the Port of Coronel south of this site, during the same earthquake.

Because predictions from Faris et al. (2006) appear to be conservative, the same reduction factor used by Cetin et al. (2009) for settlement was applied to DPI values in an effort to improve

agreement with measured displacement. A similar reduction factor for lateral spread displacements is implemented in the CLiq program and is recommended by Robertson to avoid excessive lateral displacements. The equation for the reduction factor (DF_i) from Cetin et al. (2009) is shown in equation (3-5). The term d_i represents the depth at the middle of each soil layer, and 18 meters was chosen by Cetin et al (2009) as the denominator because settlement below this depth is assumed to contribute negligibly to surface settlement. This equation can reasonably be applied to liquefaction as soil is more difficult to move laterally due to overburden pressure with increasing depth. When applied to reduce displacements from the Faris et al. (2006) method, a DF value is calculated for each layer then multiplied by the DPI for each layer before DPI is summed.

$$DF_i = 1 - \frac{d_i}{18\,meters} \tag{3-5}$$

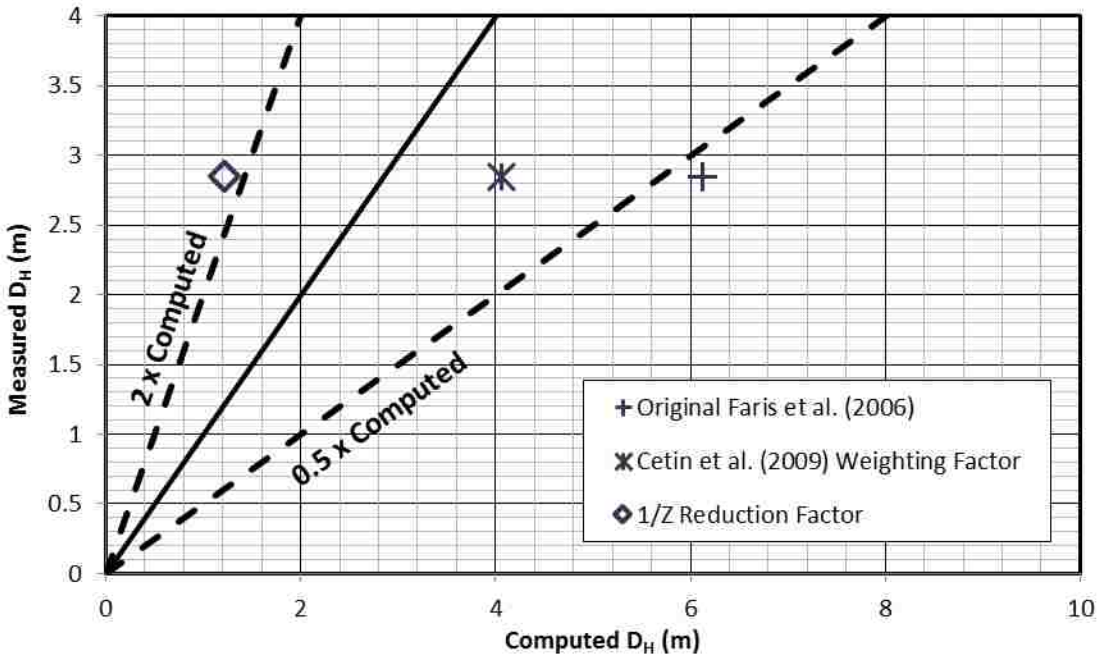

Figure 55. Predicted vs. measured displacement using Faris et al. (2006) model and a reduced modifications of the same model.

A reduction factor of 1/z was similarly applied to produce a third predicted displacement for comparison. This reduction factor has been suggested by van Ballegooy et al. (2013) based on experience with liquefaction induced settlement in Christchurch, New Zealand.

Both the original and reduced displacement predictions from Faris et al. (2006) are shown in Figure 55. Even with the Cetin et al. (2009) weighting factor reduction of the Faris et al. (2006) method the lateral displacement is still overpredicted; however, the predicted displacement is less than two times the measured displacement. In contrast, the 1/z reduction factor considerably under predicts, falling outside a factor of two of measured displacement. The Cetin et al. (2009) Weighting Factor reduction of the Faris et al. (2006) method results in the closest prediction to measured displacement. This result is consistent with findings from Tryon (2014) for lateral spreads at the Port of Coronel.

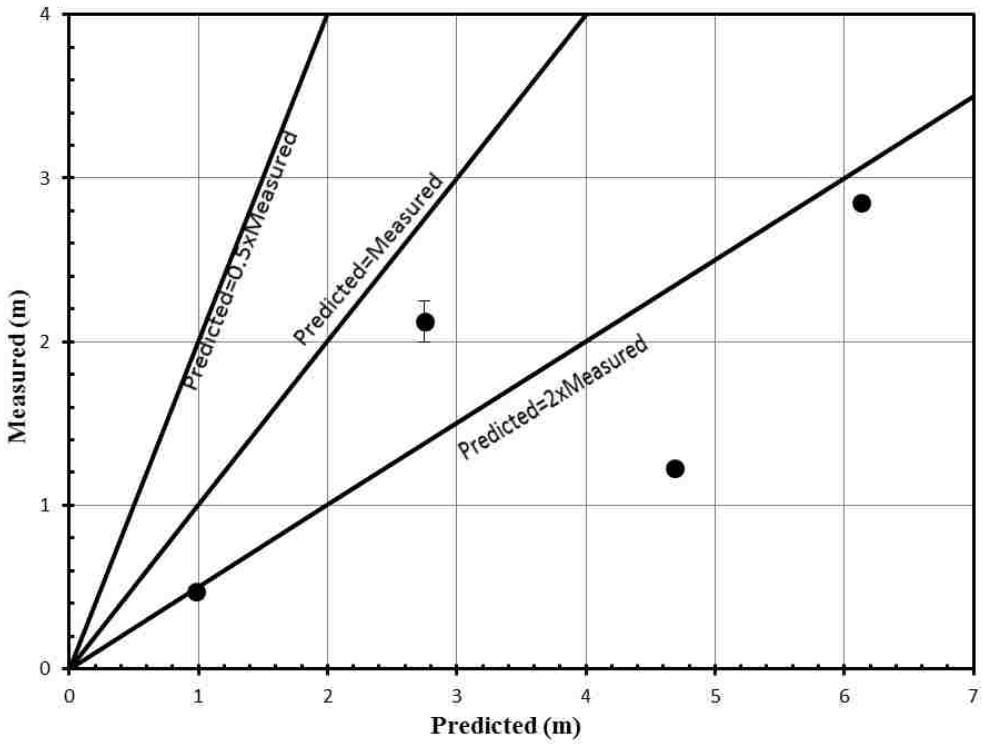

Figure 56. Faris et al. (2006) predictions for the Lo Rojas and Tryon (2014) sites in Port Coronel.

All displacement vectors from Port Cornel analyzed with the Faris et al. (2006) method from this study and Tryon (2014) are shown in Figure 56. All predicted displacements are overpredictions of measured displacement, with only one displacement prediction within a factor of two of measured displacement.

3.6.6 Lateral Spread Evaluation using Zhang et al. (2004)

The program CLiq v.1.7.6.34 developed by GeoLogismiki Geotechnical Software in collaboration with Peter Robertson (http://www.cpt-robertson.com) and Gregg InSitu. Inc. (http://greggdrilling.com) applies the Zhang et al. (2004) method. The program installer and user's manual can be found at www.geologismiki.gr. CPT data can be imported directly from a text file, but in this case was imported first into CPeT-IT, a companion program developed by the same parties, then exported to CLiq.

Depth, tip resistance, sleeve friction, and pore pressure are the required inputs from CPT testing. The depth to the GWT is also input manually. Options and settings selected in "Liquefaction assessment parameters" are shown in Figure 57 through Figure 61 for CPT5. Options modified in subsequent runs are specified.

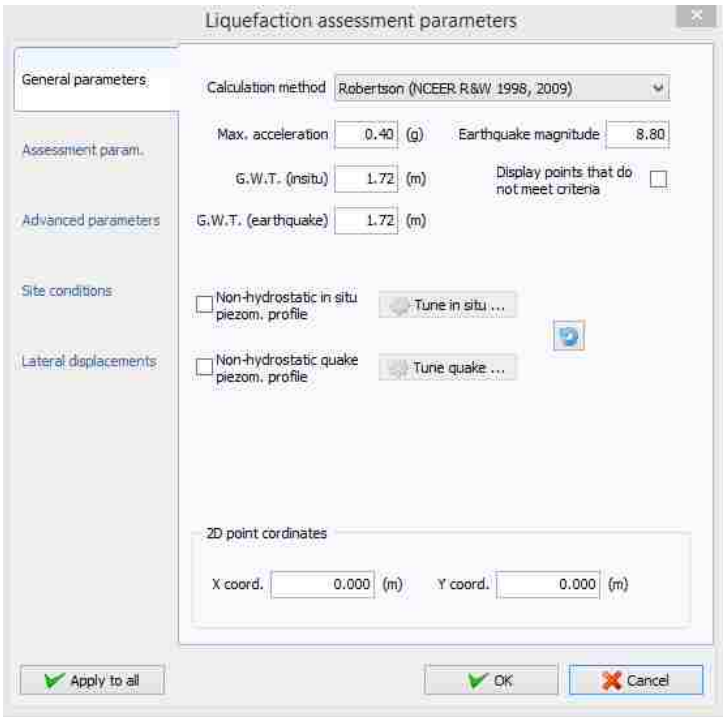

Figure 57. General parameters for liquefaction assessment in CLiq.

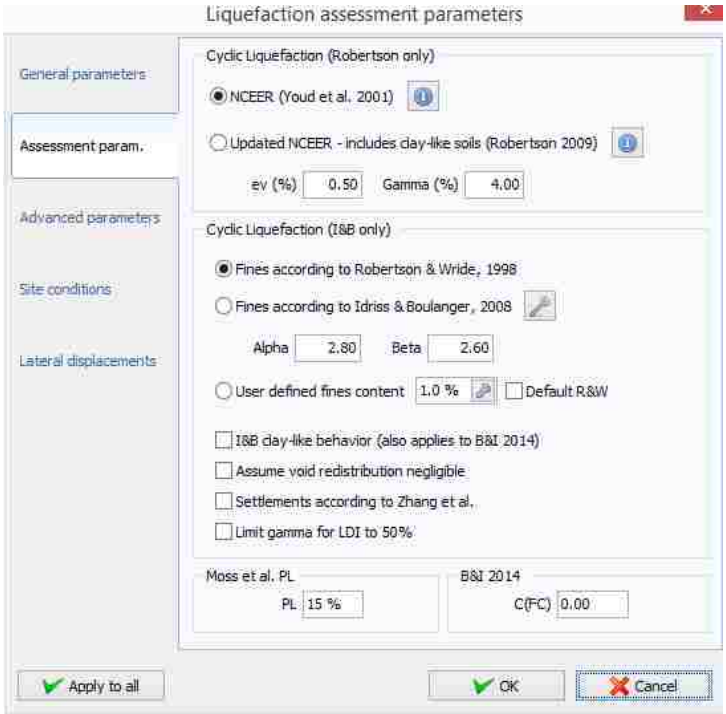

Figure 58. Assessment parameters for liquefaction assessment in CLiq.

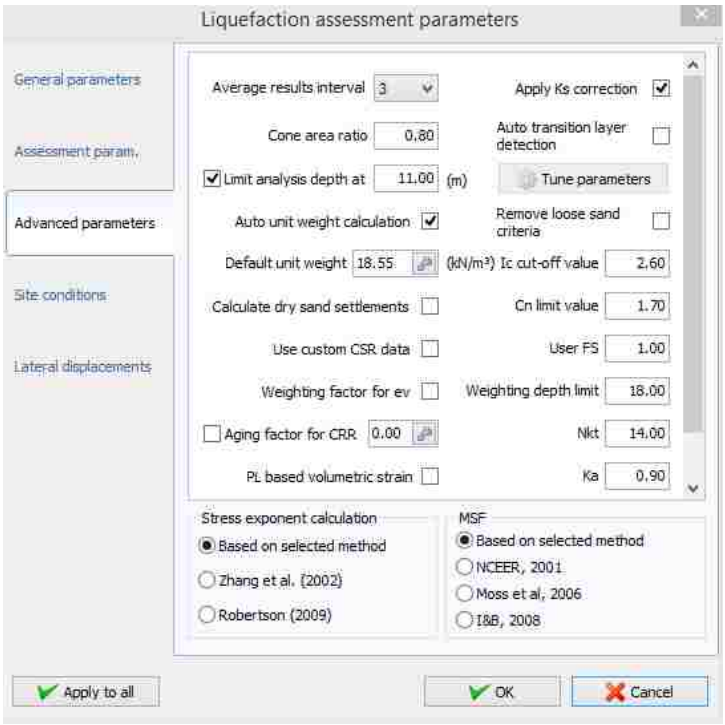

Figure 59. Advanced parameters for liquefaction assessment in CLiq.

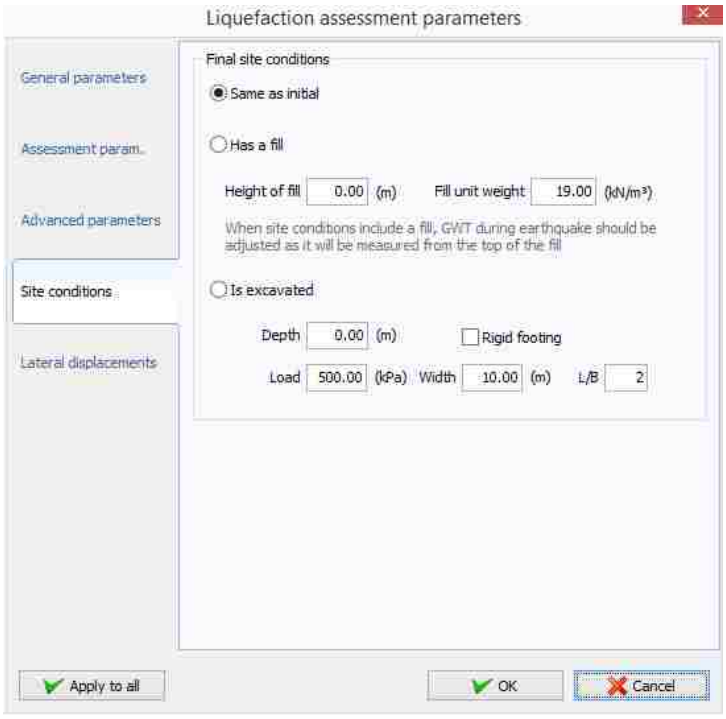

Figure 60. Site conditions for liquefaction assessment in CLiq.

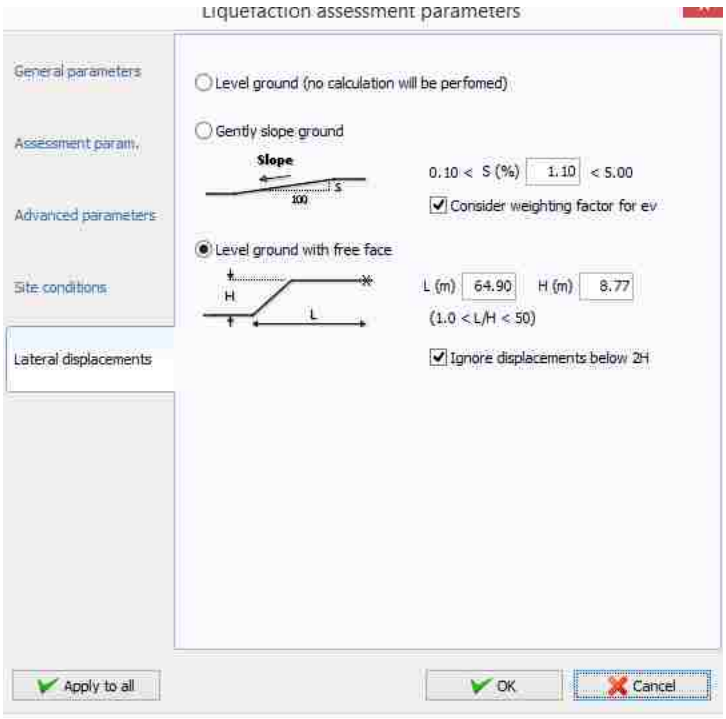

Figure 61. Lateral displacement parameters for liquefaction assessment in CLiq.

The GWT found during SPT testing is used, as it is frequently more reliable since it can be physically observed instead of interpolated. Seismic parameters discussed in the section 3.2 are included, and the NCEER 2001 or Youd et al. (2001) liquefaction method is used as recommended by Zhang et al. (2004), though other options are available within the program. The default was used for most parameters during the first run, with the exception of depth limits and site geometry. Options to automatically calculate unit weight and apply a K_σ correction for overburden strength were selected in the default version, as shown in Figure 59. Depth is limited to the base of a consistent layer with a factor of safety less than 1.0, which is 10.5 m for both CPT5 and CPT6. The factor of safety against liquefaction calculated for CPT5 were shown in Figure 37 and for CPT6 in Figure 38 in the liquefaction triggering section.

Both the free face and gentle slope cases are examined. The free face height and length are the same as those obtained for the Youd et al. (2002) method, shown in Table 11: L (km) is from the base of the free face base to the start of the lateral spread line; H (m) is from the base of the free face to nearest point of the lateral spread line. The slopes input into CLiq represent average slope over 20 m at each displacement point considered, the same values used for the Youd et al. (2002) method shown in Table 12. Since Zhang et al. (2004) method restricts slopes to below 5%, a slightly reduced slope of 5% is used in CLiq instead of 5.5%.

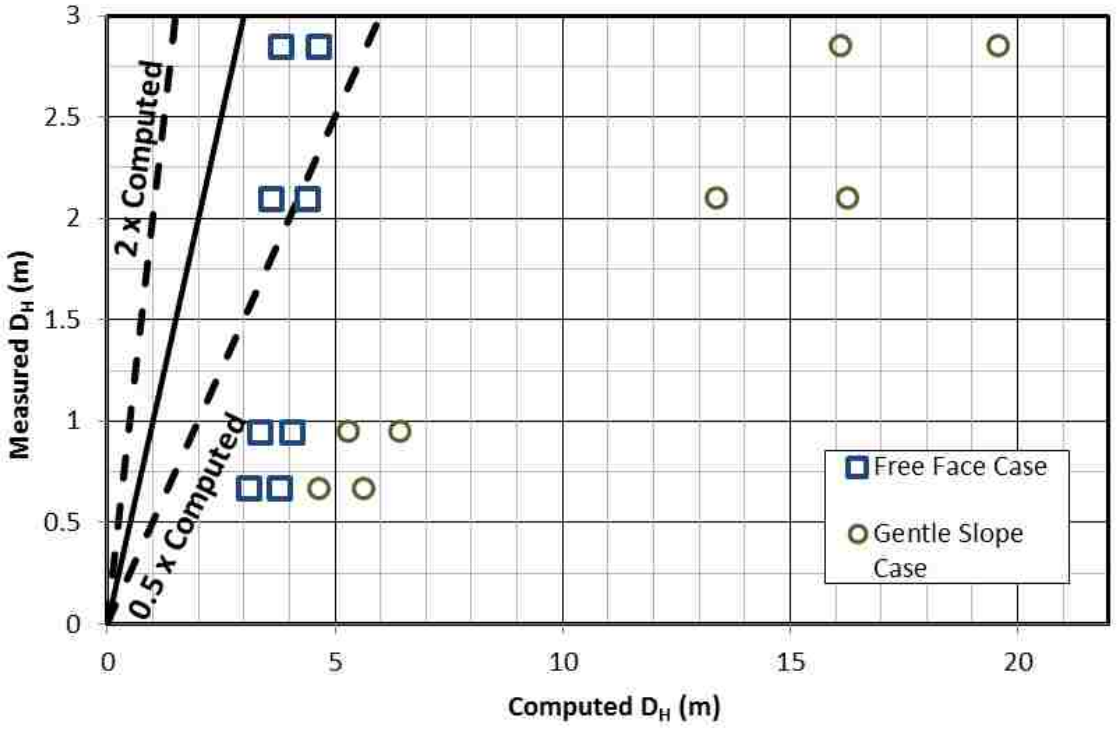

Figure 62. Original CLiq predicted displacement from CPT5 and CPT6 data without any depth weighting factors.

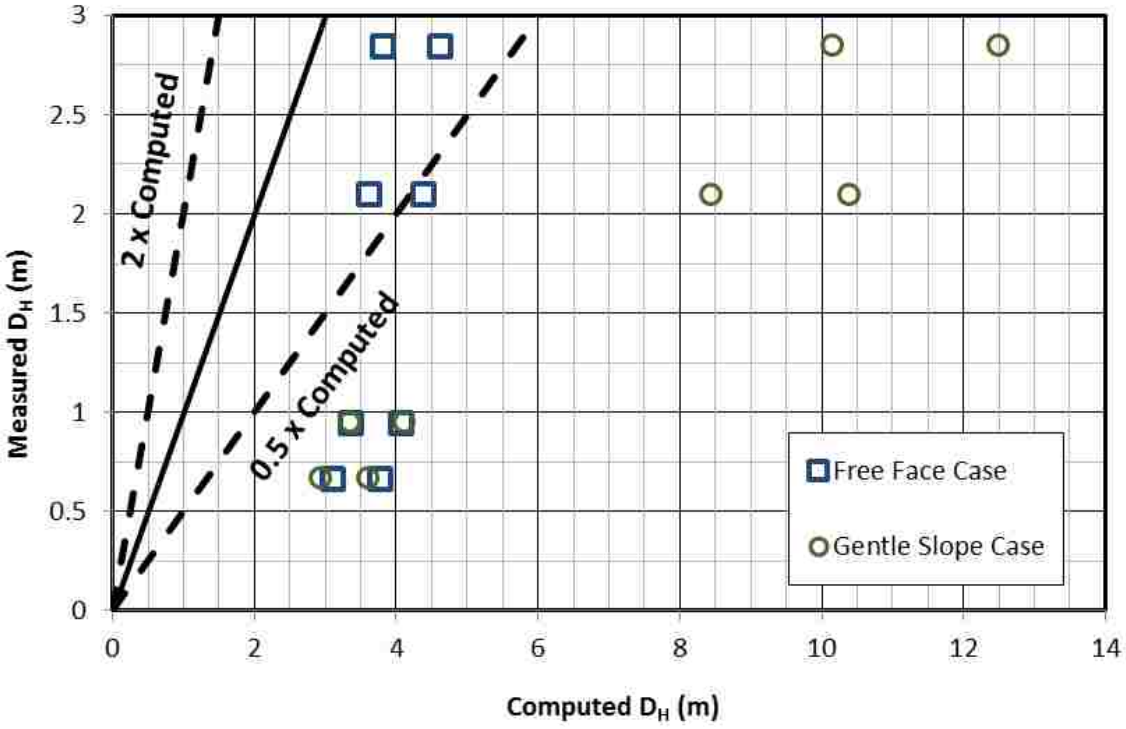

Figure 63. CLiq predicted displacement considering ε_v weighting factor.

Displacement predictions for these initial assumptions are shown in Figure 62 relative to the measured value. All the approaches overestimate the measured value; however for the two highest measured displacements, the predictions based on the free-face geometry are less than two times the measured value. For the slope based methods, predicted values were roughly 6 to 8 times larger than measured values.

Because the predictions based on slope geometry were generally high compared to the measured displacement, the depth (or ε_v) weighting factor defined by equation (3-5) was subsequently selected for all slope scenarios, as shown in Figure 63 relative to measured displacement. Free face predictions for Figure 62 and Figure 63 are the same because CLiq apparently does not apply the depth weighting factor for this geometry. Again, all approaches overperdict measured displacement, with only the free-geometry computing predictions less than

two times the measured value. However, predicted values for the slope based methods are improved slightly when the ε_v depth weighting factor is applied, predicting values roughly 3.5 to 5.5 times larger than measured values instead of 6 to 8 times larger when no depth weighting factor is applied.

Because CLiq continues to over predict even after including the ε_v depth weighting factor, the influence of the Auto Transition option was subsequently investigated. The Auto Transition option eliminates predicted displacement from zones that are transitioning between sand and clay, according to user specification. Layers with I_C values between 1.70 and 3.00 with a fast enough rate of change such that delta I_C is greater than 0.1 are eliminated, as shown in red on the SBTn Plot for CPT 5 in Figure 64 and CPT 6 in Figure 65. A review of the data in Figure 64 and Figure 65 indicates that red layers are more pronounced for CPT 6.

The predicted values using the Auto Transition option are compared with the measured value in Figure 66. Generally, applying the Auto Transition option reduces the computed displacement obtained from CPT 6 and brings it more in agreement with the predicted the measured displacement. However, all predictions with the Zhang et al. (2004) method are still overestimating measured displacement. Although the addition of the ε_v depth weighting and Auto Transition options improve predictions, the slope based methods remain 3.5 to 5 times greater than the measured displacement. CPT6 always predicts more displacement than CPT5, regardless of Auto Transition or ε_v depth weighting options selected.

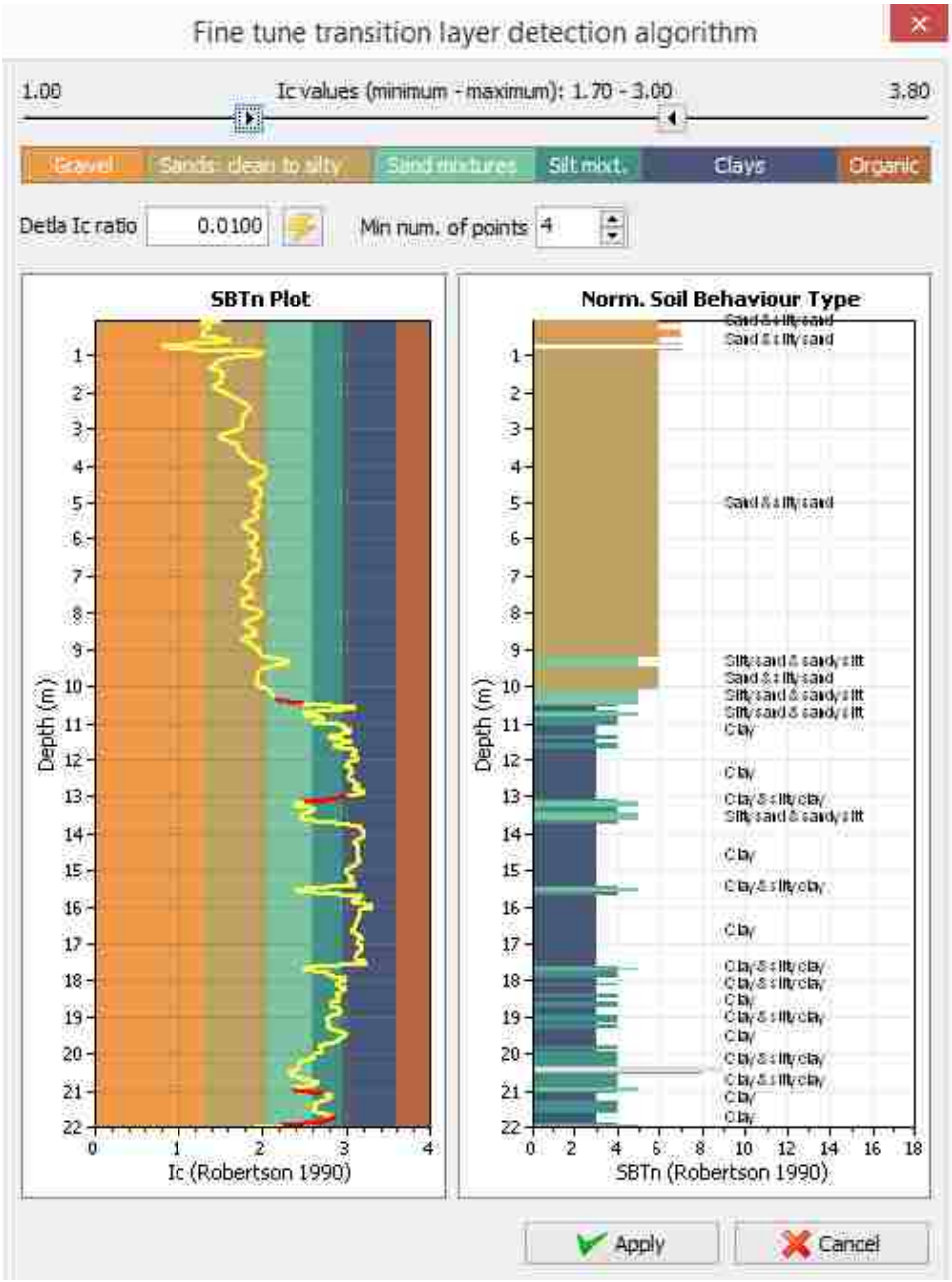

Figure 64. CLiq SBTn Plot and Auto Transition Zones (in red) for CPT5.

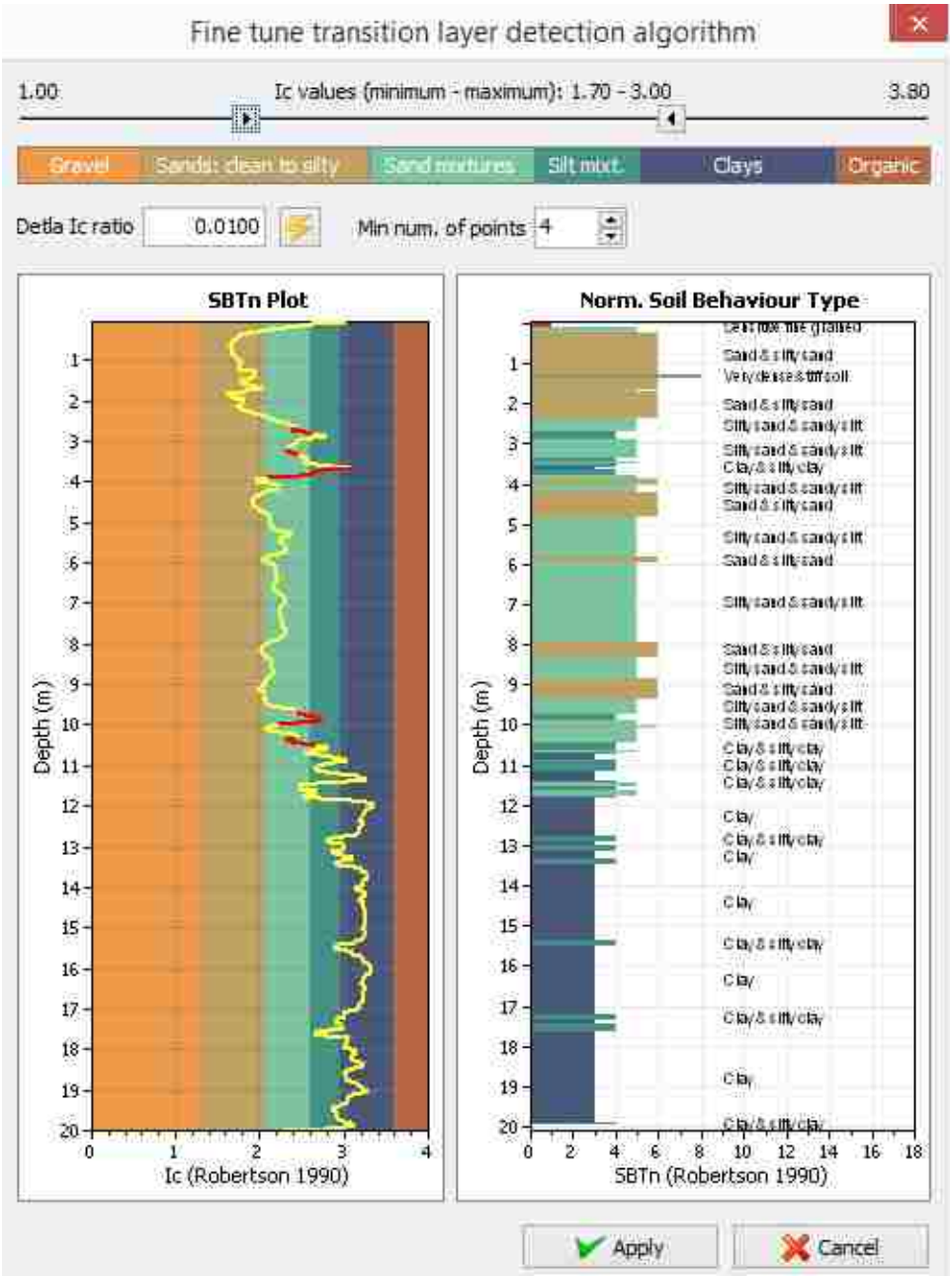

Figure 65. CLiq SBTn Plot and Auto Transition Zones (in red) for CPT6.

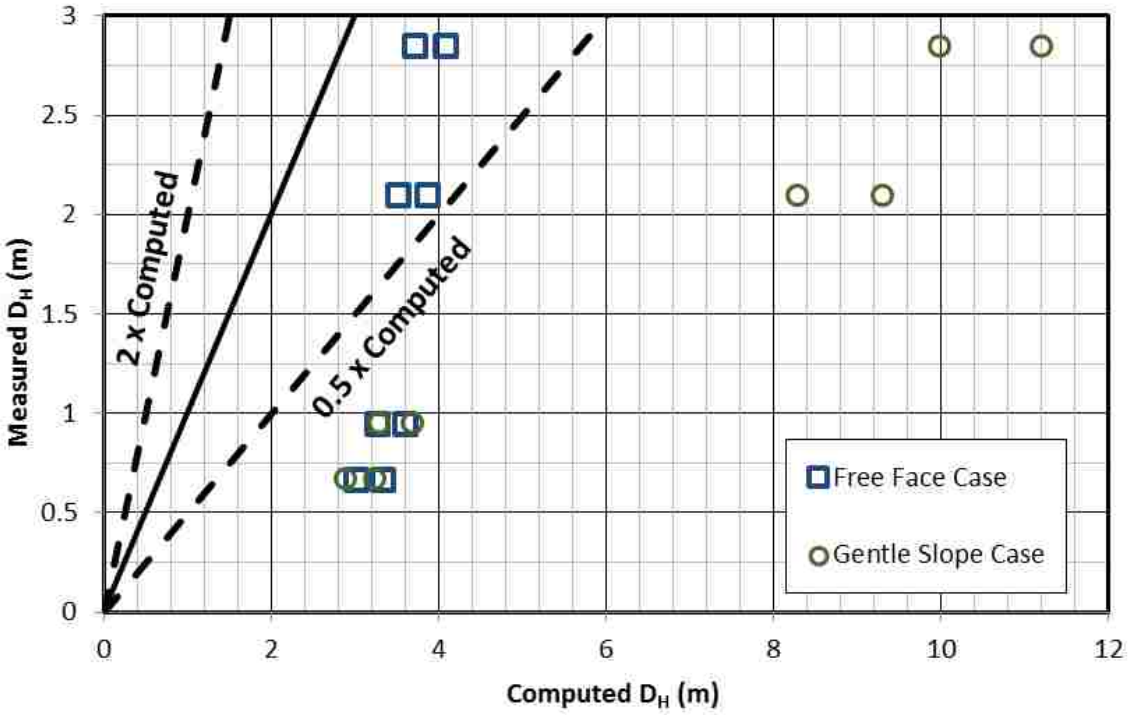

Figure 66. CLiq predicted displacement considering ε_v weighting factor and Auto Transition option.

As noted previously, the predicted displacements based on free face geometry are conservative but not unreasonable for the two highest measured displacements; however, for the two lower measured displacements, predictions using the free face based geometry are four to five times higher than measured displacements. Additionally, the overall geometry of the cross-section seems to resemble that of a slope somewhat more than a free face.

All displacement vectors from Port Cornel analyzed with the Zhang et al. (2004) method from this study and Tryon (2014) are shown in Figure 74. For the Lo Rojas site, the gentle slope case is used for comparison because this geometry is assumed to most closely resemble actual site geometry. All predicted displacements are overpredictions over a factor of two of measured displacement.

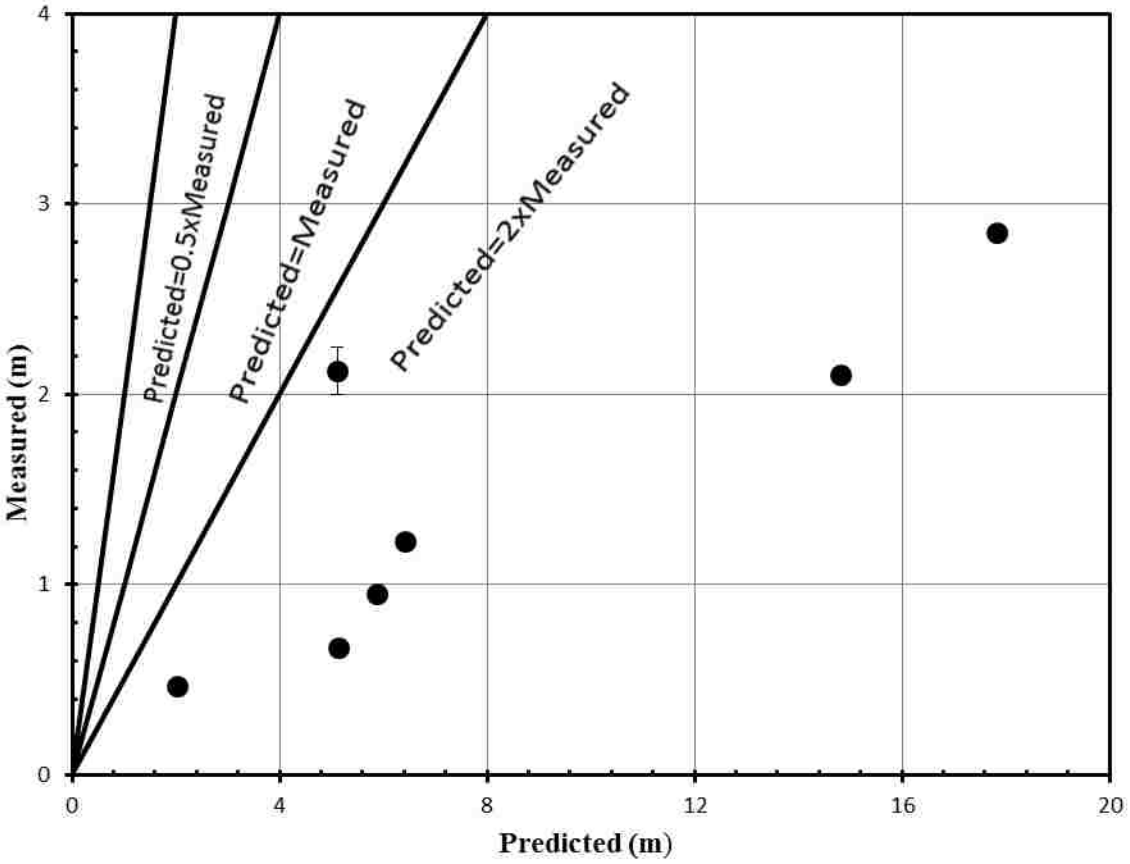

Figure 67. Faris et al. (2006) predictions for the Lo Rojas and Tryon (2014) sites in Port Coronel.

3.6.7 Comparison

For both Youd et al. (2002) and Bardet et al. (2002), the distance term has a huge impact on the amount of displacement predicted. If the equations are used as originally intended, R would be taken as zero because the fault ruptured below the site. However, this approach results in unrealistic over predictions. Substituting the distance to the maximum zone of uplift also results in an unrealistic over prediction, while substituting the distance to the surface fault rupture results in significant underpredictions for both methods. A distance of 104 km predicts displacements within a factor of two of measured displacement for the Youd et al. (2002) slope case if a smaller slope taken over the 20 m is used for each of the four considered displacement vectors. Predictions

corresponding to the three highest measured displacements are within a factor of two of measured displacement for the Youd et al. (2002) free face based method, with the predicted displacement corresponding to the smallest displacement vector falling just outside a factor of two of measured displacement. However, 104 km fit well for many of the sites in Tryon (2014). A value of 104 km represents a distance equal to about 65% of the length to the surface manifestation of the fault.

For both the free face and slope based versions of the Bardet et al. (2002) method, an R value of 79 to 80 km, or approximately 50% of the length to the surface manifestation of the fault, brings predicted displacement within a factor of two of measured displacement for all four displacement vectors considered. The only predictions within a factor of two of measured displacement found using R=104 km were the lowest two predictions. An R value of 160 km resulted in unrealistically high predictions over 8 m, and an R value of 47 km resulted in unrealistically low predictions bordering 0 m.

Even when the R value was assumed to be zero, the Rauch and Martin (2000) method resulted in significant under predictions if the true distance to the minimum factor of safety was used. However, if the distance to the bottom of the liquefiable layer was used, which has a factor of safety only 0.02 higher, the predictive capability is improved significantly.

Zhang et al. (2012) provides reasonable predictions, with both the free face and slope cases falling within a factor of two of the measured displacement. However, the slope case is a better predictor for this particular case history than the free face case.

Zhang et al. (2004) computed with CLiq consistently over predicts, particularly for the slope case. However, predicted displacement is reduced when options to linearly weight maximum shear strain with depth and automatically account for transition layers are selected. When applying the automatic transition option, predictions using the free face based method fall within a factor of

two from measured displacement for the two highest measured displacement vectors. Predictions for all slope based methods fall well outside a factor of two of measured displacements, even after strain depth weighting reductions and transition layer options are applied.

Faris et al. (2006) predicts more than twice the measured displacement. When the Cetin et al. (2009) weight factor originally used on settlement is applied to limit lateral displacement, as performed in CLiq and recommended by Robertson, predicted displacement is within a factor of two of measured displacement. A 1/Z reduction factor is also applied, as recommended by van Ballegooy et al. (2014), but predicts less than 50% of measured displacement.

3.6.8 Slope Stability Analysis

Field investigations of the Lo Rojas pier showed concrete cracks indicating that the soil displaced in blocks downslope toward a free face. In the event that a flow failure had occurred, a slump at the head of the slide with a flow of material downstream from the head would be expected, but was not evident during the time of the field investigation. However, had the evidence not supported lateral spreading as the primary mechanism for displacement, extremely low $(N_1)_{60\text{-}CS}$ values averaging around 6 in the liquefiable layer may have indicated a high likelihood of flow failure.

To investigate whether a flow slide would have been predicted, a slope stability analysis was performed to determine if the factor of safety would be less than 1.0 after liquefaction. The slope stability analysis was performed using the computer program UTEXAS4 developed by Stephen Wright at the University of Texas (Wright, 2004). Simplified layer profiles were entered into UTEXAS, as shown in Table 17, along with a simplified cross section elevations. The first layer is sand which is liquefiable below the water table. The sand layer is typically about 10.5 m thick, and saturated below a depth of 1.7 m. Two clay layers are also included, the first layer

extending from 10.5 to a depth of 18 m below the ground surface based on CPT-6 and the second from a depth of 18 m to a depth of 68 m below the ground surface. Bedrock is assumed at this depth of 68 m due to extremely dense material that prevented the SPT drill rig from advancing normally. Undrained shear strength values were estimated from CPT-5 and CPT-6 data using equation (3-6):

$$Su = (q_c - \sigma)/15 \tag{3-6}$$

Table 17. Slope Stability Model Parameters for the Lo Rojas Site

	Depth of Layer Base (m)	Su (psf)	Unit Weight (pcf)
Sand Layer	8.8	N/A	118
Upper Clay Layer	18	1284	110
Lower Clay Layer	68	5323	125

A residual undrained shear strength in the liquefied sand was obtained from correlations with $(N_1)_{60\text{-}CS}$ values proposed by Seed and Harder (1990) as shown in Figure 68. The average $(N_1)_{60\text{-}CS}$ in the liquefiable layer is 6, resulting in a residual strength of about 100 psf if a conservative estimate of the bottom third of the range shown in Figure 68 is assumed. A value of 150 psf falls about in the middle of the probable range proposed by Seed and Harder (1990), and 300 psf corresponds to the maximum proposed range. The saturated unit weight was assumed to be 118 psf for all cases.

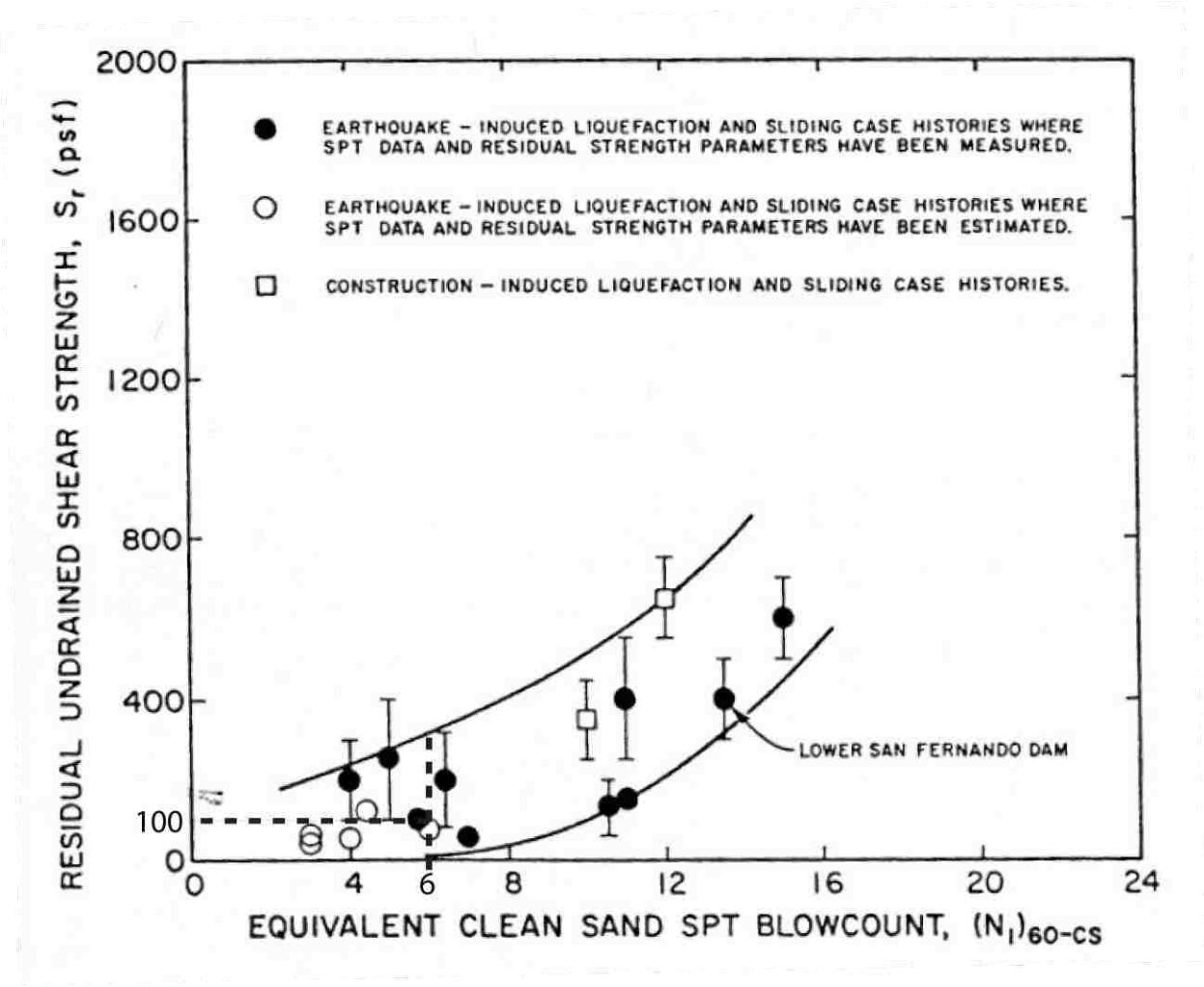

Figure 68. $(N_1)_{60\text{-}CS}$ and undrained residual strength from Seed and Harder (1990)

The UTEXAS model profile layout is shown in Figure 69. A sliding block failure along the base of the liquefiable layer as well as a circular failure surface were both examined, but only the latter is discussed as this failure mechanism had a smaller factor of safety. Using the more conservative estimate of residual undrained strength, the factor of safety against flow failure is 0.80. However, if the shear strength is increased to the average value of 150 psf from the Seed and Harder (1990) correlation, the factor of safety increases to 1.2. If the maximum residual shear strength from the Seed and Harder (1990) correlation is used, the factor of safety is computed to

be 2.4, which is well over one. This demonstrates that while a flow failure is not unreasonable, the assumption that a flow failure did not occur based on field observations is also supported based on the average residual strength. If the residual undrained shear strength is increased to 126 psf, the factor of safety against flow failure is one. The results of the model run using a residual shear strength of 126 are shown in Figure 70.

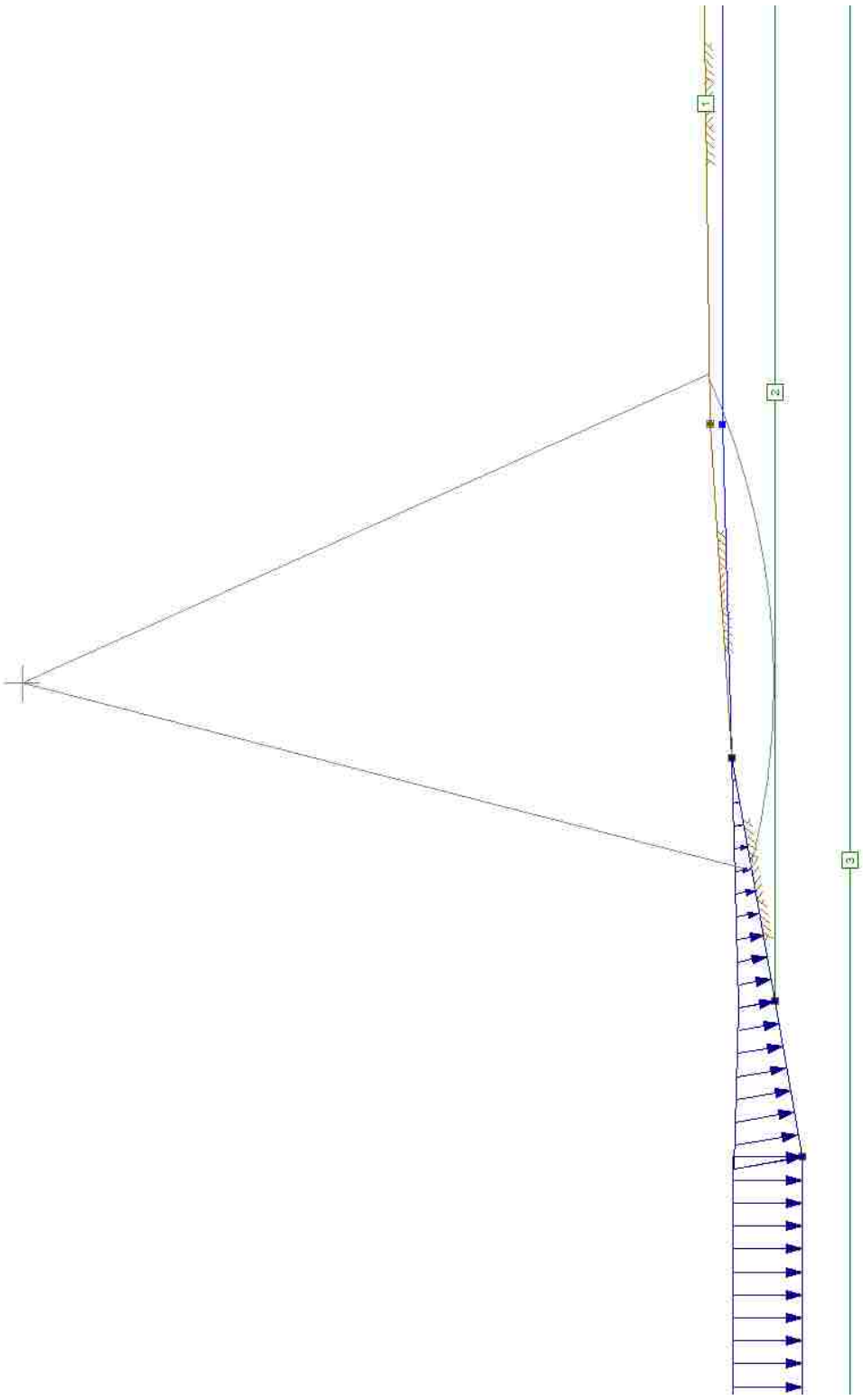

Figure 69. UTEXAS slope stability model cross section profile.

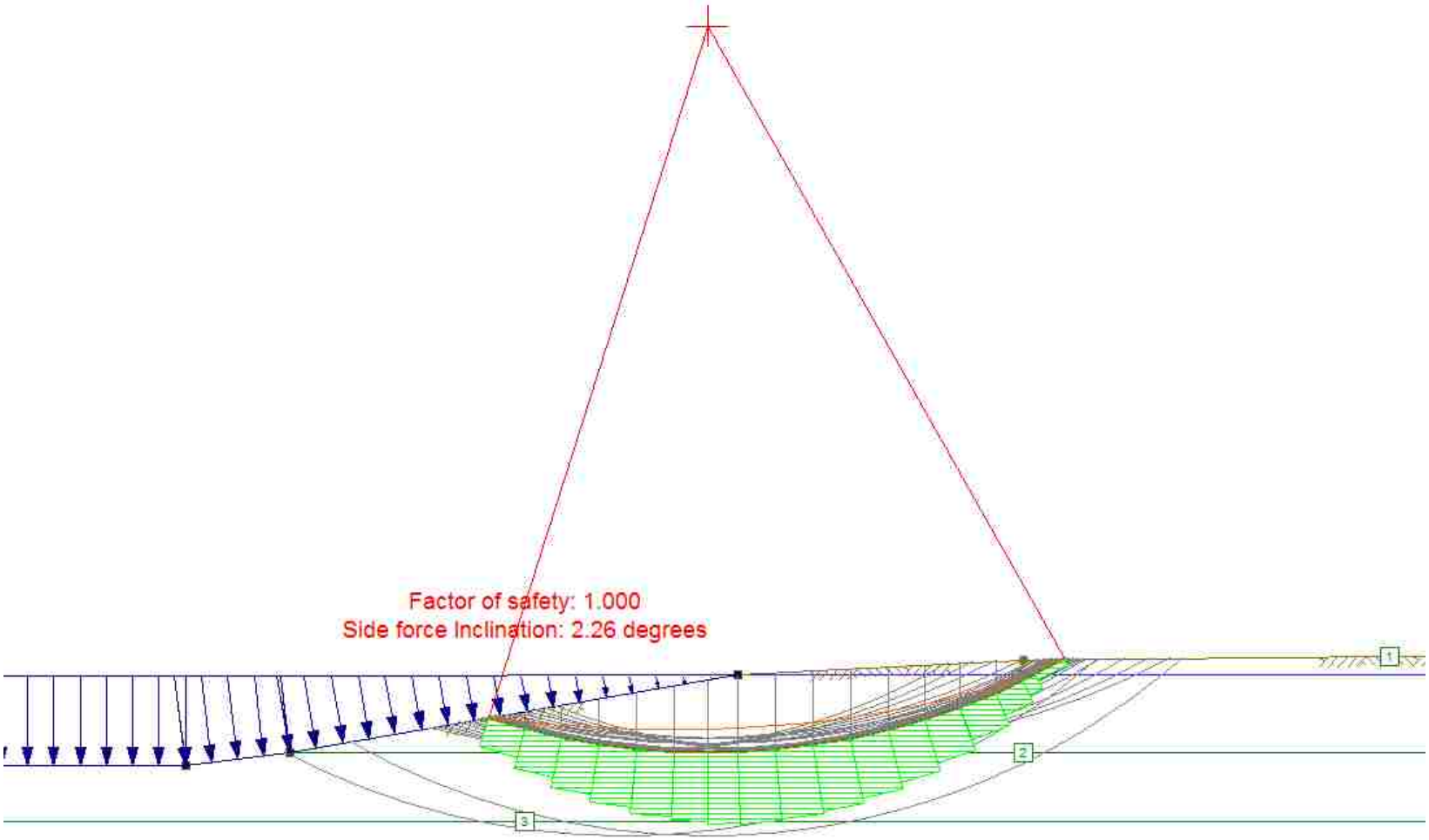

Figure 70. UTEXAS slope stability model failure surface using an undrained residual strength of 126 psf in the sand layer.

4 GRANELERO CASE STUDY

Terminal Granelero, or Granelero Port, also referred to as the Carbonero port, is a large pier on the south end of Port Cornel. This 1400 meter long pier contains a large pipeline to import and export large quantities of wheat, soy, corn, and coal (Puerto de Coronel, n.d.). Importing coal is an important function of the pier, as it supplies the thermoelectric plant Santa María owned by Colbún S.A (González and Verdugo, n.d).

4.1 Site Characteristics

Figure 11 shows the location of the Granelero pier in relation to the Lo Rojas pier and other piers in Port Coronel. Several tests were performed by EMPRO Ltda. and FCQ Geotechnical Engineering before construction of the pier in 2008, including 9 SPT borings. The pier was under construction on Feb. 27, 2010 when the earthquake hit Port Coronel, with no known displacements or damages noted (Verdugo, personal communication).

4.2 Seismic Parameters

Seismic parameters for the Granelero pier are the same as described for the Lo Rojas pier in section 3.2.

4.3 Cross-section Profile

The Granelero cross section profile is more clearly a free face scenario, as the best available data supports that the slope steepens near the shore then becomes relatively flat behind the retaining wall at the head of the pier. Elevation profile data is limited, but the fairly steep slope of 6.1 % between the nearest marine boring and on shore boring in addition to similarly steep slopes from the nearby South Pier indicate free face behavior can be expected (Tryon, 2014), as seen in Figure 72. The height of the free face is about 15.1 m, with a length between these points of 247 m, as interpolated from the vertical and horizontal distances between borings ET-1 and SM-1. Figure 72 from section 4.4 shows cross section data along with SPT blow count data from 10 borings.

4.4 Geotechnical Site Characteristics

Nine borings were performed by EMPRO Ltda. in Feb. 2008, eight in the ocean and one on shore. An additional SPT borings titled SPT-5 was performed on shore by JQ Engineering in April 2014 as a part of this study. Boring locations are shown in Figure 71, and corrected $(N_1)_{60}$ blow counts in Figure 72. The ground surface is assumed to follow the top of each borehole, and 0 m in elevation is assumed to be Mean Sea Level (MSL). The ground water table was recorded at about 3.6 m below the ground surface or an approximate elevation of 1.5 m for the 2008 on shore boring, and at about 4.2 m below the ground surface or an approximate elevation of 0.9 m for the 2014 boring.

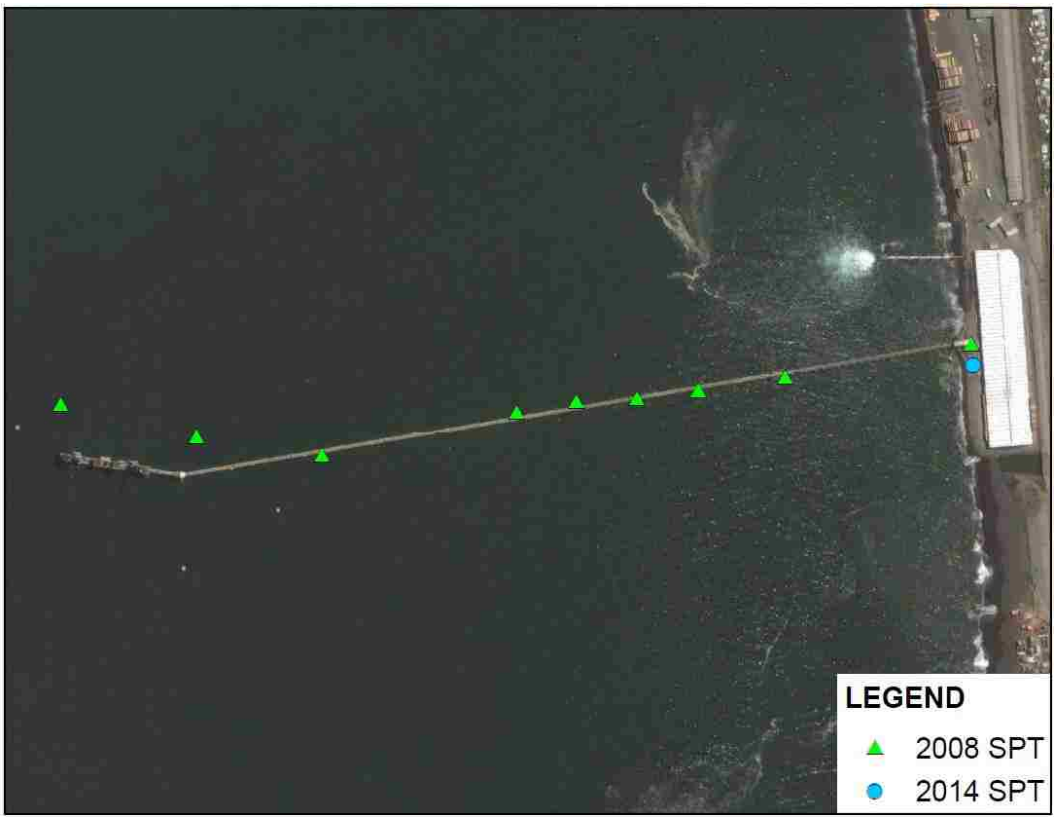

Figure 71. SPT boring locations from 2008 and 2014 at Granelero Pier.

Grain size and fines content data was not obtained for the 2008 data, so estimations are made from the USCS classification. Results are thus considered rough estimates due to a general lack of soil data. Fines content and water content tests were conducted on samples from borehole SPT-5, as shown in Table 18. Samples were not recovered at 8.3 and 12.3 m depths, so interpolations were made at these depths from the samples above and below this depth. Additionally, Atterberg Limit tests were performed on two samples between 14 m and 15.5 m below the surface, with results shown in Table 19.

Table 18. Gradation and Water Content Results from SPT-5 near Granelero Pier.

Sample Depth (m)	Fines (%)	Water Content (%)
1.3	3.4	0.5
2.3	1.8	7.5
3.3	4.3	0.8
4.3	1.9	0.8
5.3	4.9	2.5
7.3	2.8	10.1
8.3	3.5	8.4
9.3	4.3	6.8
10.3	4.2	7.2
11.3	4.5	13.8
12.3	2.3	3.4
13.3	2.3	3.4
14.3	11.4	5.2
15.3	22.5	21.7

Table 19. Atterberg Limit Results for Samples from Boring SPT-5

Sample Depth (m)	USCS Classification	Liquid Limit (LL)	Plastic Limit (PL)	Plasticity Index (PI)
14	SP-SC	32.4	22.8	9.6
15	SM	36.4	26.5	9.9

The soil layers are identified based on $(N_1)_{60}$ values and classification data. On shore, dense sand extends about 14 m below the ground surface to an elevation of approximately 9 m below MSL. The dense sand layer is underlain by a thin layer of loose poorly graded sand to sandy silt that becomes the seafloor surface and extends about 400 m off shore (see Figure 72). The loose sand layer is underlain by dense silt with high blow counts over 50 on shore, and alternating clay, sand and silt with relatively high blow counts off shore. The surface layer changes from sand to silt and clay beyond about 400 m from the shore surface but maintains low blow counts (< 15) for about 5 to 10 meters below the ground surface. This layer is underlain by denser silt, sands, and

clays. The exception to this pattern is boring S-7, which lies farthest from shore and exhibits loose sand and silt extending approximately 25 m below the surface.

The loose sand layer that lies underneath the dense sand on shore and extends through the seafloor surface represents a potentially continuous liquefiable layer which could lead to lateral spread. However, the continuity of the loose sand layer at this depth is called into question in a number of instances by the presence of non-liquefiable dense sand or clayey layers. For example, Borehole SM-8 approximately 270 m offshore shows sand with high blow counts over 30 from the ground surface to a depth of about 15 m below the surface, underlain by clay, which in turn is underlain by extremely dense silt that could not be penetrated during SPT sampling. Though the high density of the sand in this layer decreases the probability of a continuous layer of liquefied soil, liquefiable layers are present in borings on either side of SM-8 at approximately the same depth and potentially influenced soil behavior in this zone.

Measured PI values of 9 are greater than the limit of 7 proposed by Idriss and Boulanger (2004) which suggests the loose soil layer is unlikely to liquefy. However, because some authors suggest a more conservative PI value of 12 as a limit between cohesive and non-cohesive soil behavior (Bray and Sancio, 2006), liquefaction triggering and lateral spread equations were still evaluated.

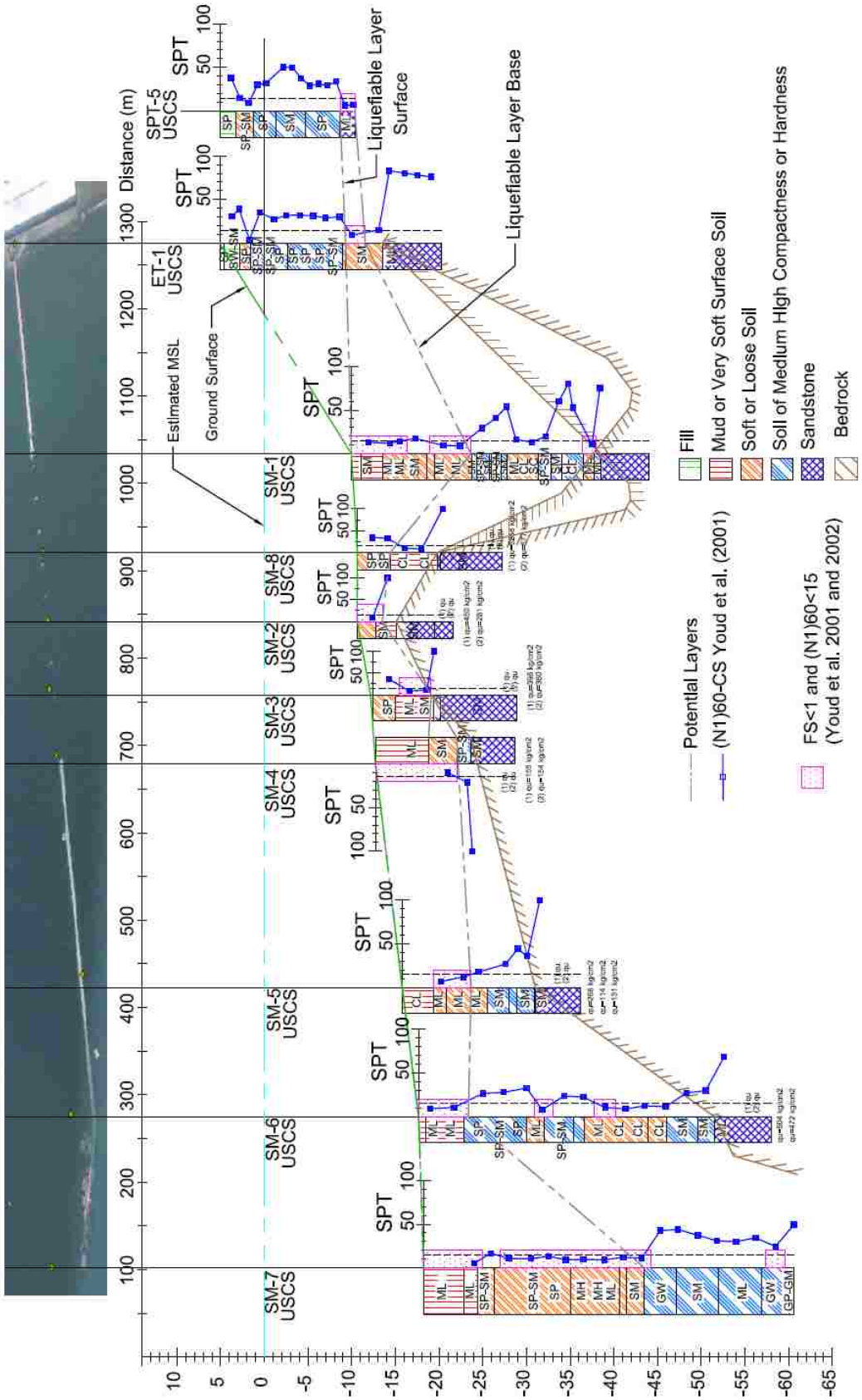

Figure 72. SPT data and liquefiable zones with SPT<15 near Granelero Pier.

4.5 Liquefaction Triggering

SPT data from all 10 boreholes was analyzed using the Youd et al. (2001), Cetin et al. (2004) and Idriss and Boulanger (2004) liquefaction triggering methods, with FS against liquefaction shown in Figure 73. Again, a peak ground acceleration of 0.40g and the appropriate magnitude scaling factors for the M_w 8.8 earthquake were applied.

As described in geotechnical site characterization (section 4.4), a layer of loose sand which covers the sea floor surface and is covered by about 15 m of dense sand on shore represents a potentially liquefiable layer that could lead to a lateral spread. This is consistent with the findings of all three liquefaction triggering methods. Layers indicating a FS less than 1 and a $(N_1)_{60\text{-}CS}$ less than 15 according to Youd et al. (2001) are outlined in magenta, and are considered to have a higher probability of producing lateral spread displacements. Bartlett and Youd (1995) indicate that no lateral spreads have been identified when SPT $(N_1)_{60}$ values were greater than 15 for M7.5 earthquakes. Other depths with FS values less than one that are shown in Figure 73 without an outlined had $(N_1)_{60\text{-}CS}$ values greater than 15 but less than 30, indicating a lower potential for lateral spread displacements.

The liquefiable layer is assumed to follow the loose sand layer from on shore through the layers with $(N_1)_{60}$ less than 15 in borings SM-1 and SM-2. The critical liquefiable layer is assumed to be the 2.3 m thick layer on shore overlain by dense sand which might also displace in the event of lateral spreading. Though a liquefiable layer can be drawn traveling through boring SM-8, the probability of liquefaction is decreased in this vicinity due to relatively denser sand indicated by blowcounts around 30. The Cetin et al. (2004) and Idriss and Boulanger (2004) methods calculate FS against liquefaction between 0.7 and 0.8 about 3.5 m below the surface, but this depth is considered non-liquefiable according to the Youd et al. (2001) method due to high blow counts.

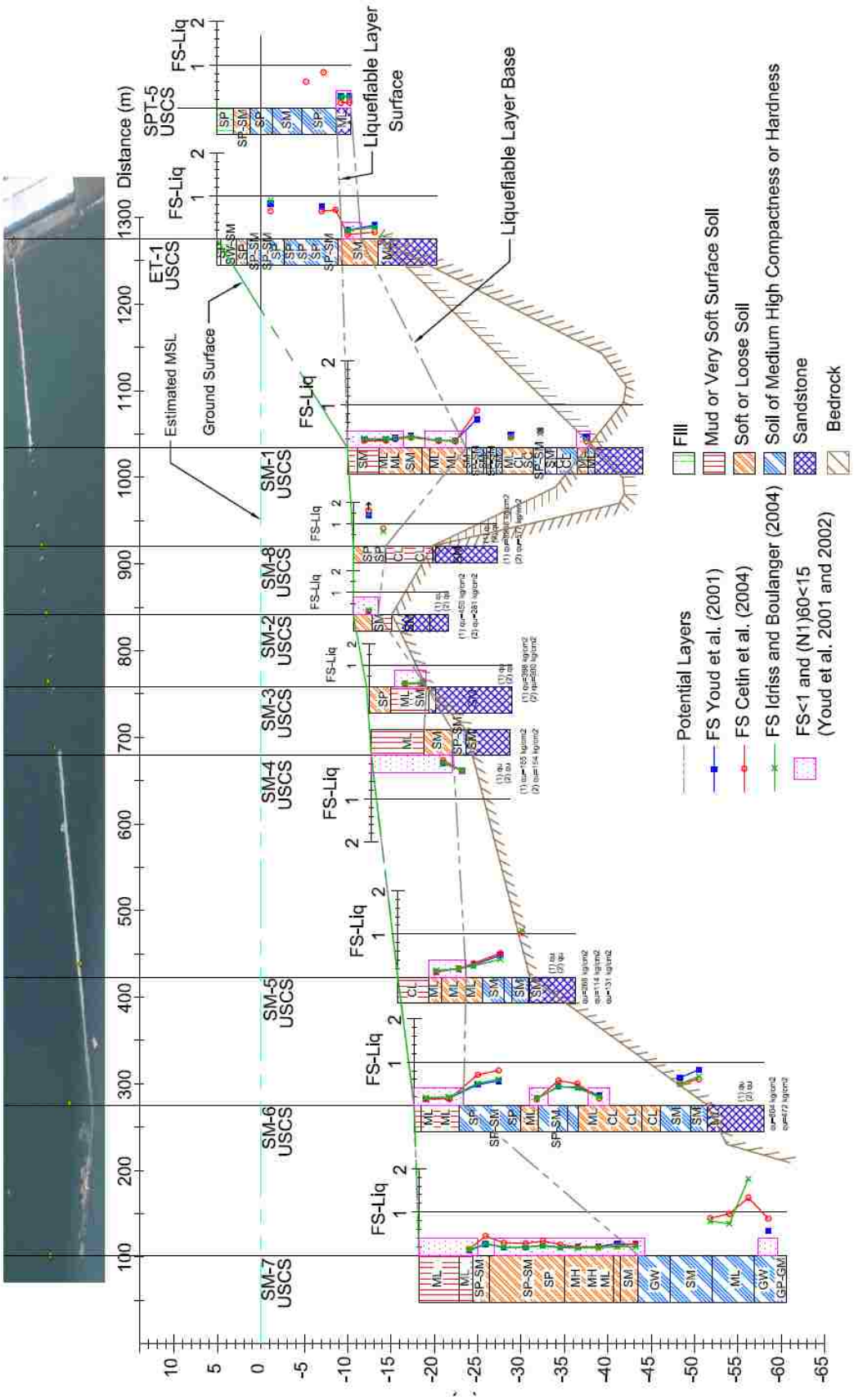

Figure 73. FS against liquefaction and zones with FS<1 and SPT<15 near Granelero Pier.

Though the presence of a high bedrock layer may have hindered lateral displacements, a potentially liquefiable layer is possible moving seaward from the bottom of boreholes SPT-5 and ET-1 through the top of borehole SM-2. Though no actual displacement occurred, this small layer is further analyzed for lateral spread potential to investigate the displacement predicted by the various analysis procedures.

4.6 Lateral Spread

All five SPT based methods analyzed in section 3.6 for the Lo Rojas pier are also analyzed for the Granelero Pier, including Youd et al. (2002), Rauch and Martin (2000), Bardet et al. (2002), Zhang et al. (2012), and Faris et al. (2006). Zhang et al. (2004) is not analyzed because no CPT data was collected for the Granelero pier.

4.6.1 Youd et al. (2002) Lateral Spread

All variables used for the Youd et al. (2002) method are specified in Table 20. As the best available data indicates that the Granelero pier resembles a free face, only the free face scenario is considered. T_{15} is the smallest observed thickness of the liquefiable layer which was observed in ET-1. Fines content is averaged from the two samples in SPT-5 in the loose sand layer, and $D50_{15}$ is calculated using a geometric average from the same samples, which are located about 15 m below the ground surface.

The free face ratio is estimated as the difference in height over the difference in length between borehole ET-1 and SM-1, the nearest boreholes to the free face. Again, R = 0.5 km produces an unrealistic prediction over 17 m, so the same variations in R were investigated as described in section 3.6.1 for the Lo Rojas pier. Table 21 and Figure 74 show predicted displacement against the observed displacement of 0 m.

All cases over predict, with an R value of R = 160 km providing the closest prediction to zero. An R value of 104 km predicts 0.3 m of displacement, while an R value of 47 significantly over predicts, estimating 3.27 m of displacement which is more displacement than actually observed for the Lo Rojas pier which failed.

Table 20. Youd et al. (2002) Model Parameters for the Granelero Site

Variable	Value
R* (km)	248.6
M_w	8.8
R (km)	Varies
R_0 (km)	155.6
T_{15} (m)	2.3
F_{15} (%)	16.9
$D50_{15}$ (mm)	0.56
W (%)	6.1
H (m)	15
L (m)	247
Z_T (m)	3.6

Table 21. Predicted Displacements for Various R using the Youd et al. (2002) Lateral Spread Method

R (km)	DH (m)
160	0.08
104	0.30
47	3.27

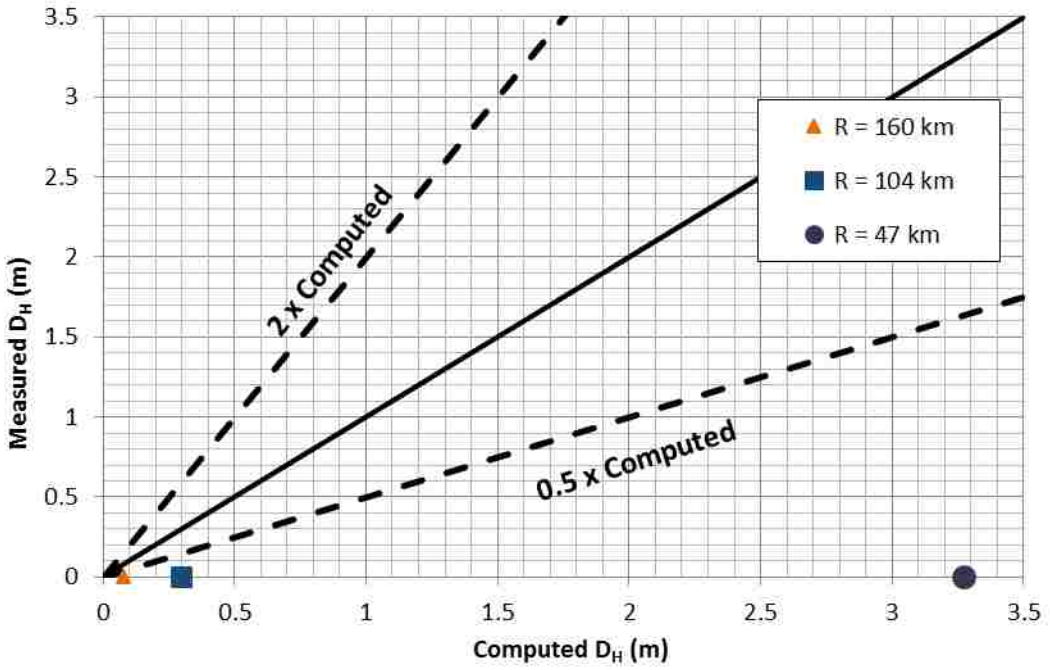

Figure 74. Predicted displacements for various R using the Youd et al. (2002) lateral spread method.

4.6.2 Rauch and Martin (2000) Lateral Spread

Parameters used for the Rauch and Martin (2000) EPOLLS model are shown in Table 22. All regional parameters are the same as listed in section 3.6.2 for the Lo Rojas pier. Since the pier did not move, L_{Slide} is assumed to be 0, and the free face height H_{face} is again assumed as the difference in height between boring ET-1 and SM-1. The ground surface behind the free face is assumed to be flat such that $S_{top} = 0$. Liquefaction analysis according to Youd et al. (2001) shows the minimum factor of safety of 0.19 occurs at a depth of 15.1 m from the surface in boring ET-1. The depth to the top of the ML layer observed in SPT-5 is used for Z_{liq}. Lateral spread predictions for various values of R are plotted against the observed displacement of zero meters in Figure 75.

The Rauch and Martin (2002) method predicts 0.48 m of displacement, which is more than likely occurred without reasonably noticeable evidence.

Table 22. Rauch and Martin (2002) EPOLLS Model Parameters for the Granelero Site

EPOLLS Model	Parameters	
Regional	M_w	8.8
	R_f (km)	0
	A_{max} (g)	0.4
	T_d (s)	120
Site	L_{slide} (m)	0
	S_{top} (%)	0
	H_{face} (m)	15.1
Geotechnical	Z_{FSmin} (m)	15.1
	Z_{liq} (m)	14

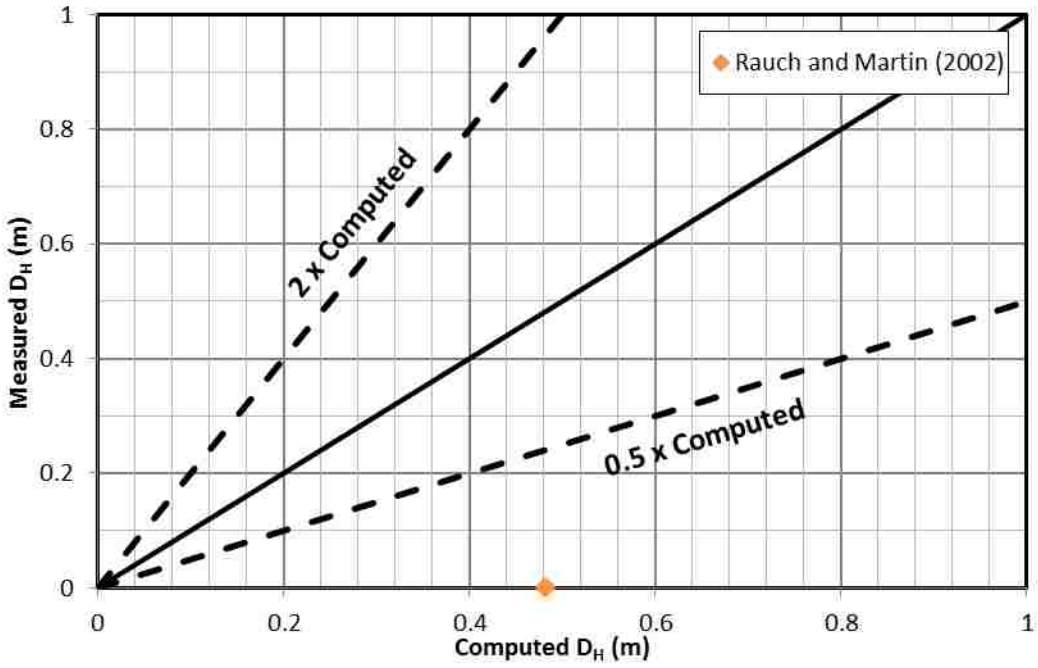

Figure 75. Predicted displacements for various R using the Rauch and Martin (2000) lateral spread method.

4.6.3 Bardet et al. (2002) Lateral Spreading

Parameters used for the lateral spreading analysis according to Bardet et al. (2002) are shown in Table 23. Again, only the free face scenario is considered and various values of R are

explored since R=0 produced unrealistic values. T_{15} and W values are the same as used for the Youd et al. (2002) method as described in section 4.6.1.

Predicted displacement versus the observed displacement of zero is plotted in Figure 76 for the same three values of R used for the Lo Rojas case study. An R value of 160 km produces negative displacement of -0.007 m, which is the closest prediction to zero. R = 104 km predicts about 0.09 m or 3.5 inches of displacement, while R = 47 again significantly over predicts 3.7 m of displacement.

Table 23. Bardet et al. (2002) Model Parameters for the Granelero Site

BARDET 2002 (Data set A)	
M_w	8.8
R (km)	Varies
T_{15} (m)	2.25
W (%)	6.10

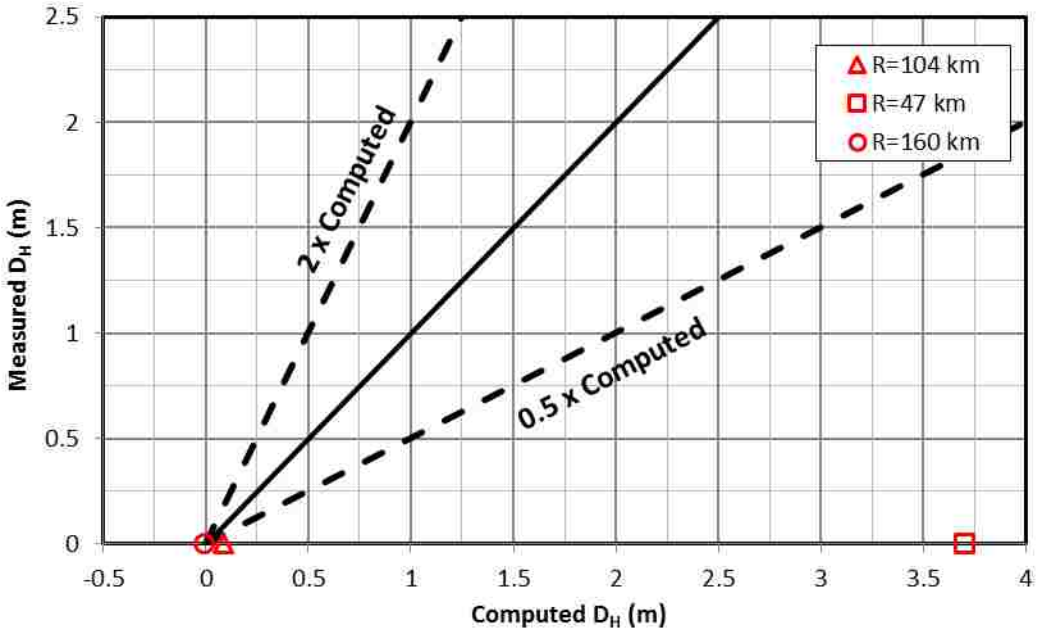

Figure 76. Predicted displacements for various R values using the Bardet et al. (2000) lateral spread method.

4.6.4 Zhang et al. (2012)

Parameters used for the lateral spreading analysis according to Zhang et al. (2012) are shown in Table 24. The same 0.054 m value of SD is used as calculated for the Lo Rojas pier in section 3.6.4. The same values of T_{15}, F_{15}, W and $D50_{15}$ that were calculated for the Youd et al. (2002) method were also used.

Table 24. Zhang et al. (2012) Model Parameters for the Granelero Site

Parameters	
SD (m)	0.054
T_{15} (m)	2.3
F_{15} (%)	16.9
$D50_{15}$ (mm)	0.56
W_{ff} (%)	6.1

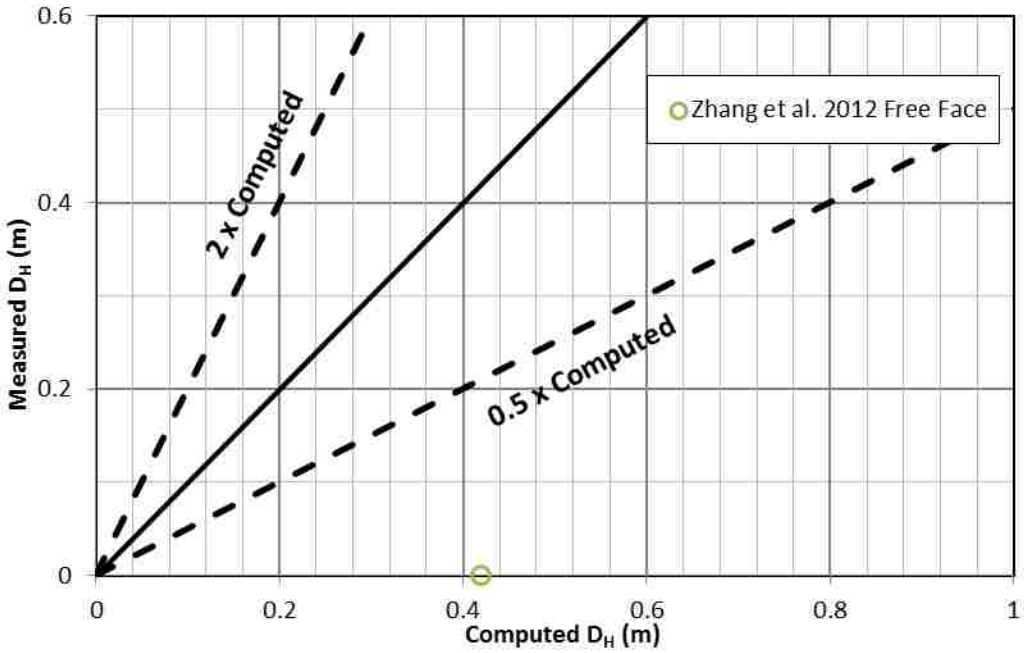

Figure 77. Predicted displacements for various R values using the Zhang et al. (2012) lateral spread method.

Zhang et al. (2012) also over predicts displacement with a value of 0.42 m, as shown in Figure 77, which is again over the amount that is considered reasonable without noticeable evidence.

4.6.5 Faris et al. (2006)

Values used in the Faris et al. (2006) model are shown in Table 25. The value α is calculated using only the free face case, with the length and height of the free face the same as used for the Youd et al. (2002) method. Figure 78 shows predicted displacement against the observed displacement of zero. In addition, displacements were computed using the same reduction factors that were applied to the Lo Rojas case study in section 3.6.5.

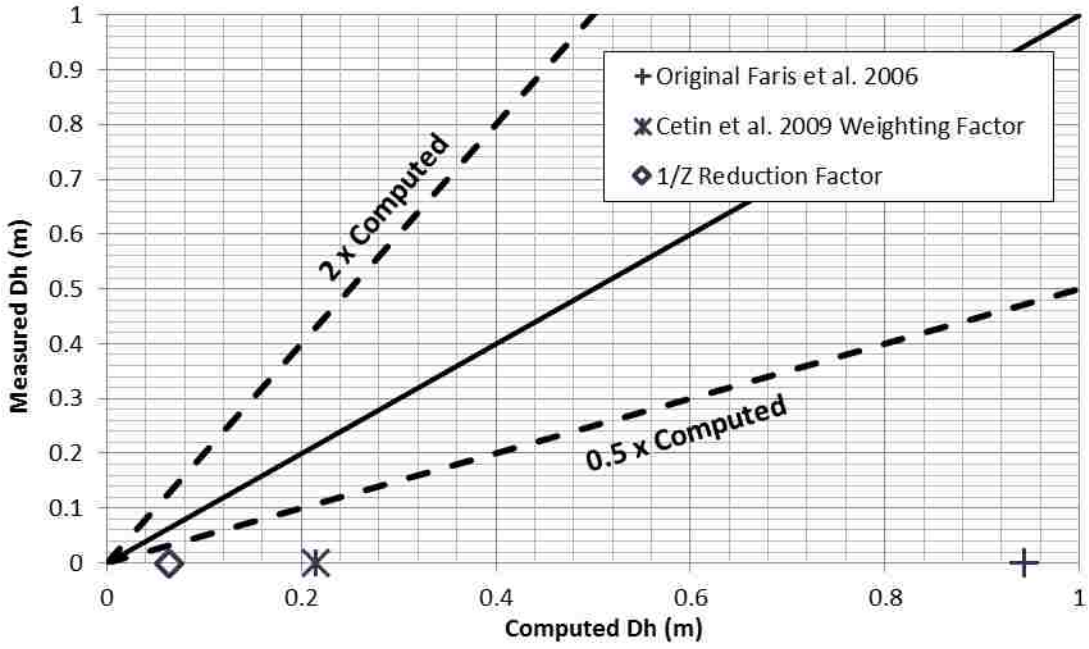

Figure 78. Predicted displacements for various R values using the Faris et al. (2006) lateral spread method.

Table 25. Faris et al. (2006) Model Parameters for the Granelero Site

Parameters	
H (m)	15.1
L (m)	247
S (%)	0.0
α (%)	24.4
M_W	8.8
DPI_{max} (m)	0.94

The prediction with the 1/Z reduction factor is closest to zero, predicting only 0.06 m of displacement. The prediction including the Cetin et al. (2009) ε_v depth weighting factor is the next best fit to observed displacement, predicting 0.21 m of displacement. The original method predicted a displacement of 0.94 m which is the highest prediction compared to observed displacement.

4.6.6 Discussion of Results

Results from each method are summarized in Table 26. As several methods include multiple predictions obtained by adjusting the distance parameter R or inclusion of reduction factors in the case of Faris et al. (2006), maximum and minimum values show the range of predictions. The Bardet et al. (2002) method resulted in the closest prediction; however, this prediction estimated displacement away from the free face. Youd et al. (2002) and Faris et al. (2006) both also provide close approximations, but also have maximum predictions that are much higher than likely occurred as no signs of displacement were apparent. The Youd et al. (2002) and Bardet et al. (2000) also produce gross over predictions of over 3 meters when using the lowest R value, which is much more displacement than was observed for even the failed Lo Rojas pier.

Table 26. Faris et al. (2006) Model Parameters for the Granelero Site

Method	Max. Prediction (m)	Min. Prediction (m)
Youd et al. (2002)	3.27	0.08
Rauch and Martin (2000)	0.48	0.48
Bardet et al. (2002)	3.70	-0.01
Zhang et al. (2012)	0.42	0.42
Faris et al. (2006)	0.94	0.06

Though all methods analyzed in this section result in significant over predictions, it is possible there are other reasons outside of the proper application of each lateral spread prediction method that no displacement was observed near the Granelero pier. Lateral spread analysis requires a consistent layer of liquefied soil. Some possible reasons that no displacement was observed, including reasons a consistent liquefiable layer may not have been present, are listed:

1. About 270 m off-shore and 350 m from the land borings, borehole SM-8 showed denser sand than the surrounding borings, with corrected $(N_1)_{60}$ values near 30, underlain by clay. It is possible the denser sand and clay in this layer prevented liquefiable layers found in boreholes SM-1, ET-1, and SPT-5 from moving.
2. A non-continuous soil layer may have existed, as boreholes provide only snapshots into the soil layering. The distance between boreholes ET-1 and SM-2 is about 400 m, and it is possible the soil layers changed significantly across this distance.
3. From the 2008 borings, there appears to be a fairly sharp increase in the elevation of the bedrock between SM-1 and SM-8, with SM-2 showing only about 4.5 m of soil above the bedrock layer. This high bedrock layer might have acted as a buttress against lateral spreading in the liquefied soil thereby preventing displacement.
4. Since the liquefiable layer on shore underneath the dense sand is at approximately the same elevation as the mud layer on the seafloor, it is possible this layer has similar

characteristics as the rest of the seafloor throughout Port Coronel. As observed in Tryon (2014), the seafloor mud is sometimes heterogeneous, showing pockets of clay and silt with a high plasticity index, as also observed in farther seaward borings near the Granelero pier. It is possible there were sufficient pockets of high plasticity soils that were not observed in the boring which did not liquefy and prevented the formation of a continuous liquefied layer necessary for lateral spread development.

5. Off-shore, the liquefiable layer consists primarily of very low $(N_1)_{60}$ values near the ground surface, occasionally overlain by very weak clay. Even if this soil layer displaced, it is possible the layer flowed around the piles supporting the pier without inducing enough pressure to cause any damage.
6. On shore, the dense sand layer above the liquefiable sand is about 15 m thick, with $(N_1)_{60\text{-}CS}$ values mostly around 30, ranging from 28 to 54. The shear strength from the upper layer of soil may have resisted displacement, even if the loose sand underneath liquefied and would have otherwise displaced.
7. Similarly, perhaps the loose sand layer did shift slightly, but the dense sand layer was able to accommodate the movement causing it to appear as if no displacement occurred. Even if the sand displaced closer to the liquefiable layer, less and less displacement may have occurred in higher layers, with displacement indiscernible at the surface.
8. Atterberg Limit tests measured a PI greater than 7 for the critical sand layer, indicating the soil may have behaved more like a clay than a sand.
9. Even if none of these reasons alone prevented displacement, it is possible a combination of factors were sufficient.

5 CONCULSION

Two piers in Port Cornel that underwent the 2010 Maule, Chile M_W 8.8 earthquake have been presented as case studies, and used to evaluate empirical methods for predicting lateral spreading for large magnitude subduction zone events. For the Lo Rojas pier, which experienced a maximum of 2.85 m of displacement, SPT, CPT, and V_S data was obtained. For the Granelero pier, only SPT data was available and no lateral displacement was observed. The following lateral spread methods were evaluated: Youd et al. (2002), Rauch and Martin (2000), Bardet et al. (2002), Zhang et al. (2012), Faris et al. (2006), and Zhang et al. (2004).

Table 27. Lo Rojas Lateral Spread Prediction Summary

Method	Best Prediction of Maximum Displacement (m)	Corresponding Method Adjustment
Maximum Measured Displacement	2.85	
Youd et al. (2002)	2.23	R = 104 km, Slope averaged over a smaller distance of 20 m
Rauch and Martin (2000)	2.45	Distance to base of liquefiable layer used for Z_{FSmin}, Slope averaged over a smaller distance of 20 m
Bardet et al. (2002)	2.41	R = 80 km using the slope based method
Zhang et al. (2012)	3.4	No adjustments made
Faris et al. (2006)	4.06	E_v depth weighting factor applied
Zhang et al. (2004)	3.71 – 4.08	Auto Transition option applied to the free face based method

Uncertainty over several parameters or proposed adaptations of the method to better predict lateral spread displacement for large magnitude earthquakes resulted in multiple displacement predictions for most methods. Table 27 shows the method adjustment and resulting prediction that fit best with maximum measured displacement for the Lo Rojas pier, while Table 26 from section 4.6.6 summarizes the range of values the Granelero pier. Since so many possibilities were explored for the Lo Rojas pier, a range of values is not provided. The following points are considered of particular significance:

1. The Youd et al. (2002) and Bardet et al. (2002) lateral spreading prediction methods are extremely sensitive to the distance term R, and the current definition of R for these two methods (Joyner-Boore distance) resulted in predictions that were more than two times the measured values for the Lo Rojas site. Using the distance from the site to the surface rupture plane (trench) produced displacements that were less than half the measured displacement, while using the distance to the zone of maximum coastal uplift again overestimated displacements. The best prediction of measured displacement was obtained using a distance of 104 km (about 65% of the distance to the trench). With this same R value, the Youd et al. (2002) method also yielded reasonable predictions of measured displacements for several nearby piers in Port Coronel (see Tryon, 2014). Predicted displacements fit well with the measured displacements when using an R value of 104 for the Youd et al. (2002) slope based method at the Lo Rojas site. However, this method did not work well for sites from the 1964 Alaskan earthquake.
2. The Lo Rojas case study is not an obvious free face or gentle slope case scenario as described by several authors, including Youd et al. (2002), but instead falls somewhere in between. Instead of using the free face ratio or using a slope averaged across the

entire length of the lateral spread, a smaller average capturing the slope at the specific point where the most lateral displacement was measured was explored, and found to provide the best prediction of lateral displacement for the Lo Rojas pier when compared to measured displacement. The smaller average used for this study was 20 m, 10 m before and 10 m after the displacement point of interest.

3. The Rauch and Martin (2000) method is sensitive to the depth to the lowest FS against liquefaction Z_{FSmin}. Because the liquefiable layer at the Lo Rojas site is comprised of consistently low blow counts, calculated FS against liquefaction is low and similar throughout the layer. The difference in the minimum FS and the FS at the base of the liquefiable layer (0.11) is less than 0.02, however the base of the liquefiable layer is 5 m lower than the technical depth of the minimum FS. By using the depth to the base of the liquefiable layer, predictions fall well within a factor of 2 from measured displacement, instead of around 50% of measured displacement when using Z_{FSmin} as defined.
4. Zhang et al. (2012) provided reasonable predictions for three of four considered displacements with no adjustments necessary. Use of local attenuation relations from Chile appears to help compensate for lack of large magnitude earthquakes used in the development of most empirical prediction methods, and eliminates the difficulty defining R as observed with Youd et al. (2002) and Bardet et al. (2002).
5. Faris et al. (2006) over predicts displacement in comparison to measured displacement near the Lo Rojas pier. Two weighting factors were applied to reduce the amount of displacement predicted, and the ε_v depth weighting factor originally intended for settlement calculations by Cetin et al. (2009) successfully reduced predictions to within

a factor of two of measured displacement. Application of the 1/Z reduction factor resulted in an under prediction below a factor of two of measured displacement.

6. The Zhang et al. (2004) CPT-based method used in the program CLiq also predicted displacements roughly 6 to 8 times larger than the measured displacements using the original formulation. More reasonable predictions of displacement were obtained when using the ε_v depth weighting factor and the auto transition option, which allows the user to define a transition layer between sand and clay that is excluded from further calculations. Nevertheless, resulting displacement predictions remained high for the Lo Rojas pier with only the two highest measured displacements assuming a free face geometry falling within a factor of two of measured displacement.
7. No method provided a good prediction of measured displacement for the Granelero pier. All predictions were outside a factor of two from measured displacement because no displacement was actually observed. Several hypothesis are presented to explain why no movement was observed, including:
    a. A high plasticity index greater than 7 present in the loose liquefiable soil layer may have prevented lateral displacements according to Idriss and Boulanger (2006)
    b. A dense sand layer and high bedrock layer which may have provided a buttress for liquefiable soils
    c. An insufficiently continuous liquefiable soil layer was present
    d. Pockets of clay and silt as observed near other piers in Port Coronel at approximately the same depth may have prevented the development of a consistent failure surface and displacements

e. Off-shore and past the dense sand high bedrock region, the soft liquefiable layer at the surface may have moved without causing damage, flowing around piers instead of displacing them

f. A thick layer of dense sand above liquefiable soils on shore which may have either prevented displacement from occurring or dampened the impact of the displacement, resulting in indiscernible displacement at the surface

REFERENCES

Abrahamson, N.A., and Silva, W.J., 1997. "Empirical response spectral acceleration relations for shallow crustal earthquake." *Seismol. Res. Lett.,* 68(1), 94-127.

Bardet, J., Tobita, T., Mace, N., Jianping, H., 2002. "Regional Modeling of Liquefaction-Induced Ground Deformations." *Earthquake Spectra*, Vol. 18, No. 1, pp. 19-46.

Bartlett, S. F., and Youd, T. L., 1995. "Empirical Prediction of Liquefaction-Induced Lateral Spread." *Journal of Geotechnical Engineering*, Vol. 121, No. 4.

Boore, D., Joyner, W., Fumal, T., 1997. "Equations for estimating horizontal response spectra and peak acceleration for western North American earthquakes: A summary of recent work." *Seismol. Res. Lett.,* 68(1), 128-153.

Bray, J., Elderidge, T., Frost, D., Hashash, Y., Kayen, R., Ledezma, C., Moss, R., Verdugo, R., 2010. "Geo-engineering Reconnaissance of the 2010 Maule, Chile Earthquake". *Veo-Engineering Extreme Events Reconnaissance Association*. Version 2: May 25, 2010.

Bray, J.D., Sancio, R. B., 2006. "Assessment of the liquefaction susceptibility of fine-grained soils." *Journal of Geotechnical and Geoenvironmental Engineering*, ASC, Vol. 132, No. 9, pp. 1165-1177.

Bedient, P. B. and Huber, W. C., 1988. *Hydrology and Floodplain Analysis*, Addison-Wesley.

Campbell, K., 1997. "Empirical near-source attenuation relationships or horizontal and vertical components of peak ground acceleration, peak velocity, and pseudo-absolute acceleration response spectra." *Seismol. Res. Lett.,* 68(1), 154-179.

Cetin, K. O., Seed, R. B., Kiureghian, A. D., Tokimatsu, K., Harder, L. F. Jr., Kayen, R. E., Moss, R. E. S., 2004. Standard Penetration Test-Based Probabilistic and Deterministic Assessment of Seismic Soil Liquefaction Potential, *Journal of Geotechnical and Geoenvironmental Engineering*, Vol. 130, No. 12, pp. 1314-1340.

Cetin, K. O., Bilge, H. T., Wu, J., Kammerer, A. M., Seed, R. B., 2009. "Probabilistic Model for the Assessment of Cyclically Induced Reconsolidation (Volumetric) Settlements." *Journal of Geotechnical and Geoenvironmental Engineering, ASCE*.

Contreras V., and Boroschek, R., 2012. Strong Ground Motion Attenuation Relations for Chilean Subduction Zone Interface Earthquakes, *Proceedings in 15th World Conference on Earthquake Engineering*, Lisboa 2012.

Delouis, B., Nocquet, J., Vallée, M., 2010. "Slip distribution of the Februrary 27, 2010 M_w = 8.8 Maule Earthquake, central Chile, from static and high-rate GPS, InSAR, and broadband teleseismic data." *Geophysical Research Letters*, Vol. 37, L17305.

Faris, Alison T., Raymond B. Seed, Robert E. Kayen, and Jiaer Wu., 2006. "A Semi-Empirical Model for the Estimation of Maximum Horizontal Displacement Due to Liquefaction-Induced Lateral Spreading." *Procceedings of the 8th U.S. National Conference on Earthquake Engineering*, paper 1323, San Francisco.

Gillins, D. T., 2012. "Mapping the Probability and Uncertainty of Liquefaction-induced Ground Failure." PhD Dissertation, Civil and Environmental Engineering, University of Utah.

González, J., Verdugo, R. "Efectos del Terremoto del 27F en el Subsuelo del Puerto de Coronel." Department of Civil Engineering, University of Chile, Santiago, Chile.

Idriss, I. M., and Boulanger, R. W., 2004. Semi-Empirical Procedures for Evaluating Liquefaction Potential During Earthquakes, *Soil Dynamics and Earthquake Engineering*, Vol. 26, pp. 115-130.

Kaklamanos, J., Baise, L., Boore, D., 2011. "Estimating Unknown Input Parameters when Implementing the NGA Ground-Motion Prediction Equations in Engineering Practice." *Earthquake Spectra*, Vol. 27 (4), 1219-1235.

Kramer, S. L., 1996. *Geotechnical Earthquake Engineering*, Prentice-Hall Inc., Upper Saddle River, NJ, 349 pp.

Maza, G., Williams, N., Sáez, E., Rollins, K., 2014. "Liquefaction-induced lateral spreading in Lo Rojas, Coronel. Field study and numerical modeling." *VIII Congreso Chileno de Ingeniería Geotécnica 2014*. Santiago, Chile.

Mobile Geographics. *Talcahuano, Chile Tide Chart*. http://tides.mobilegeographics.com/locations/6338.html?y=2010&m=2&d=27 (accessed April 16, 2015).

National Oceanic and Atmospheric Administration. *High and Low Water Predictions, West Coast of North and South America*. Tide Tables 2010. http://tidesandcurrents.noaa.gov/tidetables/2010/wctt2010book.pdf (accessed April 16, 2015).

Puerto de Coronel. *Granales*. http://www.puertodecoronel.cl/ (accessed May 4, 2015).

Rauch, A. F., and Martin, J. R., 2000. EPOLLS Model for Predicting Average Displacement Lateral Spreads, *Journal of Geotechnical and Geoenvironmental Engineering*, Vol. 126, No. 4.

Robertson, P., Gregg Drilling & Testing Inc., 2014. "CLiq User's Manual." Geologismiki. http://www.geologismiki.gr/Documents/CLiq/HTML/

Sáez, E., Ledezma, C., De La Maza, G., Cortés, M., Brunet, S., 2013. "Case Study of Two Piers Affected by Liquefaction-Induced Lateral Spreading for the 2010 Maule Earthquake: Geophysical Survey." *New Zealand – Japan Workshop on Soil Liquefaction during Recent Large-Scale Earthquakes.*

Seed, R. B., Harder, L. F., 1990. "SPT-Based Analysis of Cyclic Pore Pressure Generation and Undrained Residual Strength." *Earthquake Engineering Handbook edited by Charles Scawthorn, Wai-Fah Chen,* 2003.

U.S Geological Survey. *M8.8 – Maule, Chile*. Earthquake Hazard Program. http://earthquake.usgs.gov/earthquakes/eventpage/duputel201002270634a#scientific_summary (accessed March 4, 2015).

van Ballegooy, S., Malan, P., Lacrosse, V., Jacka, M. E., Cubrinovski, M., Bray, J. D., O'Rourke, T. D., Crawford, S. A., Cowan, H. 2014. "Assessment of Liquefaction-Induced Land Damage for Residential Christchurch." *Earthquake Spectra*, Vol. 30, No. 1, pp. 31-55.

Vargas, G., Farías, M., Carretier, S., Tassara, A., Baize, S., Melnick, D., 2011. "Coastal uplift and tsunami effects associated to the 2010 M_w 8.8 Maule earthquake in Central Chile". *Andean Geology*, Vol. 38, 219-238.

Wright, S. G., 2004. "UTEXASED4: A Computer Program for Slope Stability Calculations (Educational version of the UTEXAS4 and TexGraf4 software)." Austin, Texas. http://www.ce.utexas.edu/prof/wright/UTEXASED4/UTEXASED4%20Manual.PDF

Wu, J., 2002. "Liquefaction Triggering and Post Liquefaction Deformations of Monterey 0/30 Sand under Uni-Directional Cyclic Simple Shear Loading." PhD Dissertation, Department of Civil and Environmental Engineering, University of California, Berkeley, CA.

Youd, T. L., DeDen, D. W., Bray, J. D., Sancio, R., Cetin, K. O., Gerber, T. M., 2009. Zero-Displacement Lateral Spreads, 1999 Kocaeli, Turkey, Earthquake, *Journal of Geotechnical and Geoenvironmental Engineering*, Vol. 135, No. 1, pp. 46-61.

Youd, T. L., Hansen, C. M., Bartlett, S. F., 2002. Revised Multilinear Regression Equations for Prediction of Lateral Spread Displacement, *Journal of Geotechnical and Geoenvironmental Engineering*, Vol. 128, No. 12.

Youd, T. L., Idriss, I. M., Andrus, R.D., Arango, I., Castro, G., Christian, J. T., Dobry, R., Finn, W. D. L., Harder, L. F., Hynes, M. E., Ishihara, K., Koester J. P., Liao, S. C., Marcuson, W. F., Martin, G. R., Mitchell, J. K., Moriwaki, Y., Power, M. S., Robertson, P. K., Seed, R. B., Stokoe, K. H., 2001. Liquefaction Resistance of Soils: Summary Report from 1996 NCEER/NSF Workshops on Evaluation of Liquefaction Resistance of Soils, *Journal of the Geotechnical and Geoenvironmental Engineering*, vol. 127 (410), pp. 817-833.

Youd, T. L. (2002). Youd, Hansen, and Bartlett database for induced lateral spreads, <http://www.et.byu.edu/cc/ccweb/faculty/youd/data.html>.

Zhang, G., Robertson, P. K., Brachman, R. W. I, 2004. Estimating Liquefaction-Induced Lateral Displacements Using the Standard Penetration Test or Cone Penetration Test, *Journal of Geotechnical and Geoenvironmental Engineering*, Vol. 130, No. 8, pp. 861-871.

Zhang, J., Changwei, Y., Zhao, J. X., McVerry, G. H., 2012. Empirical Models for Predicting Lateral Spread Considering the Effects of Regional Seismicity, *Earthquake Engineering and Engineering Vibrations*, vol. 11, No. 1, pp. 121-131.

APPENDIX A. DATA LOGS

OBRAS PORTUARIAS
& GEOTÉCNIA

Ingeniería

RESUMEN DE OPERACIÓN Y MUESTRAS
DETERMINACIÓN DEL SPT

Proyecto: Reconocimiento Suelo de Fundación Construcción Muelles Artesanales Caletas Lo Rojas y Lota Bajo
Localidad: Caleta Lo Rojas
Sondaje N°: SM-1 Marítimo Operador: Hernando Rojas
Ubicación: 5.900.731 Norte Inicio: 03 de Mayo del 2010 Término: 11 de Mayo del 2010
663.994 Este Equipo: Maquina de Sondaje Boyles Bros
Altura agua: 9.20 m Día: 07 de Mayo del 2010 Hora: 08:45 hrs.

Herramienta	PENETRACIÓN SPT tramo (metros) Inicial	final	N1	N2	N3	NF	Muestra N°	Largo Testigo Rec. (cm)	OBSERVACIONES
NQ	10,00	10,45	4	5	2	7	3	45	limo
NQ	10,55	11,00	2	4	2	6	4	42	limo
NQ	11,00	11,45	14	25	27	52	5		arena media fina
NQ	11,55	12,00	18	33	45	78	6	45	arena media fina
NQ	12,00	12,45	9	12	10	22	7	25	arena media fina
NQ	12,55	13,00	9	16	21	37	8	35	arena media fina
NQ	13,00	13,45	2	3	3	6	9	45	limo arenoso
NQ	13,55	14,00	2	6	8	14	10	45	limo arenoso
NQ	14,00	14,45	2	2	4	6	11	45	limo arenoso
NQ	14,45	15,00	6	31	R	100	12	40	arena media fina
NQ	15,00	15,45	11	12	15	27	13	45	arena fina
NQ	15,55	16,00	3	4	11	15	14	45	arena fina
NQ	16,00	16,45	9	27	R	100	15	45	arena fina
NQ	17,00	17,45	14	22	23	45	17		arena fina
NQ	18,00	18,45	15	50	R	100	19	30	arena fina
NQ	19,00	19,45	24	50	R	100	21	28	arena fina
NQ	20,00	20,45	5	5	10	15	23	40	arena fina
NQ	21,00	21,45	10	14	20	34	25	40	arena fina
NQ	22,00	22,45	10	35	44	79	27	45	arena fina
NQ	23,00	23,45	11	22	33	55	29	45	arena fina con fino limoso
NQ	24,00	24,45	14	24	27	51	31	45	limo
NQ	25,00	25,45	14	31	38	69	33	45	limo , arena limosa cementada
NOTAS:									
Las muestras de los primeros 10 m corresponden a limos y arenas finas sueltas con SPT< 5, por lo cual se obtuvieron un par de muestras a modo de referencia									Las barras AW y la masa del SPT, bajaban sólo con el peso propio
	0,00	4,50					1		limo
	4,50	10,00					2		arena fina
NOTA: Al rechazo se le asigna el valor maximo solo para graficar la secuencia.									

Casing	Cant. m	Fecha	Hora	Prof (m)	Observación

Observaciones
(*) De acuerdo a la norma ASTM D1586, para considerar rechazo se debe cumplir alguna de las siguientes condiciones:

1. Se aplica un total de 60 golpes, durante cualquiera de los tres incrementos de 15 cm que componen la prueba.
2. No se observa avance de la cuchara, durante la aplicación de 10 golpes sucesivos

Figure A - 1. SM-1 Boring Log at Lo Rojas.

OBRAS PORTUARIAS
& GEOTECNIA

Ingeniería

RESUMEN DE OPERACIÓN Y MUESTRAS

Proyecto: Reconocimiento Suelo de Fundación Construcción Muelles Artesanales Caletas Lo Rojas y Lota Bajo
Localidad: Caleta Lo Rojas
Sondaje N°: SM-2 Marítimo Operador: Hernando Rojas
Ubicación: 5.900.771 Norte Inicio: 19 de Mayo del 2010 Término: 26 de Mayo del 2010
663.976 Este Equipo: Maquina de Sondaje Boyles Bros
Altura agua: 8,10 m Dia: 19 de Mayo del 2010 Hora: 08:30 hrs

Herramienta	PENETRACIÓN SPT tramo (metros) Inicial	final	N1	N2	N3	NF	Muestra N°	Largo Testigo Rec. (cm)	OBSERVACIONES
	0,00	0,45	6	8	9	17	1	45	Arena media fina
	1,00	1,45	3	4	1	5	3	5	Arena media fina
	2,00	2,45	3	4	3	7	5	45	Arena media fina
	3,00	3,45	3	3	2	5	7	10	Arena media fina
	4,00	4,45	1	2	1	3	9	45	Gravas medias gruesas
	5,00	5,45	1	1	2	3	11	45	Limo arcilloso
	6,00	6,45	2	1	2	3	13	15	Limo arcilloso
	7,00	7,45	1	1	2	3	15	45	Limo arcilloso
	8,00	8,45	1	2	2	4	17	40	Limo arcilloso
	9,00	9,45	2	1	2	3	19	45	Limo arcilloso
	10,00	10,45	4	6	7	13	21	40	Limo arenoso
	10,55	11,00	2	5	14	19	22	14	Limo arcilloso
	11,00	11,45	12	27	42	69	23	30	Arena media fina
	12,00	12,45	12	27	R	100	24	40	Arena media fina
	14,40	14,90	2	1	2	3	25	45	Limo arenoso
	15,00	15,45	22	45	50	95	26	45	Arenas
	15,55	16,00	13	20	26	46	27	45	Arenas
	16,00	16,45	4	17	31	48	28	45	Arenas
	16,55	17,00	4	10	24	34	29	20	Arenas
	17,55	18,00	8	27	50	77	31	30	Arenas
	18,00	18,45	14	27	50	77	32	40	Arenas
	18,55	19,00	13	20	45	65	33	40	Arenas
	19,00	19,45	14	35	50	85	34	40	Arenas
	19,55	20,00	6	16	29	45	35	40	Arenas
	20,55	21,00	10	16	28	44	37	40	Arenas
	21,55	22,00	18	50	R	100	38	15	Arena media fina
	22,55	23,00	6	10	15	25	40	15	Arena media fina
	23,55	24,00	11	25	33	58	42	15	Arena media fina
	25,00	25,45	3	7	12	19	44	15	Arcilla
	28,05	28,50	7	11	18	29	48	23	Limo arcilloso

NOTA: Al rechazo se le asigna el valor maximo solo para graficar la secuencia.

Casing	Cant. m	Fecha	Hora	Prof (m)	Observación

Observaciones
(*) De acuerdo a la norma ASTM D1586, para considerar rechazo se debe cumplir alguna de las siguientes condiciones:

1. Se aplica un total de 50 golpes, durante cualquiera de los tres incrementos de 15 cm que componen la prueba.
2. No se observa avance de la cuchara, durante la aplicación de 10 golpes sucesivos

Figure A - 2. SM-2 Boring Log at Lo Rojas.

EMPRO LTDA.
Ensaye de Materiales y Prospecciones
Paicavi N°3001 Fono: (041)2741727 Fax: (041)2741757 e-mail: empro@entelchile.net
Suelos – Hormigones –Asfaltos
Concepción

RESULTADOS DE EXPLORACIÓN DEL SUBSUELO
PASEO LA OLA LO ROJAS, CORONEL
Sondaje S-1

Informe N° 94730-14-00
O.T. N° 422229

UBICACIÓN: Indicada por Mandante

FECHA DE INICIO: 18//03/14
TERMINO: 19/03/14

COTA INICIO: 0,00
TERMINO: 21,82

PROFUNDIDAD DE	PROFUNDIDAD A	DESCRIPCIÓN VISUAL DEL SUBSUELO	MUESTRA N°	MUESTRA TIPO	PENETRACIÓN DE	PENETRACIÓN A	ENSAYO DE PENETRACIÓN ESTANDAR N1	N2	N3	N	L (m)
0,00	1,00	Arena fina a media con algunos restos de gravas aisladas de tamaño máximo 3/4", compacidad baja, humedad baja, color gris oscuro.	1	CN	0,60	1,05	2	2	3	5	0,33
1,00	1,73	Base estabilizada y bolones de tamaño máximo 7", humedad media, compacidad alta.									
1,73	3,59	Arena fina a media, compacidad baja, humedad alta, color gris oscuro,	2	CN	1,73	2,18	10	5	3	8	0,31
			S/M	CN	2,59	3,04	1	1/30			
3,59	5,60	Arena media a gruesa, compacidad baja, humedad alta, color gris oscuro.	3	CN	3,59	4,04	1	2	1	3	0,26
			4	CN	4,63	5,08	1	1	2	3	0,38
5,60	7,59	Arena media a gruesa con gravas aisladas de tamaño máximo 1", compacidad baja, humedad alta, color gris oscuro.	5	CN	5,60	6,05	3	3	2	5	0,20
			6	CN	6,60	7,05	3	2	2	4	0,21
7,59	8,60	Arena fina, compacidad baja, humedad alta, color gris oscuro.	7	CN	7,59	8,04	2	2	4	6	0,13
8,60	9,61	Arena muy fina con lentes aislados de carboncillo, compacidad baja, humedad alta, color gris oscuro.	8	CN	8,60	9,05	4	3	6	9	0,36
9,61	10,63	Arena fina algo limosa con alto porcentaje de carboncillo, compacidad baja, humedad alta, color gris oscuro.	9	CN	9,61	10,06	2	2	1	3	0,44
10,63	12,57	Arena fina limosa, plasticidad media, compacidad baja, humedad alta, color gris oscuro, con restos de carbón.	10	CN	10,63	11,08	2	1	2	3	0,67
			11	CN	11,54	11,99	5	2	1	3	0,60

CONTROL NAPA DE AGUA		
Fecha	Hora	Profundidad (m)
19-03-14		1,72

MUESTREADOR TIPO
CN: Cuchara Normal
SH: Tubo Shelby
NQ3: Barril testigo 45mm
HQ3: Barril testigo 63mm

ENSAYO SPT
N1: Número de golpes para penetrar los primeros 15cm
N2: Número de golpes para penetrar los segundos 15cm
N3: Número de golpes para penetrar los terceros 15cm
N: N2 + N3

SIMBOLOGÍA DE MUESTRA
S/M: Sin muestra recuperada
L: Longitud de muestra
R: Rechazo
R: Rechazo

Figure A - 3. S-1 boring log at Lo Rojas.

EMPRO LTDA.
Ensaye de Materiales y Prospecciones **Suelos – Hormigones –Asfaltos**
Paicaví N°3001 **Fono: (041)2741727** **Fax: (041)2741757** **e-mail: empro@entelchile.net** **Concepción**

RESULTADOS DE EXPLORACIÓN DEL SUBSUELO
PASEO LA OLA LO ROJAS, CORONEL
Sondaje S-1

Informe N° 94730-14-00
O.T. N° 422229

UBICACIÓN: Indicada por Mandante

FECHA DE INICIO: 18//03/14
TERMINO: 19/03/14

COTA INICIO: 0,00
TERMINO: 21,82

PROFUNDIDAD DE	PROFUNDIDAD A	DESCRIPCIÓN VISUAL DEL SUBSUELO	MUESTRA N°	MUESTRA TIPO	PENETRACIÓN DE	PENETRACIÓN A	ENSAYO DE PENETRACIÓN ESTANDAR N1	N2	N3	N	L (m)
12,57	13,62	Limo arcilloso con alto porcentaje de conchuelas fracturadas descompuestas, consistencia baja, humedad alta y algunos restos de carboncillo, color gris verdoso.	12	CN	12,57	13,02	2	1	1	2	0,45
13,62	15,62	Limo arcilloso, color gris verdoso, plasticidad alta, humedad alta, consistencia muy baja.	13	CN	13,62	14,07	1/30		1	1	0,45
			14	SH	14,20	14,50					0,48
			15	CN	14,60	15,05	1/30		2	2	0,45
15,62	17,62	Limo arcilloso, color gris verdoso, con lentes de conchuelas intercaladas, humedad alta, consistencia baja.	16	CN	15,62	16,07	1/30		1	1	0,50
			17	CN	16,52	17,07	1/30		2	2	0,45
			S/M	SH	17,15	17,45					
17,62	18,60	Arena fina limosa, compacidad media, humedad alta, con algunas gravillas aisladas y trozos de carbón, color gris plomizo	18	CN	17,62	18,07	2	4	9	13	0,26
18,6	19,63	Limo arcilloso, con lentes de carboncillo, intercalados, consistencia alta, humedad alta, color gris claro.	19	CN	18,60	19,05	7	7	10	17	0,30
19,63	20,57	Limo arcillo con un estrato de 19 centímetros de carboncillo, consistencia alta, humedad alta, color gris cafesoso.	20	CN	19,63	20,08	14	10	12	22	0,39
20,57	21,82	Limo arcilloso, algo cementado algo arcilloso, consistencia muy alta, color plomizo	21	CN	20,57	20,86	28	50/14			0,33
			22	CN	21,56	21,82	27	50/11			0,37

CONTROL NAPA DE AGUA		
Fecha	Hora	Profundidad (m)
19-03-14		1,72

MUESTREADOR TIPO
CN: Cuchara Normal
SH: Tubo Shelby
NQ3: Barril testigo 45mm
HQ3: Barril testigo 63mm

ENSAYO SPT
N1: Número de golpes para penetrar los primeros 15cm
N2: Número de golpes para penetrar los segundos 15cm
N3: Número de golpes para penetrar los terceros 15cm
N: N2 + N3

SIMBOLOGÍA DE MUESTRA
S/M: Sin muestra recuperada
L: Longitud de muestra
R: Rechazo
r: recuperación

Figure A - 4. S-1 boring log at Lo Rojas continued.

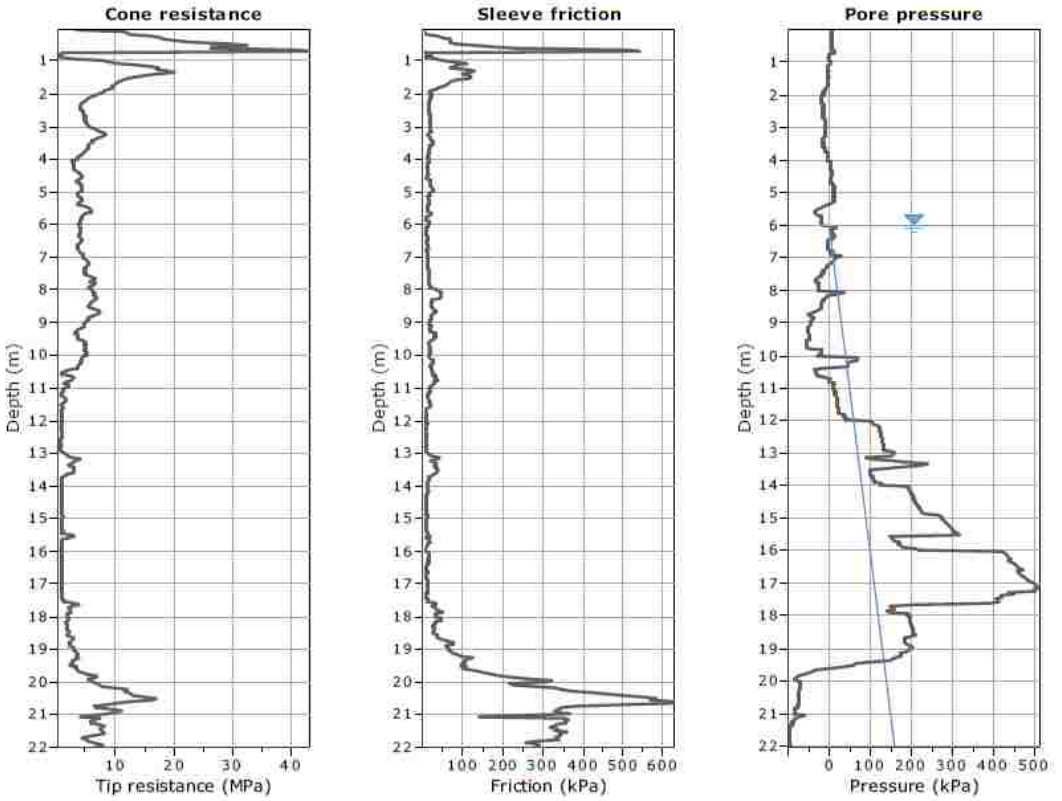

The plot below presents the cross correlation coeficient between the raw qc and fs values (as measured on the field). X axes presents the lag distance (one lag is the distance between two sucessive CPT measurements).

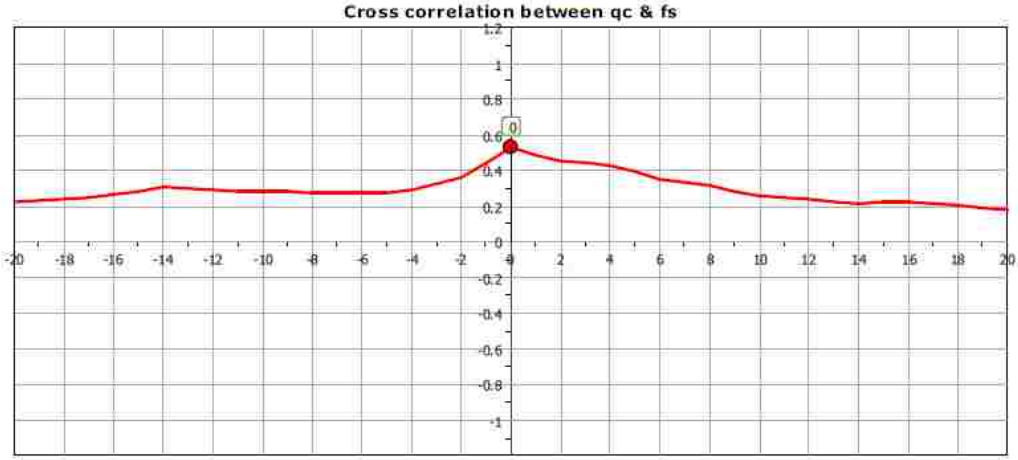

Figure A - 5. CPT5 sounding log near Lo Rojas.

LMMG
Geotechnical Engineers
www.LMMG.CL

Project:
Location:

CPT: CPT-06
Total depth: 20.00 m, Date: 06-04-2014
Surface Elevation: 0.00 m
Coords: X:0.00, Y:0.00
Cone Type: Uknown
Cone Operator: Uknown

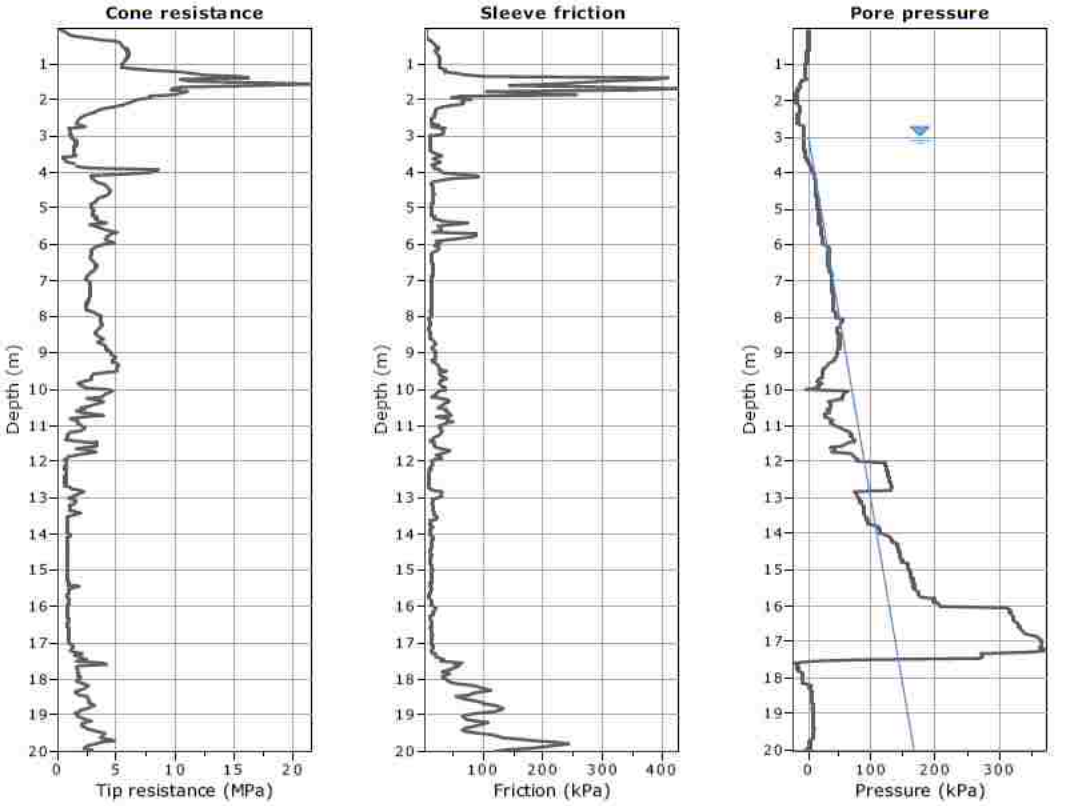

The plot below presents the cross correlation coeficient between the raw qc and fs values (as measured on the field). X axes presents the lag distance (one lag is the distance between two sucessive CPT measurements).

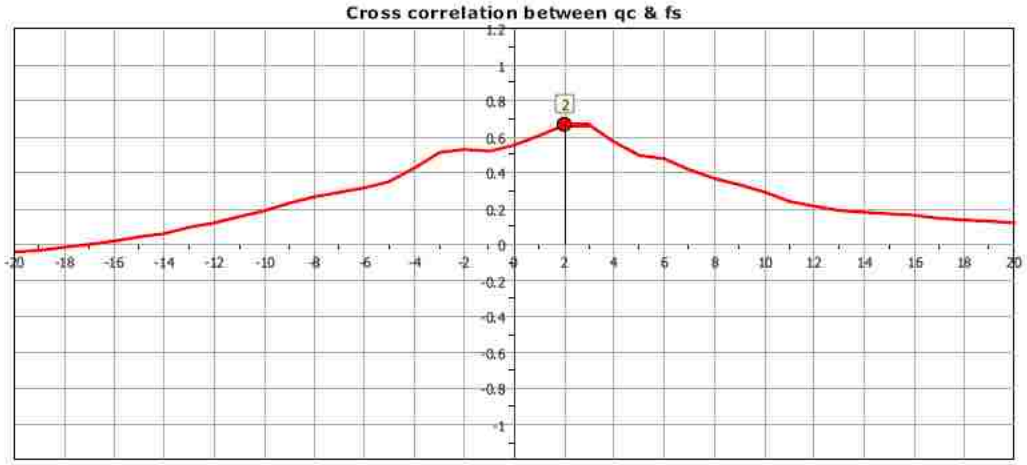

Figure A - 6. CPT6 sounding log near Lo Rojas.

JQ Ingenieria Ltda.
Estudios Básicos & Geotecnia

ENSAYO SPT
RESUMEN DE OPERACIÓN Y MUESTRAS

Nombre del Proyecto: **Sondajes Geotecnicos con medición de SPT, Puerto Coronel**

Sondaje: **SPT-5** **Terrestre** Operador: **Nelson Muñoz Ferreira**
Ubicación: Norte **5899003 m** Inicio: **03-04-14** Termino: **07-04-14**
Este **664918 m** Equipo: Maquina de sondaje KSK

Fecha	Herr.	PENETRACIÓN SPT Tramo (m) Inicial	Final	N1	N2	N3	NF	Muestra N°	Largo Testigo Rec. (m)	OBSERVACIONES
04-abr	-	0,00	0,45	-	-	-		-	-	-
04-abr	SPT	1,00	1,45	12	15	15	30	1	45	Arena limpia con gravillas de tam. prom. 10 mm
04-abr	SPT	2,00	2,45	4	9	3	12	2	32	Arena con finos, grava aislada en la punta
05-abr	SPT	3,00	3,45	2	4	5	9	3	32	Arena con escaso cont. de finos, gravas aisladas
05-abr	SPT	4,00	4,45	9	11	21	32	4	35	Arena media, gravas aisladas
05-abr	SPT	5,00	5,45	10	15	18	33	5	29	Arena media, escasa presencia de finos
06-abr	SPT	6,00	6,45	-	-	-		-	s/rec.	No se hizo SPT, fue autorizado por Dr. Rollins
06-abr	SPT	7,00	7,45	19	30	27	57	6	35	Arena limosa, sin gravas
06-abr	SPT	8,00	8,45	10	29	30	59	-	s/rec.	Se hizo dos veces, la cuchara sale abollada
06-abr	SPT	9,00	9,45	13	21	23	44	7	30	Arena limosa, sin gravas
07-abr	SPT	10,00	10,45	7	16	19	35	8	33	Arena media algo limosa con carbón
07-abr	SPT	11,00	11,45	8	17	22	39	9	24	Arena media algo limosa
07-abr	SPT	12,00	12,45	13	19	19	38	-	s/rec.	-
07-abr	SPT	13,00	13,45	16	23	22	45	10	33	Arena fina a media con algo de limos
07-abr	SPT	14,00	14,45	9	5	4	9	11	40	Limo+conchuelas+carbón, con conchas al inicio
07-abr	SPT	15,00	15,45	2	3	7	10	12	45	Limo con conchitas

NOTA: Al rechazo (R) se le asigna el valor máximo sólo para gráficar la secuencia.

Casing	Cant. m	Nivel Napa (agua existente) Fecha	Hora	Prof (m)	Observación
		15-04-14	13:30	4.2 m	Medido desde la superficie de la explanada existente

Observaciones:
(*) De acuerdo a la norma ASTM D1586, para considerar rechazo se debe cumplir alguna de las siguientes condiciones:

1. Se aplica un total de 50 golpes, durante cualquiera de los tres incrementos de 15 cm que componen la prueba.

2. No se observa avance de la cuchara, durante la aplicación de 10 golpes sucesivos

Figure A - 7. SPT5 boring log near the Granelero pier.

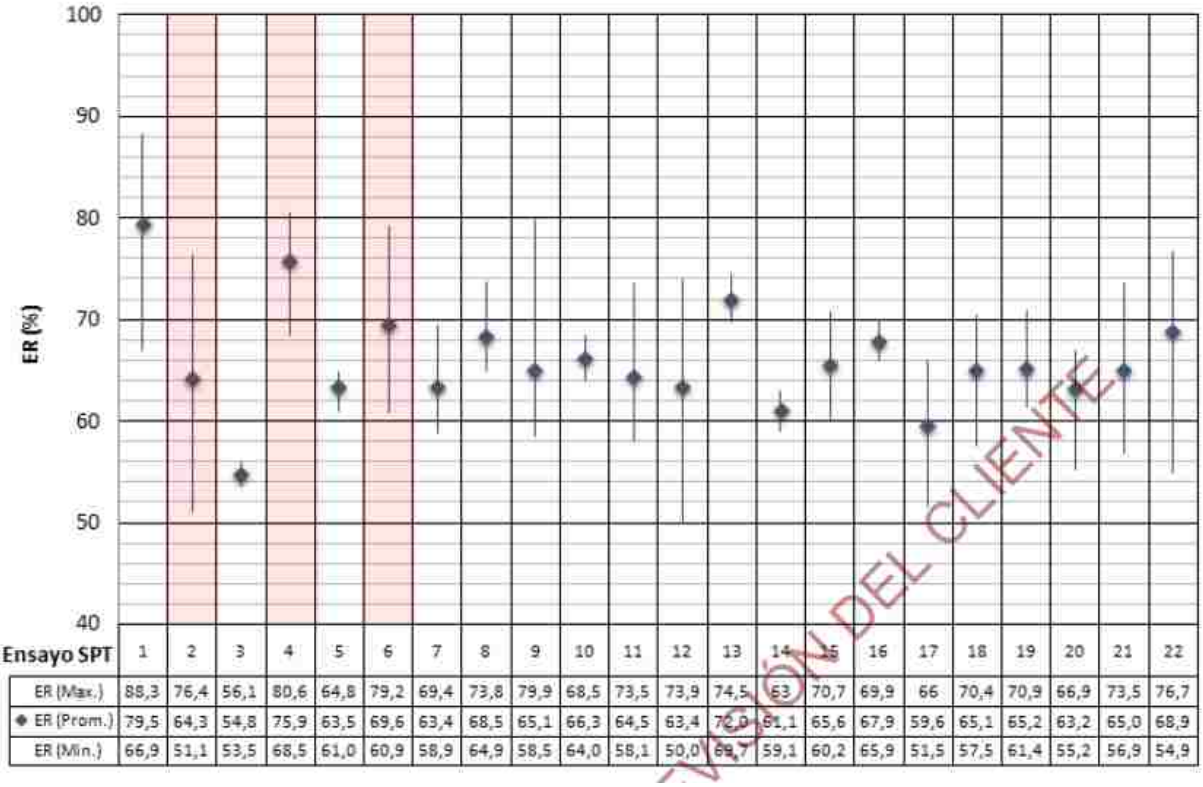

Ensayo SPT	1	2	3	4	5	6	7	8	9	10	11	12	13	14	15	16	17	18	19	20	21	22
ER (Max.)	88,3	76,4	56,1	80,6	64,8	79,2	69,4	73,8	79,9	68,5	73,5	73,9	74,5	63	70,7	69,9	66	70,4	70,9	66,9	73,5	76,7
ER (Prom.)	79,5	64,3	54,8	75,9	63,5	69,6	63,4	68,5	65,1	66,3	64,5	63,4	72,0	61,1	65,6	67,9	59,6	65,1	65,2	63,2	65,0	68,9
ER (Min.)	66,9	51,1	53,5	68,5	61,0	60,9	58,9	64,9	58,5	64,0	58,1	50,0	69,7	59,1	60,2	65,9	51,5	57,5	61,4	55,2	56,9	54,9

Figure A - 8. Energy measurement for SPT5 boring log near the Granelero pier.

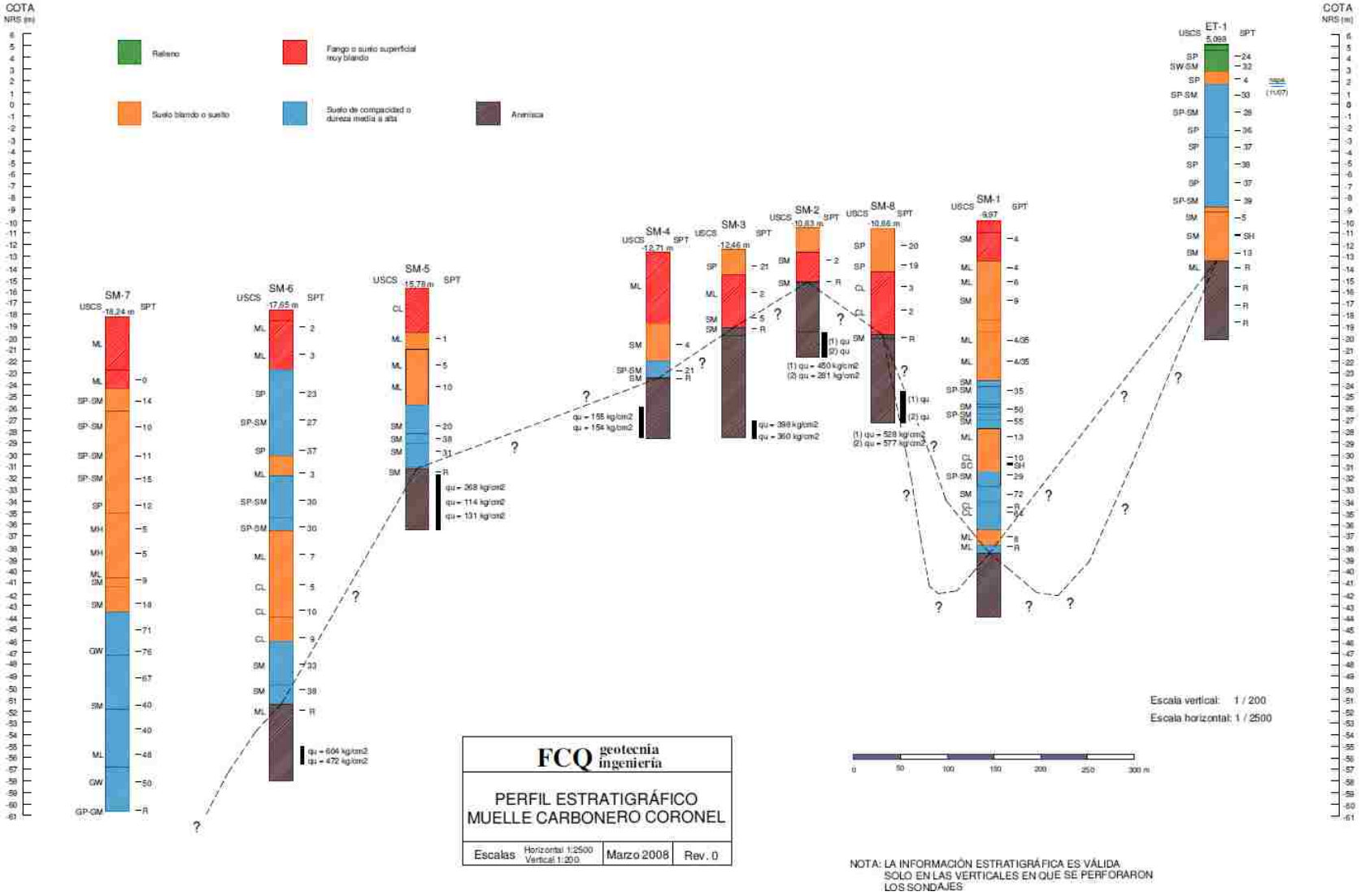

Figure A - 9. 2008 SPT borings near the Granelero pier.

APPENDIX B. FIGURES

Figure B - 1. Location of data points in Lo Rojas

Figure B - 2. CPT5 at Lo Rojas, Coronel, Chile.

Figure B - 3. CPT6 at Lo Rojas, Coronel, Chile